ISTITUTO NAZIONALE DI FISICA NUCLEARE

Sezione di Milano

INFN/TC-84/25
25 Ottobre 1984

Final version
10 Gennaio 1986

C. De Martinis and D. Giove:

THE MAGNET STRUCTURE OF THE MILAN SUPERCONDUCTING CYCLOTRON

Servizio Documentazione
dei Laboratori Nazionali di Frascati

Istituto Nazionale di Fisica Nucleare
Sezione di Milano

INFN/TC-84/25
25 Ottobre 1984

THE MAGNET STRUCTURE OF THE MILAN SUPERCONDUCTING CYCLOTRON

C. De Martinis and D. Giove
Istituto di Fisica dell'Università di Milano, and
INFN - Sezione di Milano

1.- INTRODUCTION

The construction of the superconducting cyclotron at the University of Milan, funded by the Italian National Institute for Nuclear Physics (INFN), is underway since February 1981.

It is the purpose of this paper to review in detail the design choiches and the constructional aspects of the magnetic yoke and polar expansions, which as of now, are almost completed. For the sake of completeness we briefly recall the major parameters of the machine which are extensively described elsewhere[1-3].

The machine has a 3 sectors geometry, 3 dees, with an operating magnetic field between 22 and 48 kgauss. Maximum and minimum ions energies per nucleon as a function of the ion mass number are shown in Fig. 1 for the operation of the machine as a booster for a 16 MeV Tandem. A vertical cross section and a median plane sketch of the cyclotron are shown in Figs. 2 and 3 respectively, while Table I summarizes the main cyclotron parameters.

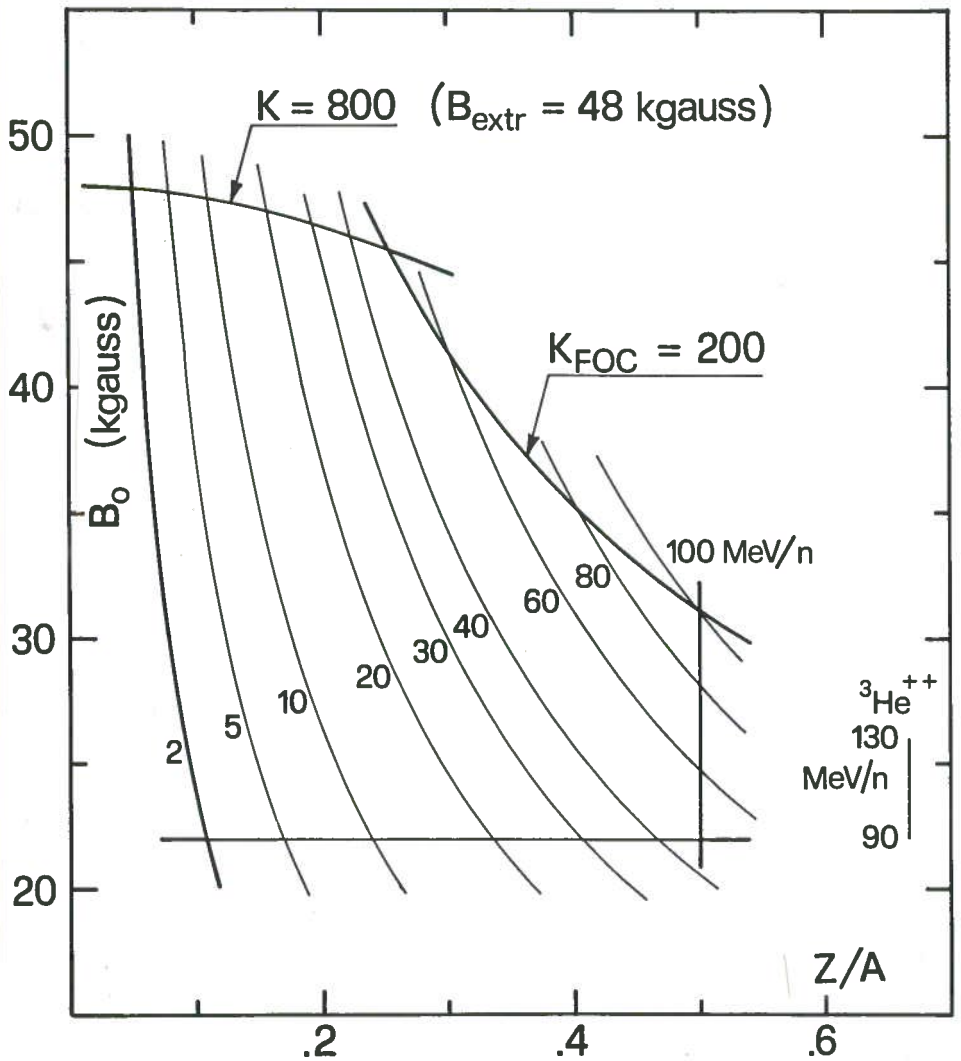

FIG. 1 - Maximum and minimum ions energies per nucleon as a function of the ion mass number.

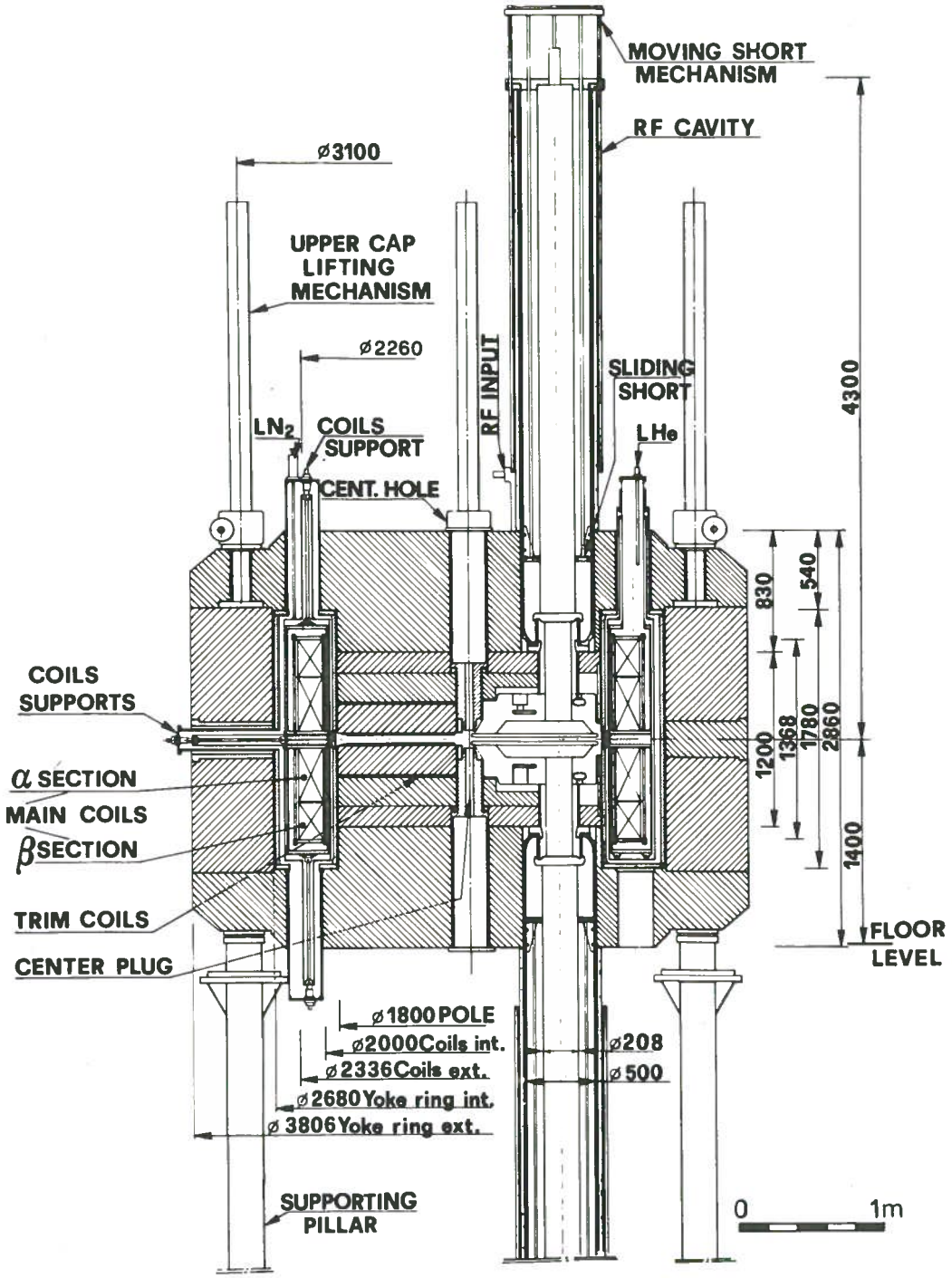

FIG. 2 - Cross section view of the cyclotron.

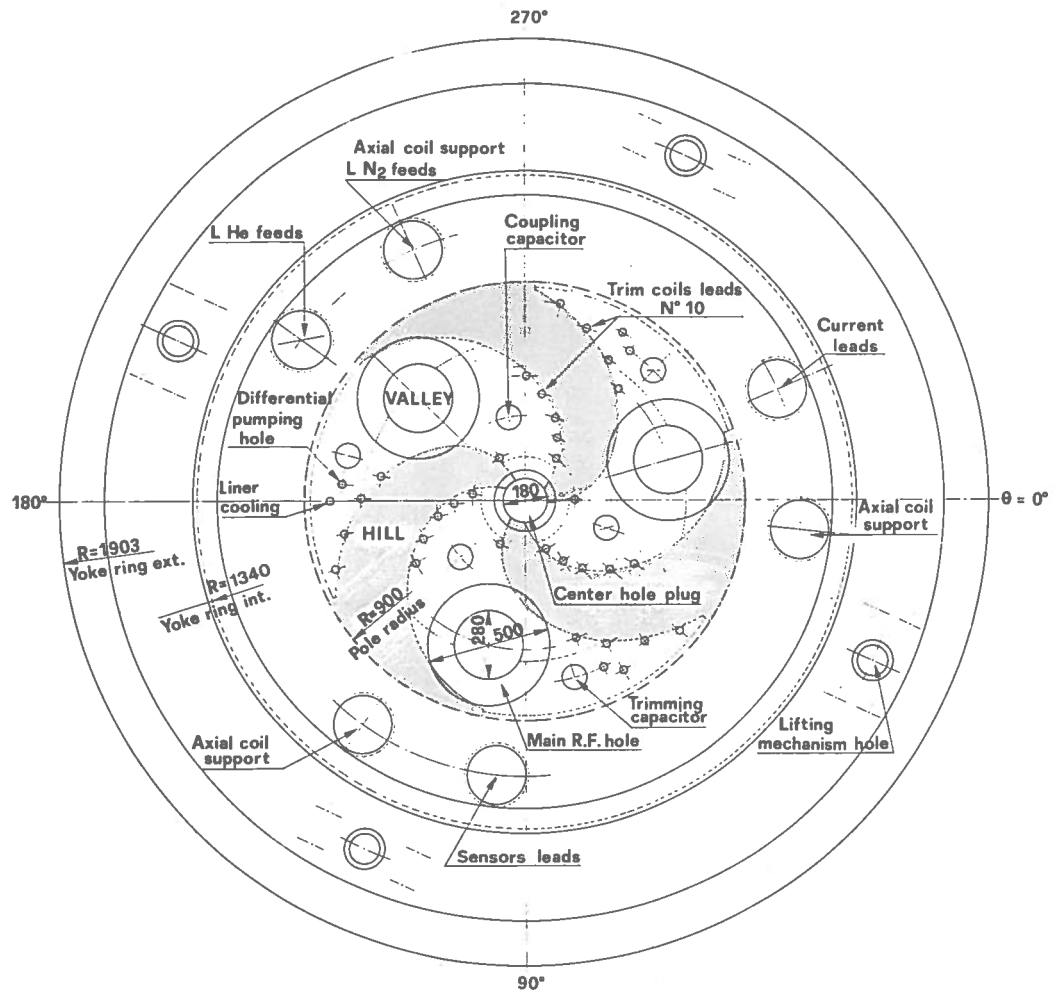

FIG. 3 - Sketch of the magnet from the top.

TABLE I - Main machine parameters.

$K_{bending}$	: 800
$K_{focusing}$	: 200
Pole diameter	: 180 cm.
Number of sectors	: 3
Average spiral constant	: 1/46 rad/cm.
Minimum hill gap	: 8.6 cm.
Maximum valley gap	: 91.6 cm.
Main coils At	: 6.55×10^6 at 3500 A/cm^2 average density
Minimum and maximum center field	: 22 and 48 kG
Number of trim coils	: 20
Maximum current in trim coils	: 400 A
Dees	: 3, in the valleys
RF frequency range	: 15 to 48 MHz
Operating harmonics	: 1,2,3,4
Peak dee voltage	: 100 kV

2.- PRELIMINARY DESIGN OF THE MAGNET YOKE

A very preliminary design of the magnet yoke was completed in June '80. This was the basis for further refinements and procurement bids and we shall refer to it for those aspects which are important for the final design. They are the compression tests for the evaluation of the mechanical deformations and stresses on the poles due to the magnetic attractive force.

A cross section and a plane view are shown in Figs. 4 and 5 in a self explanatory way.

Only the holes for the RF and the central hole for the internal source are shown in the drawings, while the holes for the trim coils leads are not presented.

2.1.- Forces acting on the structure

In order to evaluate these forces we use the following formula which gives the resultant R on a magnetized element A[4]:

$$\vec{R} = \mu_o \iint_S \left[(\vec{H}\cdot\vec{n})\vec{H} - \frac{1}{2} H^2 \vec{n} \right] dS \ ,$$

where S is a surface enclosing A and only A. This formula gives R in Newton when H, magnetic field intensity external to A, is measured in At/m, $\mu_o = 4\pi 10^{-7}$ and n is a unit vector normal to the surface S.

Assuming for simplicity a uniform axial magnetic field the formula reduces to:

$$F = \frac{1}{2\mu_o} \Delta B^2 S \ ,$$

where B^2 is the difference between the square of the magnetic induction in Tesla measured at the inner and outer surface. Using the field values obtained from Poisson calculation[5] we have assumed in our case:

B = 5 Tesla on the inner surface of the pole;

B = 0.3 Tesla on the outer surface of the pole;

B = 2 Tesla on the inner surface of the pole cap on the flux return path;

B = 0.3 Tesla on the outer surface of the pole cap.

With these values it turns out that the attractive force between the poles is:

$$F = \frac{1}{2_o} (5^2 - 0.3^2)(0.9^2) = 2.522 \times 10^7 N = 2570 \text{ tons},$$

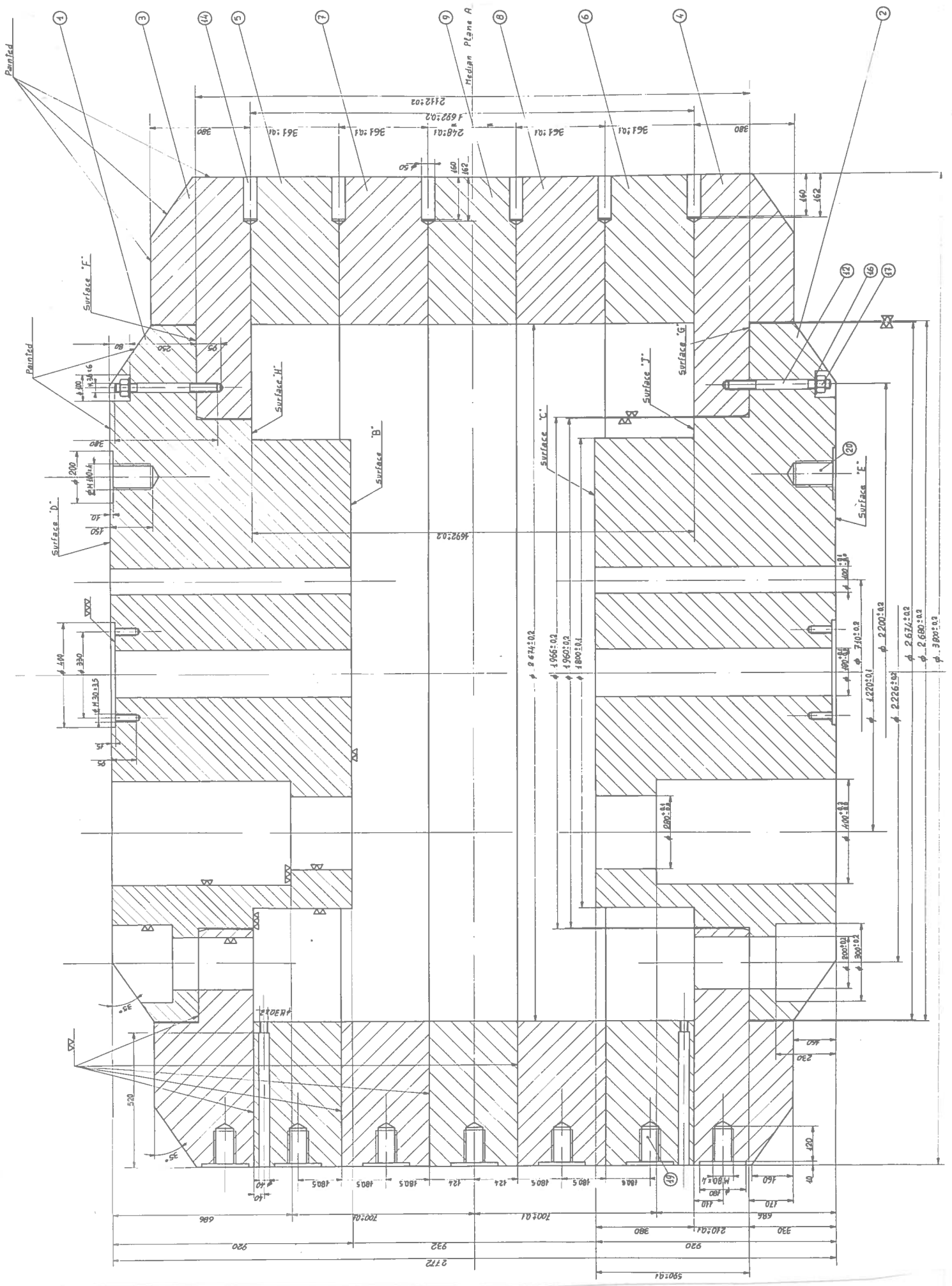

FIG. 4 - Cross section of the preliminary design of the magnet yoke.

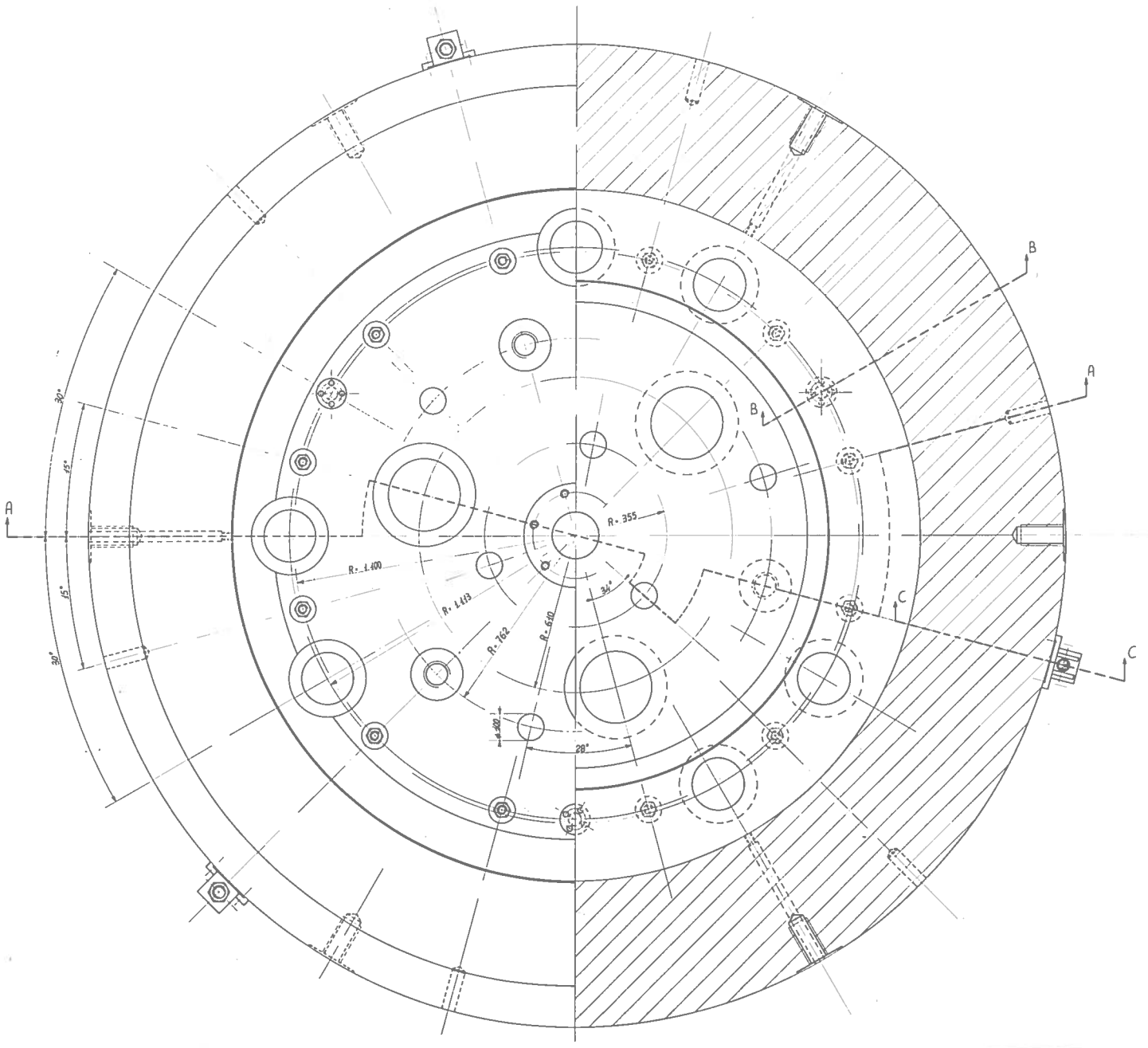

FIG. 5 - Plane view of the preliminary design of the magnet yoke.

while the packing force on the ring is:

$$F = \frac{1}{2_o}(2^2-0.3^2)(1.903^2-1.34^2) = 8.92\times10^6 N = 910 \text{ tons.}$$

The knowledge of the maximum stress and the consequent deformation experienced by the poles is important for two reasons:

- First of all the maximum stress must be well below the elastic limit of the iron.
- Second, the median plane gap variation must be kept within 0.3-0.4 mm for a reliable operation of the cyclotron.

This in order to maintain within a few gauss the first harmonic component of the field arising from a possible asymmetry in the pole deforma-

tion. Moreover, this variation must be taken into account for all those parts of the magnet yoke which have a mechanical interaction with other components of the cyclotron, like the vacuum chamber of the cryostat. For these reasons a detailed study of the deformations of the pole caps under compression and of the relevant stresses was carried out.

Because of the complexity of the yoke structure, which exhibits a number of holes (whose purposes will be described in detail later), an analytical calculation of the structure is exceedingly complex and probably not reliable enough. We have thus built a 1:10 scale model of the yoke structure and tested its behaviour under compression.

2.2.- Choice of the model for the compression tests

Two 1:10 scale model of half the structure of the magnet yoke were in fact built: the first one, labelled model n.1, according to the drawings of Figs. 4 and 5, the other, model n.2, with a slightly different configuration of the pole cap. The two models are shown in Figs. 6 and 7 respectively.

The pole cap and the upper ring of each model were machined in commercial ARMCO iron, while the remaining rings in Aq 52 steel. The attractive force between the poles is simulated by applying a variable load uniformly distributed over a surface equal to the polar one (Ø=180 mm). The magnetic stacking force between the rings has been simulated by means of 24 high stress steel tie bolts pretensioned to about 30 tons total load.

Stresses were measured by strain gauges PHILIPS PR 9832 K/d Fe positioned at some critical points while the displacements of the polar cap were detected by an electromechanical transducer PHILIPS PR 9310/03 positioned in correspondance of the central hole of the pole. Moreover when testing model n.2, two mechanical comparators were located on the edge of the pole cap and on the upper ring.

A sketch of the experimental set up is shown in Fig. 8, while model n. 2 and the experimental facility are shown in Figs. 9 and 10 respectively.

Each model was compressed with a variable load between 2 and 42 tons with and without tie bolts on the rings. Tests were carried out at the facility of the "Istituto di Macchine" of the Milan Polytechnique. Note that because of the 1:10 scale factor, loading on the model is a factor 100 lower than on the real yoke, deflections are a factor 10 lower, while stresses have the same values.

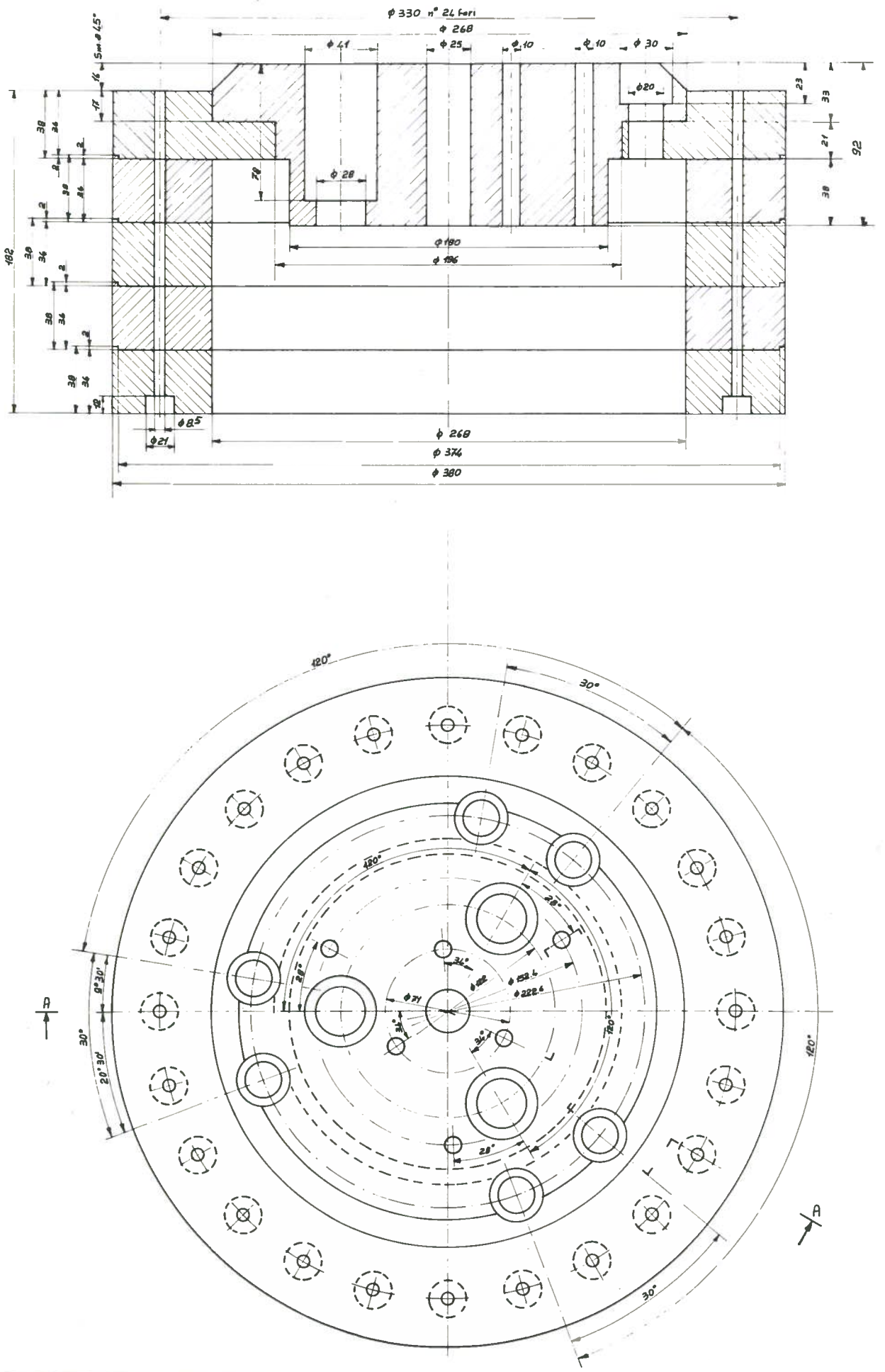

FIG. 6 - Drawing of model n. 1 for compression tests.

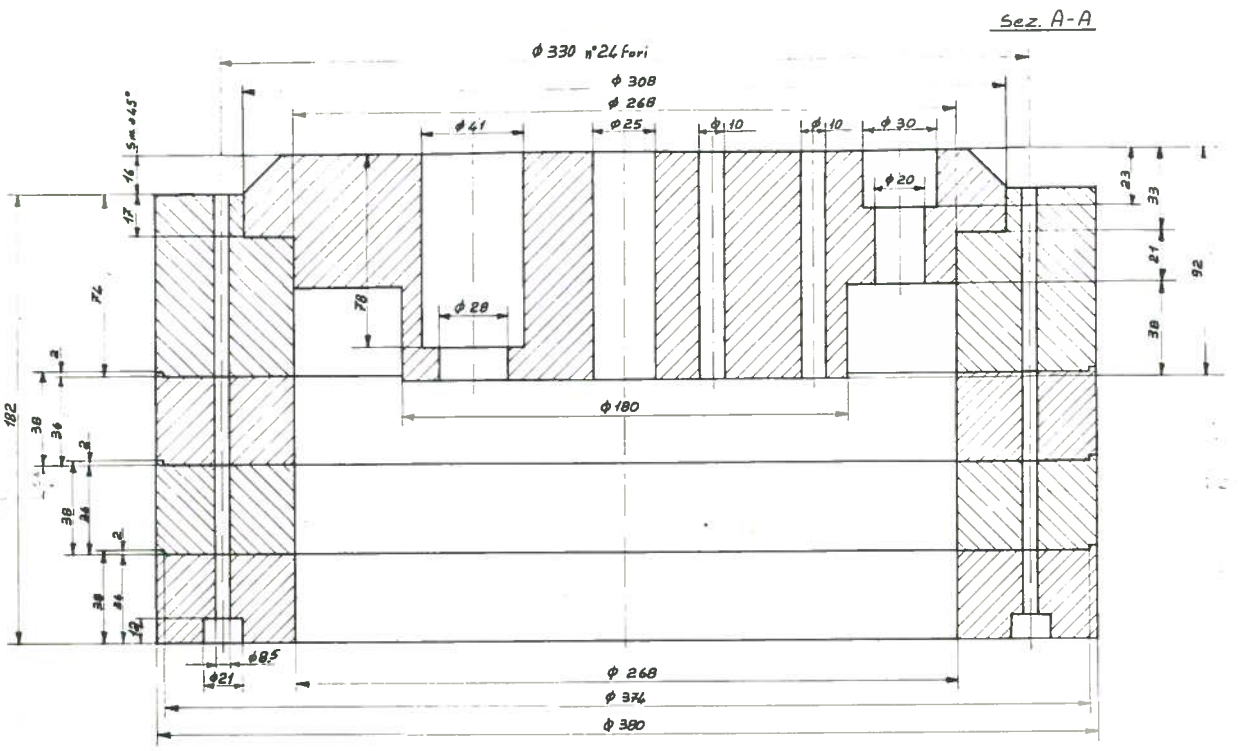

FIG. 7 - Drawing of model n. 2 for compression tests.

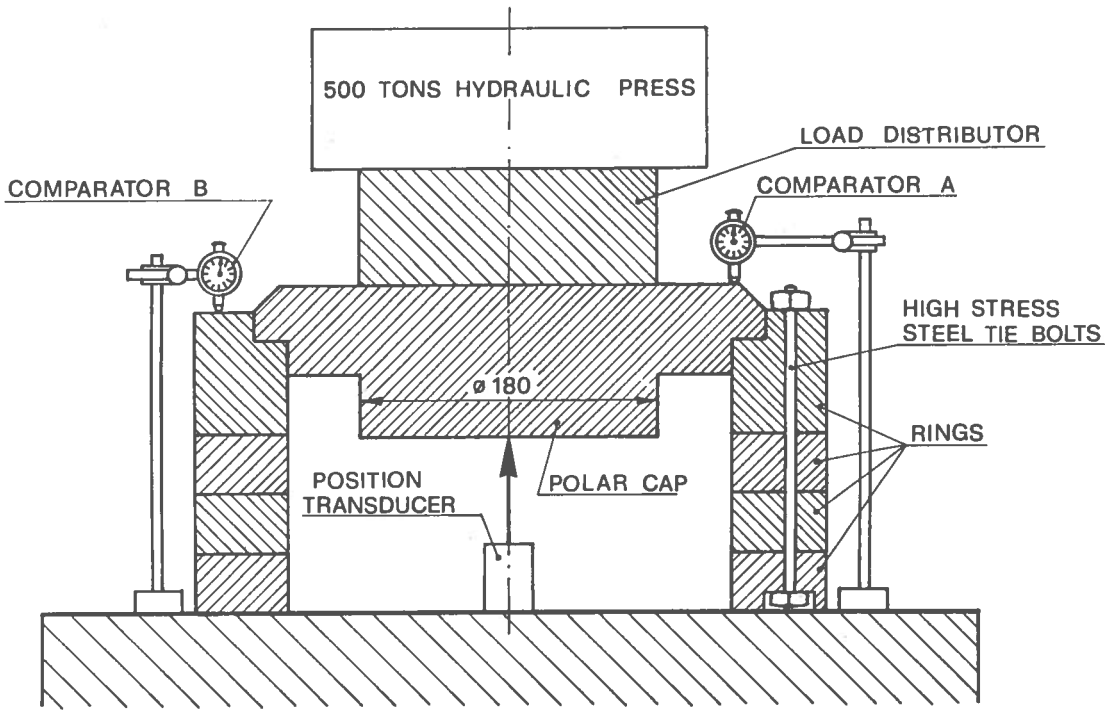

FIG. 8 - Sketch of the experimental set-up for compression tests.

The results are shown in Tables II, III, IV and V.

The test conditions nearest to the operating ones are those with pretensioned tie bolts and a load on the pole of 22 tons. The results thus obtained are respectively 0.06 mm deflection and 3.6 kg/mm stress for model n.1 and 0.046 mm deflection and 4.5 kg/mm stress for model n.2. From these results it turns out that model n.2 is better with respect to the center deflection, while the maximum stress is a 20% higher. Neverheless this value is still acceptable, being well under the elastic limit of the iron used for the yoke, which we anticipate to be about 12 kg/mm^2.

The center deflection value measured on model n.2 appears rather large compared to the goal of limiting the total pole gap variation within 0.4 mm. However we point out that this center deflection value should be regarded not as an absolute pole deflection but as an upper limit. This because the load distribution on the model combined with imperfections in the machining process results in a packing of the rings which tends to increase the true deflection value.

A more realistic evaluation of the center deflection can be obtained by subtracting from the values registered by the position transducer the values measured by comparator A. Center displacement values calculated in such a way referred to model n.2 with pretensioned tie bolts are shown on Fig. 11. The straight line represents a least squares fit to the values ob

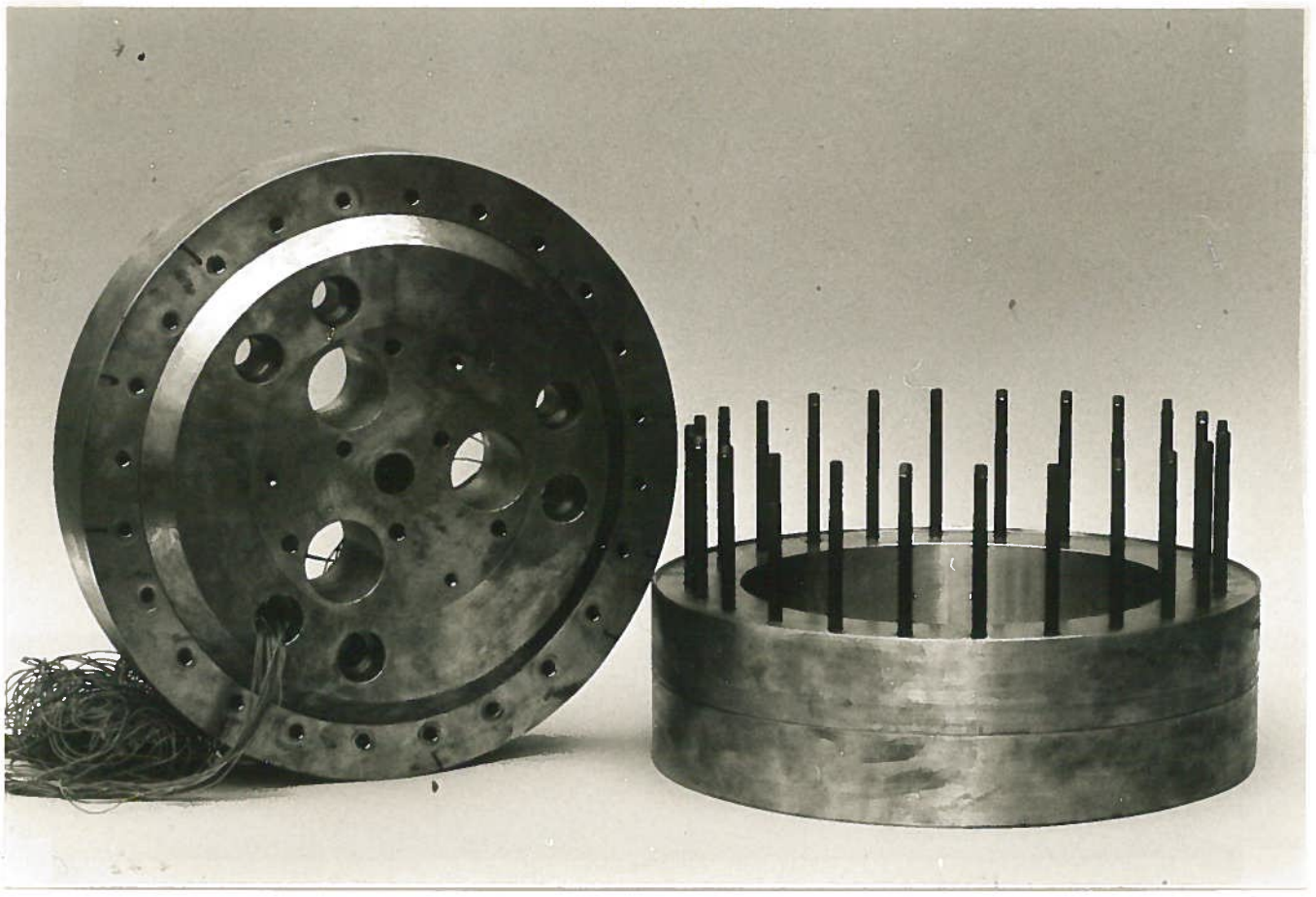

FIG. 9 - View of the model n.2 of magnet yoke for compression tests.

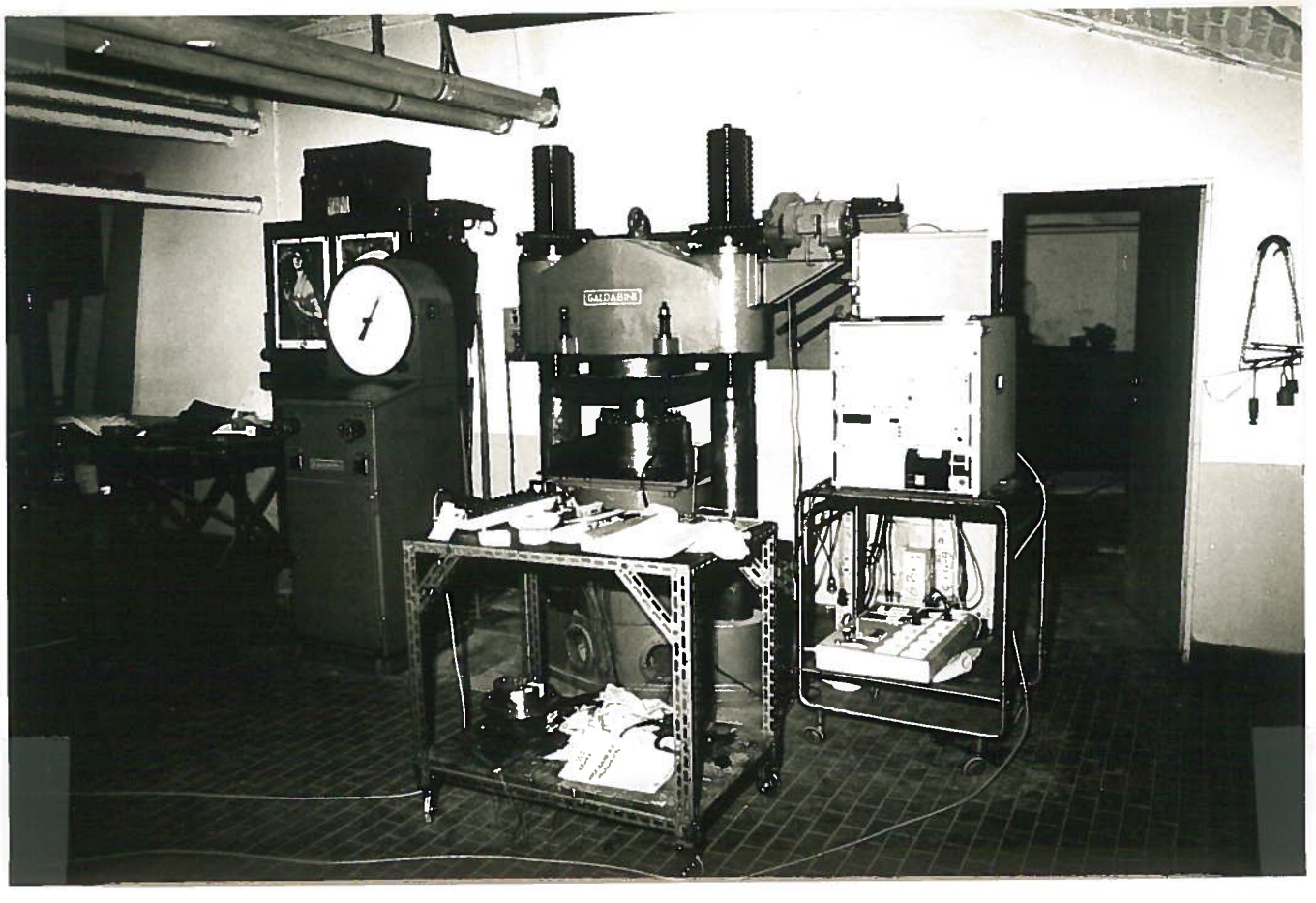

FIG. 10 - View of the experimental facility for compression tests.

TABLE II - Compression tests on model n.1 without tie bolts pretensioned.

Load (tons)	Center deflection (mm)	Maximum stress (Kg/mm^2)
0	0	
12	0.129	2.5
22	0.185	3.6
32	0.226	4.6
42	0.255	5.4

TABLE III - Compression tests on model n.1 with tie bolts pretensioned.

Load (tons)	Center deflection (mm)	Maximum stress (Kg/mm^2)
0	0	
12	0.034	2.5
22	0.060	3.6
32	0.085	4.5
42	0.107	5.4

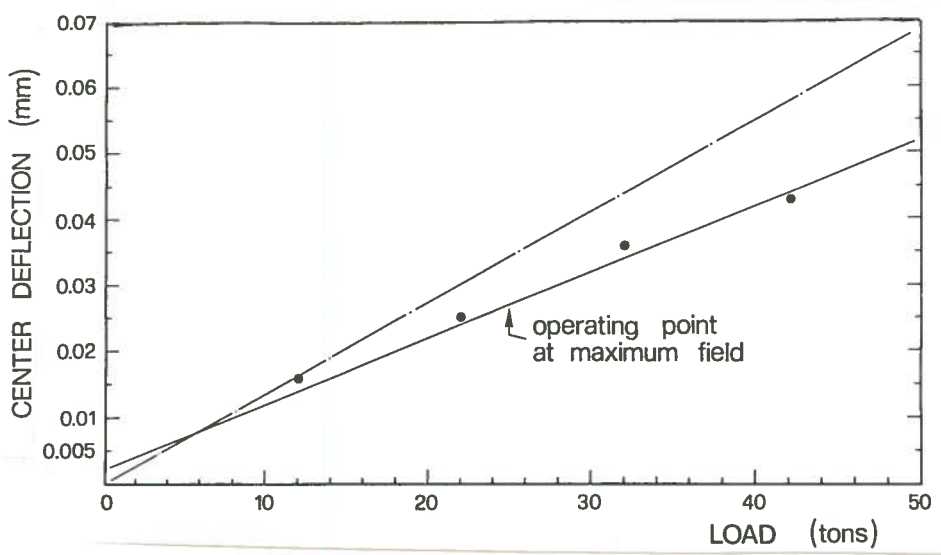

FIG. 11 - Center displacement of model n.2 with tie bolts pretensioned: straight line - estimated from measurements of Table V; dotted line - analitically calculated (see text for details).

TABLE IV Compression tests on model n. 2 without tie bolts pretensioned

Load (tons)	Center deflection (mm)	Comparators (mm)		Maximum stress (Kg/mm^2)
		A	B	
2	0	0	0	
12	0.050	0.029	0.015	2.5
22	0.080	0.045	0.016	4.5
32	0.104	0.059	0.018	6.4
42	0.123	0.068	0.021	8.3

TABLE V Compression tests on model n. 2 with tie bolts pretensioned

Load (tons)	Center deflection (mm)	Comparators (mm)		Maximum stress (Kg/mm^2)
		A	B	
0	0	0	0	
12	0.027	0.011	0.003	2.5
22	0.0465	0.020	0.006	4.5
32	0.0655	0.029	0.009	6.4
42	0.0795	0.036	0.010	8.1

tained. Center deflection at a load of 22 tons is 0.025 mm.

Although an analytical calculation applied to such a structure is somewhat unreliable, an analysis of the experimental data can be tried. This is done in the following and applied to model n.2. The upper pole cap is considered as a flat circular plate with the outer edge simply supported. Neglecting the effects due to the holes and assuming a uniform thickness equal to the average thickness of the plate, we have in the case of uniform load on the polar surface[6]:

$$W = \frac{P}{16\pi D}\left[\frac{3+v}{1+v}a^2 + c^2 \ln\frac{c}{a} - \frac{7+3v}{4(1+v)}c^2\right]$$

where the following notation applies:

D = $Et^3/12(1-v^3)$;

W = central displacement;

a = radius of the plate;

c = polar radius;

P = total load on the pole in Kg;

E = steel Young's modulus (21000 Kg/mm);

t = thickness of the plate;

v = Poisson's ratio assumed as 0.3 for steel.

Results for our case derived from this formula do not differ by more than 30% from the data and are plotted for comparison in Fig. 11. Because of the better performance of model n.2 its structure was adopted for the final design of the magnetic yoke. Further modifications introduced in the design are:

- The diameter of the three holes for the RF coaxial resonators were changed from 410 to 500 mm.
- The pole thickness with diameter 1800 mm was reduced from 920 to 820 mm.

These modifications were introduced in model n.2 which was again compressed with forces ranging between 2 and 90 tons. Results referring to tests with pretensioned tie bolts are shown in Table VI and Fig. 12. Maximum center deflection in this case at a load of 22 tons is 0.03 mm, which is a 20% higher with respect to the previous configuration.

TABLE VI - Compression tests on model n.2 modified with tie bolts pretensioned.

Load (tons)	Center deflection (mm)	Comparators (mm) A	Comparators (mm) B	Maximum stress (Kg/mm^2)
2	0	0	0	
12	0.020	0.006	0.005	1.8
22	0.042	0.012	0.008	3.5
32	0.064	0.018	0.010	5.4
42	0.087	0.025	0.012	7.4
52	0.107	0.031	0.014	9.6
62	0.115	0.037	0.016	13.7
72	0.138	0.042	0.016	19.2
82	0.165	0.049	0.021	26.2
92	0.205	0.053	0.027	32.6

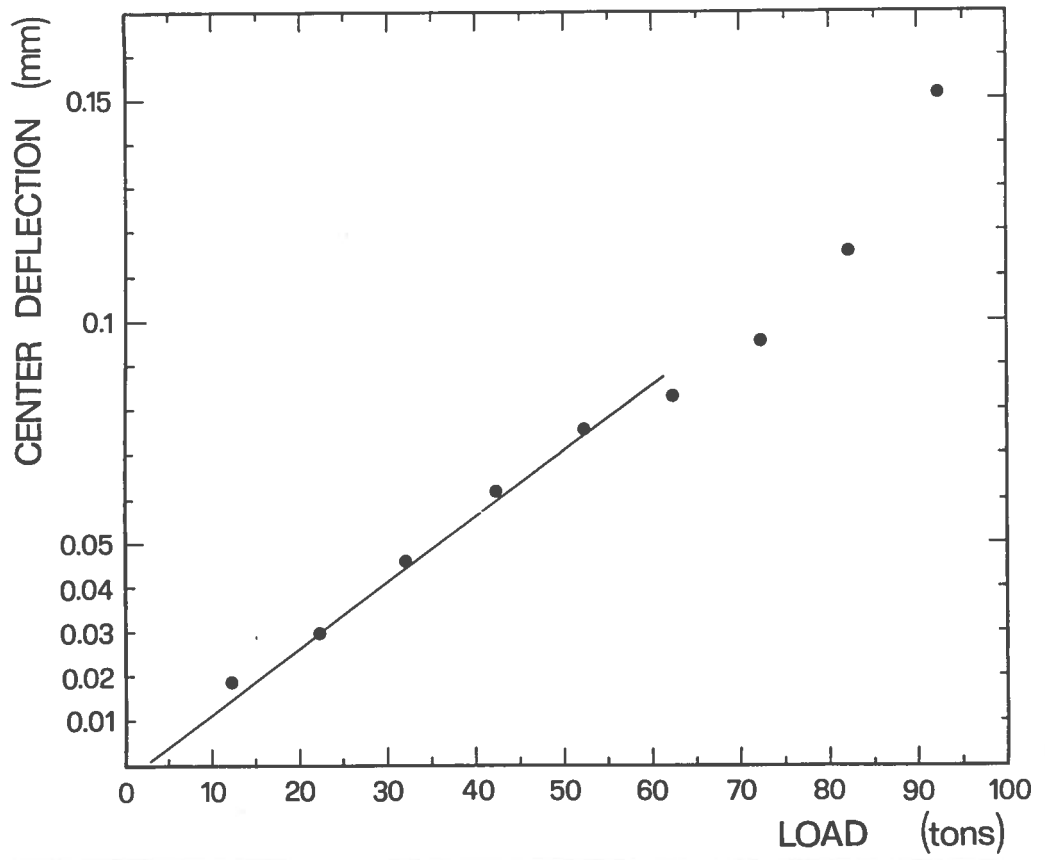

FIG. 12 - Center displacement of model n.2 modified with tie bolts pretensioned.

3.- MAGNET YOKE STRUCTURE

The magnet yoke structure has been finalized according to the above results. All the requirements stemming out of other cyclotron components, which interact closely with the magnet, were obviously taken into account.

The magnet yoke (iron casting and machining) was built by the firm HOESCH of Dortmund (W.Germany) according to our design and under our supervision. Iron casting was completed by July 1981, while machining and assembling took until March 1983. The engineering drawings of the magnet yoke are shown in Figs. 13-17 and in the following we shall refer to them.

3.1.- Main dimensions and yoke subdivision

The pole diameter is 1800 mm as determined by maximum energy requirements with an anticipated maximum magnetic field of about 5 Tesla.

For accomodating the cryostat a window 1780 mm high, and of 440 mm radial width is provided between the pole and the inner yoke wall.

The yole structure is cylindrical. Compared to an open structure yoke this choice reduces the total amount of iron, is somewhat simpler to machine and keeps to a reasonable level the fringing field. Besides, an open structure would not offer significant advantages from the point of view of the access to the machine median plane.

The flux return path has a cross section equal to 2.25 times the polar surface. Considering the radial width of 440 mm of the window for accomodating the cryostat the resulting yoke radial width is 563 mm. Thus the yoke diameter is 3806 mm. Referring to Fig. 13 the magnetic yoke is split in seven elements, namely: upper and lower pole caps, upper and lower rings, central ring, upper and lower pole plates. The number of yoke elements is substantially less than in the preliminary design of Fig. 4, a choice supported by a cost estimate from the supplier. Besides, it allows better overall mechanical tolerances, when assembled, as compared to the previous design.

The pole cap thickness is 542 mm and, as previously discussed, ensures sufficient rigidity to compression. Slightly variation are present in this design with respect to the tested one. In this configuration the pole cap is in contact with the whole surface of the relevant ring. The attractive magnetic force between them is of the order of 910 tons, as calculated in 2.1. This stacking force makes the pole cap not simply supported, but par

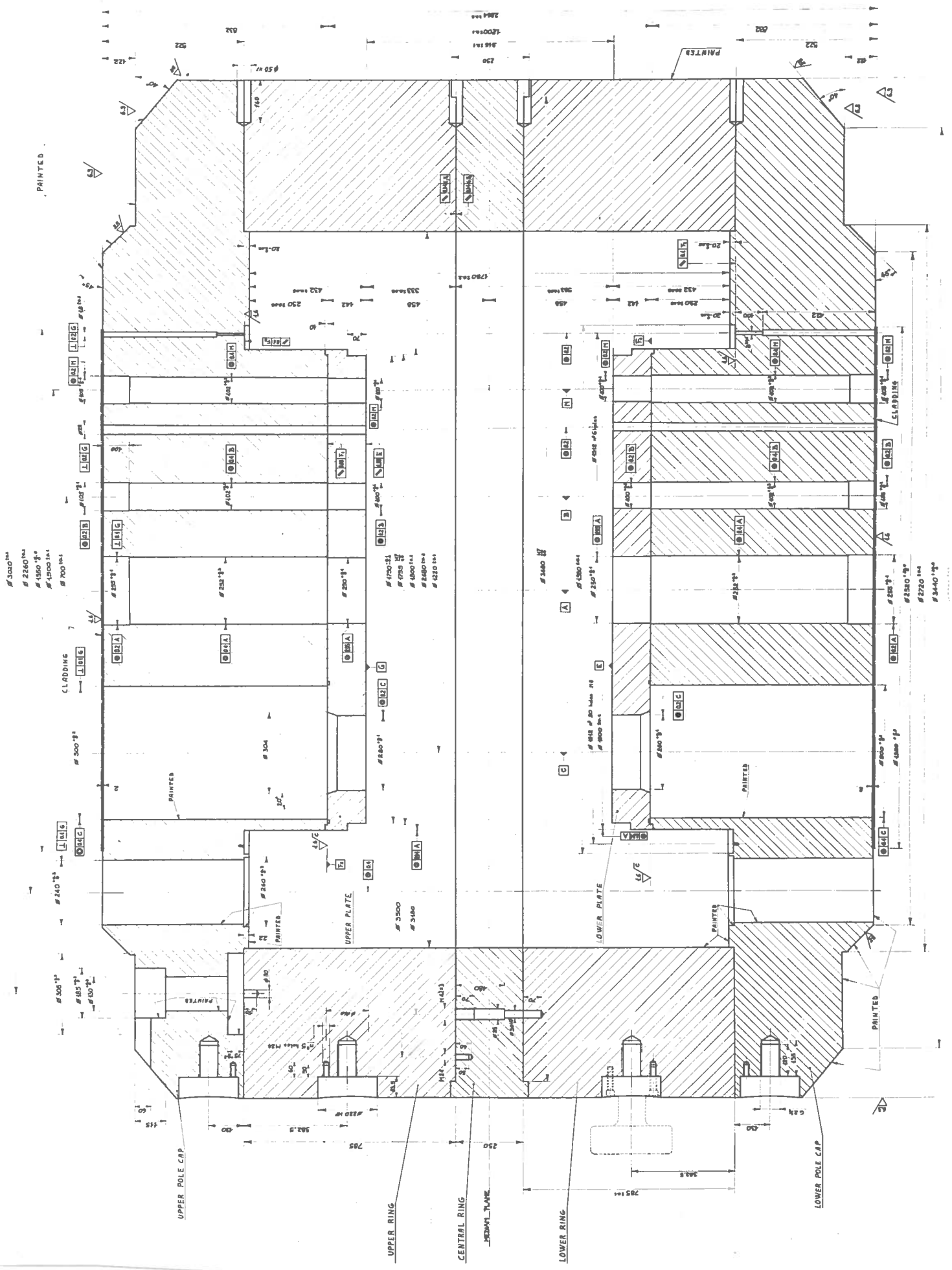

FIG. 13 - Cross section view of the magnet yoke.

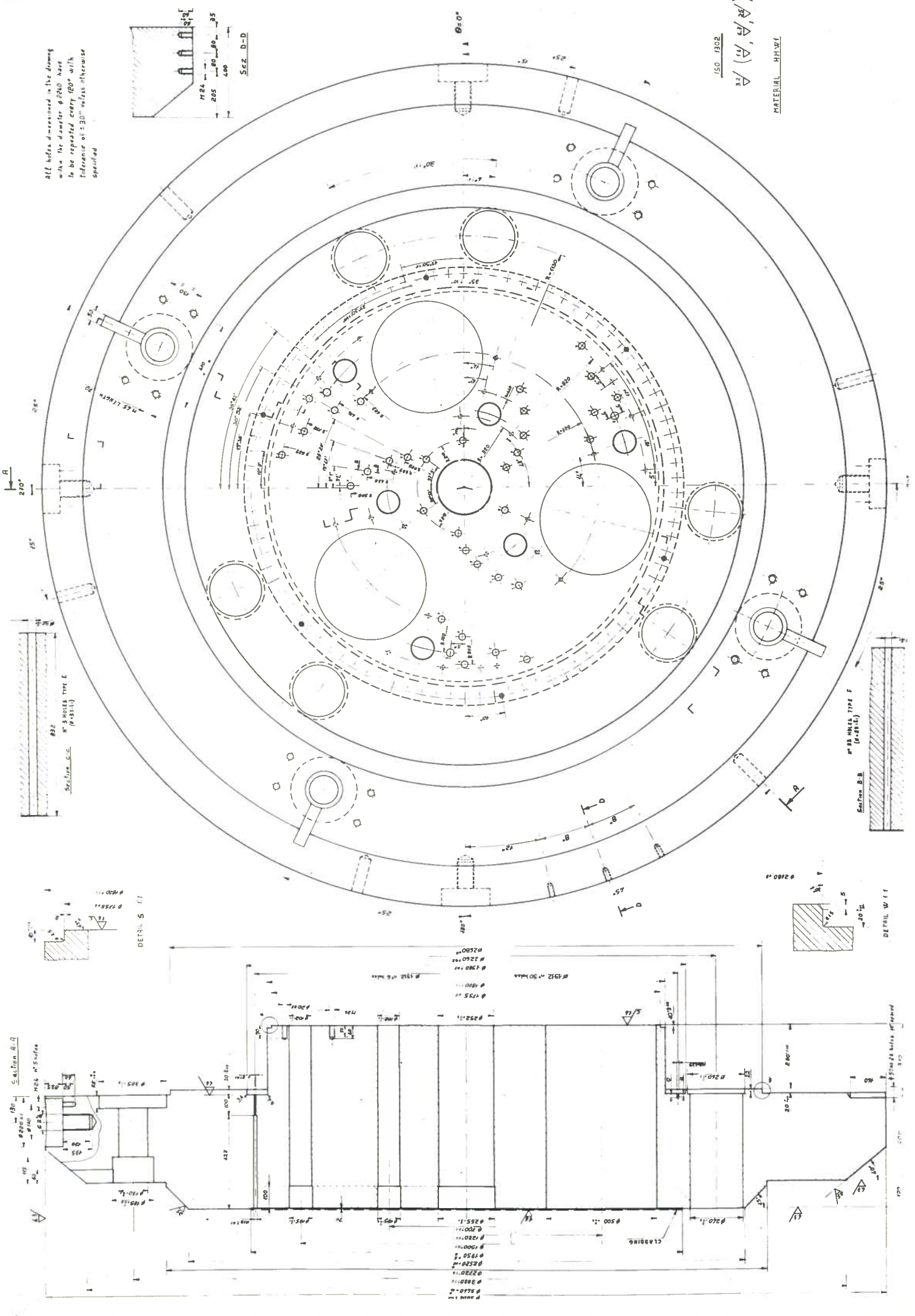

FIG. 14 - Cross section and plane view of the upper pole cap of the magnet.

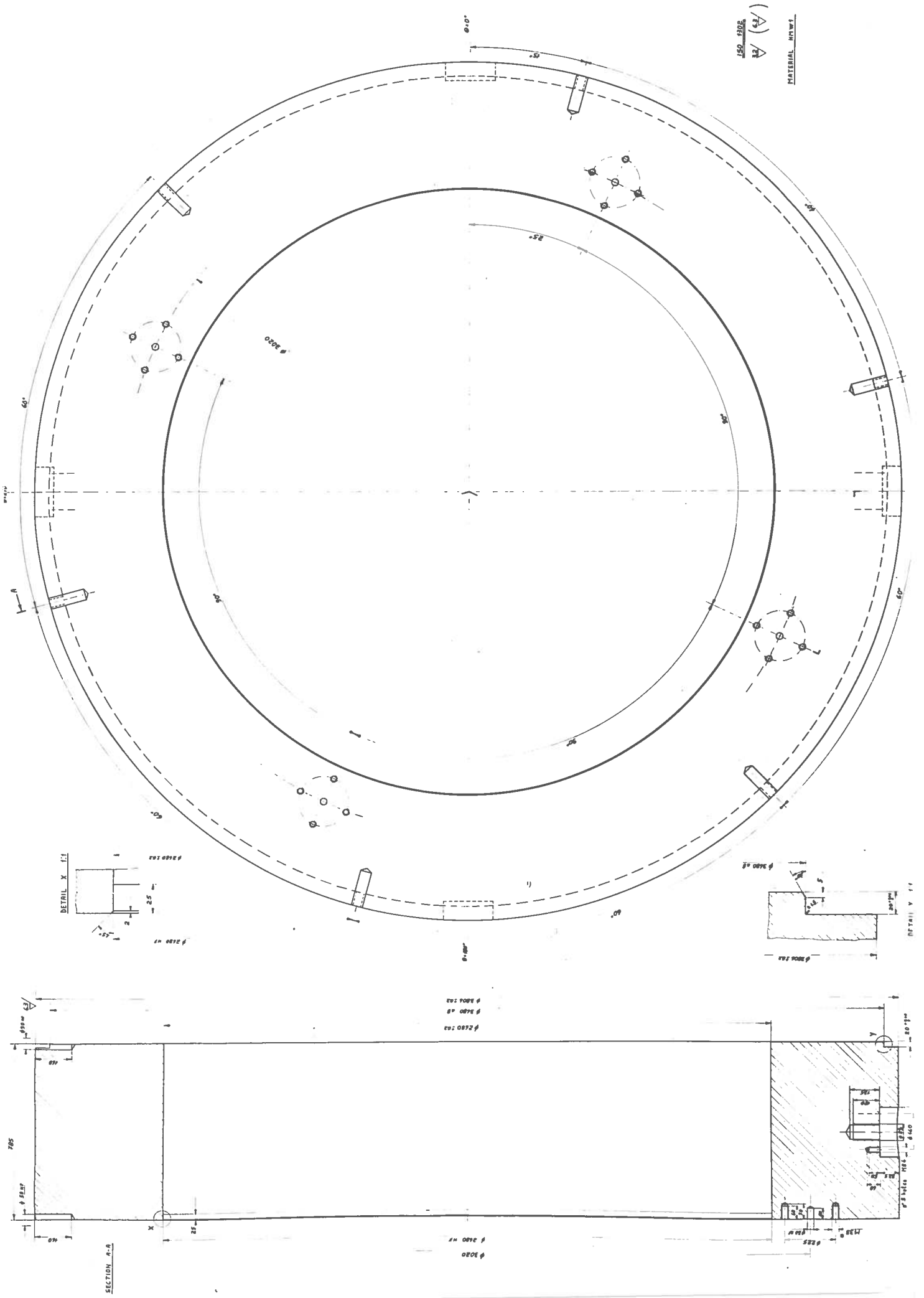

FIG. 15 - Cross section and plane view of the upper ring of the magnet.

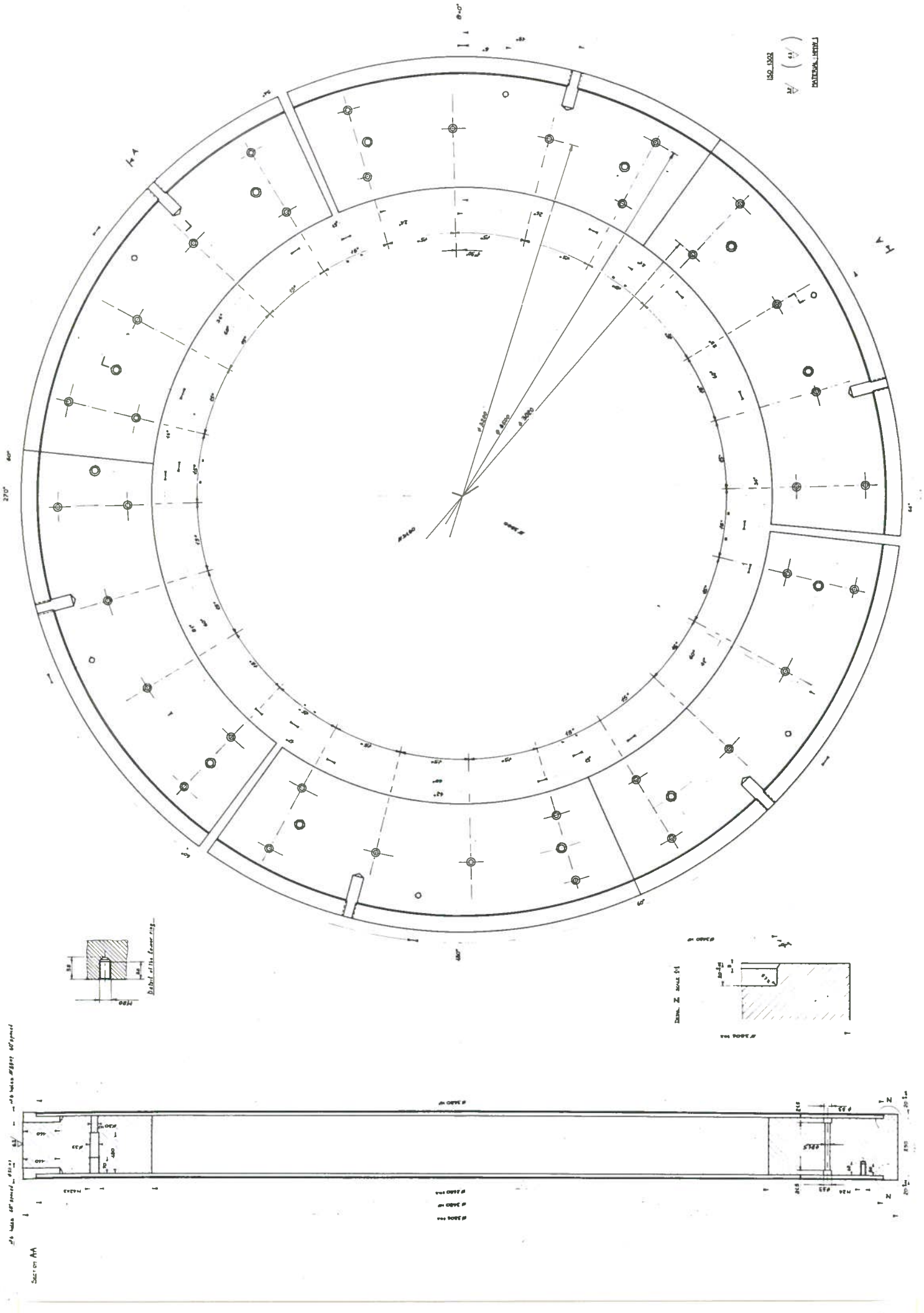

FIG. 16 - Cross section and plane view of the central ring of the magnet yoke.

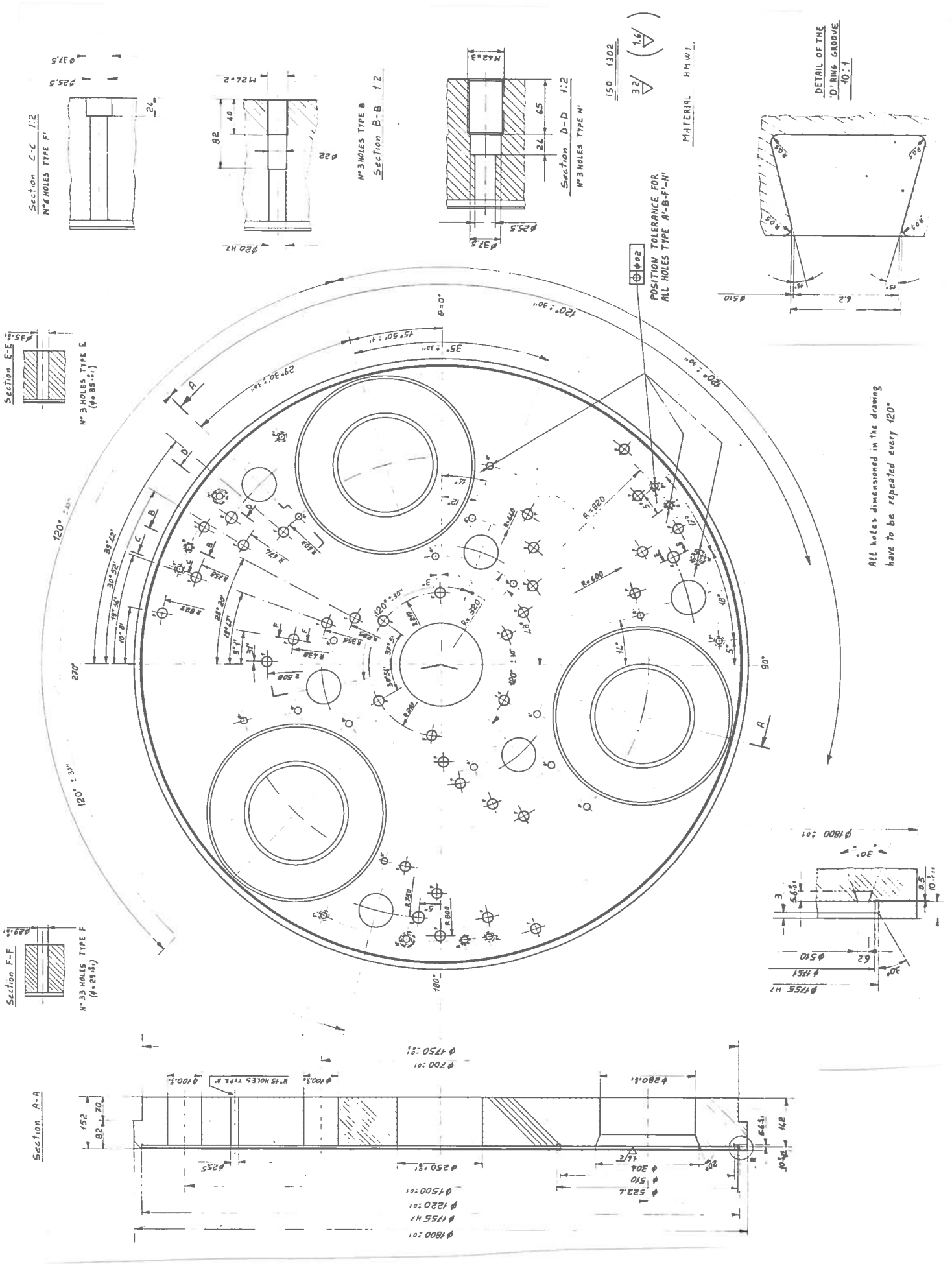

FIG. 17 - Cross section and plane view of the upper plate of the magnet yoke.

tially constrained, resulting in a lower center inflection . We expect the pole gap variation at the maximum excitation not to exceed 0.4-0.5 mm.

The central ring thickness of 250 mm is the minimum value compatible with the space necessary for the penetrations through the median plane needed for extraction and injection.

The central ring is cut in six symmetric pieces, so that the reduced weight of any single element simplifies any future machining.

The height of the upper and lower rings (785 mm) is of course a consequence of the previous choices. The resultant total height of the yoke is 2864 mm.

The upper and lower plates (142 mm thickness, 1800 mm diameter) are needed in order to assemble the pole tips in a way independent from the magnet yoke.

In Table VII we have summarized the weights of the yoke elements, the heaviest ones being the pole caps. Their weight is of 55 tons if one takes into account all the items which will be attached to them. Consequently the crane should allow a load of at least 60 tons.

TABLE VII Weights of the magnet's yoke elements

ELEMENT	MATERIAL	WEIGHT
Upper pole cap	Low carbon steel, casted	39.890 tons.
Lower pole cap	"	40.246 tons.
Upper ring	"	35.020 tons.
Lower ring	"	35.020 tons.
Central ring	"	11.416 tons.
Upper plate	"	2.533 tons.
Lower plate	"	2.533 tons.
Total weight of the yoke		166.702 tons.

3.2.- The axial holes in the pole caps

With the exception of the four holes at diameter 3020 mm on the upper pole cap, needed for the lifting system, all the holes on the pole caps are symmetric with respect to the median plane. Moreover they exhibit a 120 symmetry in order to avoid first and second harmonic components in the magnetic field, since the pole tips geometry has a threefold symmetry. In Table VIII we list all the axial holes through the pole caps, their position in the cyclotron frame of reference, and the required tolerances. The most stringent tolerances are required near the median plane, thus for the pole plates, and the values quoted in Table VIII are referred to them.

A detailed view of these holes through the yoke is shown in Fig. 14.

3.3.- Mechanical assembling and tolerances

Pole caps and rings are simply stacked together. Their own weight ensures a sufficient mechanical stability to the structure.

Referring to Fig. 13 each element of the yoke is coupled and guided with respect to the adiacent one for a length of 20 mm. This is done respectively at a diameter of 2680 mm for the coupling of the pole caps and the rings, and at a diameter of 3680 mm for the coupling of the central ring with the upper and lower ring. The coupling tolerance is of the type H7, e8. For the dimensions involved this means $2680e8^{-0.290}_{-0.510}$, $2680H7^{+0.145}_{+0}$, $3680e8^{-0.29}_{-0.62}$, $3680H7^{+0.21}_{+0}$. This coupling is made only in order to facilitate the assembling of the yoke elements and to prevent rough lateral displacement. The correct positioning of the yoke both radially and azimuthaly is accomplished by 6 cylindrical dowels for each element. They are placed radially and spaced azimuthally by 60°. The coupling tolerance of each dowel with the relative hole is of the order of 0.01 mm. At worst this should ensure the relative positioning of each element of the yoke within $0.01/\sin 60° = 0.015$ mm. Moreover, since the central ring is cut in six pieces, as mentioned above, it is fixed to the lower ring by means of 6 M 20 screws for each element and the correct positioning is given by 2 vertical dowels.

The upper and lower pole plates are bolted to the pole caps by means of 24 M 24 screws. They are also guided in the pole cap for 10 mm at a

TABLE VIII Description of the axial holes through the pole cap

N. of holes / Diameter	Function	Position in the Cyclotron frame of reference	Main tolerances (mm)	
			Position	Coaxiality
1; ϕ=250	Central hole for positioning of the plug, internal source and axial injection	R=0 θ =0°		0.05
3; ϕ=500 in the pole cap ϕ=280 in the plate	Dee stems	R= 610 θ { =104° 10' =224° 10' =344° 10'	0.1	0.2
3; ϕ=100	Coupling capacitors	R=350 θ { = 19° 10' =139° 10' =259° 10'	0.1	0.2
3; ϕ=100	Trimming capacitors	R=750 θ { = 74° 40' =194° 40' =314° 40'	0.1	0.2
30; ϕ=29	Trim coils leads	R=210 θ { =119° 04' =239° 04' =359° 04'	0.1	0.2
		R=210 θ { = 77° 05' =197° 05' =317° 05'		
		R=285 θ { = 58° 20' =178° 20' =298° 20'		
		R=355 θ { = 49° 47' =169° 47' =289° 47'		
		R=438 θ { = 39° 01' =159° 01' =279° 01'		
		R=508 θ { = 30° 31' =150° 31' =270° 31'		
		R=603 θ { = 69° 42' =189° 42' =309° 42'		

N. of holes / Diameter	Function	Position in the Cyclotron frame of reference	Main tolerances (mm)	
			Position	Coaxiality
		R=674 θ { = 60°52' =180°52' =300°52'		
		R=758 θ { = 49°36' =169°36' =289°36'		
		R=829 θ { = 40°08' =160°08' =280°08'		
3; ϕ=29	Cooling of the liner	R=800 θ { = 60° =180° =300°	0.1	0.2
3; ϕ=25	Rough pumping under the liner	R=750 θ { = 74°40' =194°40' =314°40'	0.1	0.2
6; ϕ=240	Main coils current leads; main coils vertical supports; LHe and LN_2 filling; etc.	R=1130 θ { = 6° =126° =246°	0.2	0.4
		R=1130 θ { = 96° =216° =326°		
4; ϕ=185 only in the upper pole cap	Lifting system	R=1510 θ { = 25° =115° =205° =295°	0.2	

diameter of 1755 mm, with a coupling tolerance $1755e8^{-0.240}_{-0.415}$, $1755H7^{+0.115}_{+0}$. The positioning is ensured by 3 vertical dowels.

Wearing out of the holes for the dowels between plates and pole caps could occur during the assembly because of the high softness of the low carbon iron. To prevent this, dowels are not fixed directly to the magnet iron, but by means of high stress steel ferrules.

The goal of the prescribed tolerances is mainly to obtain a mirror image symmetry around the median plane and a 120° symmetry. Prescribed tolerances refer mostly to the assembled yoke and not to the single elements and for this reason a special machining procedure has been devised. Furthermore we note that the required tolerances generally represent the best that can be granted with normal tools and at a reasonable cost for pieces of these dimensions.

In the following we list the main mechanical tolerances required:

- Pole plates parallelism : 0.08 mm;
- Pole caps parallelism : 0.08 mm;
- Pole gap : 0.1 mm;
- Holes positioning : 0.1 mm;
- Holes coaxiality : Central hole : 0.05 mm; Other holes : 0.1 mm;
- Dowels coupling tolerance : 0.01 mm.

The position of the median plane between the poles with respect to the symmetry plane of the vertical window for the cryostat may be important if the centering of the coils will be effected with reference to the vacuum chamber.

Considering all the dimensions tolerances involved the symmetry plane on the pole gap should not differ by more than 0.05 mm from the symmetry plane on the window.

3.4.- Physical and chemical properties of the iron of the yoke

The elements of the yoke have been manufactured with high purity iron with an extremely low carbon content (0.01%), cast under vacuum. This special technique developed by the firm HOESCH ensures an excellent quality, with a limited number of inclusions and a high magnetic saturation value, at a cost which is 30% lower compared to forged iron, when referred to the total cost of the machined yoke. One drawback is the relative softness of

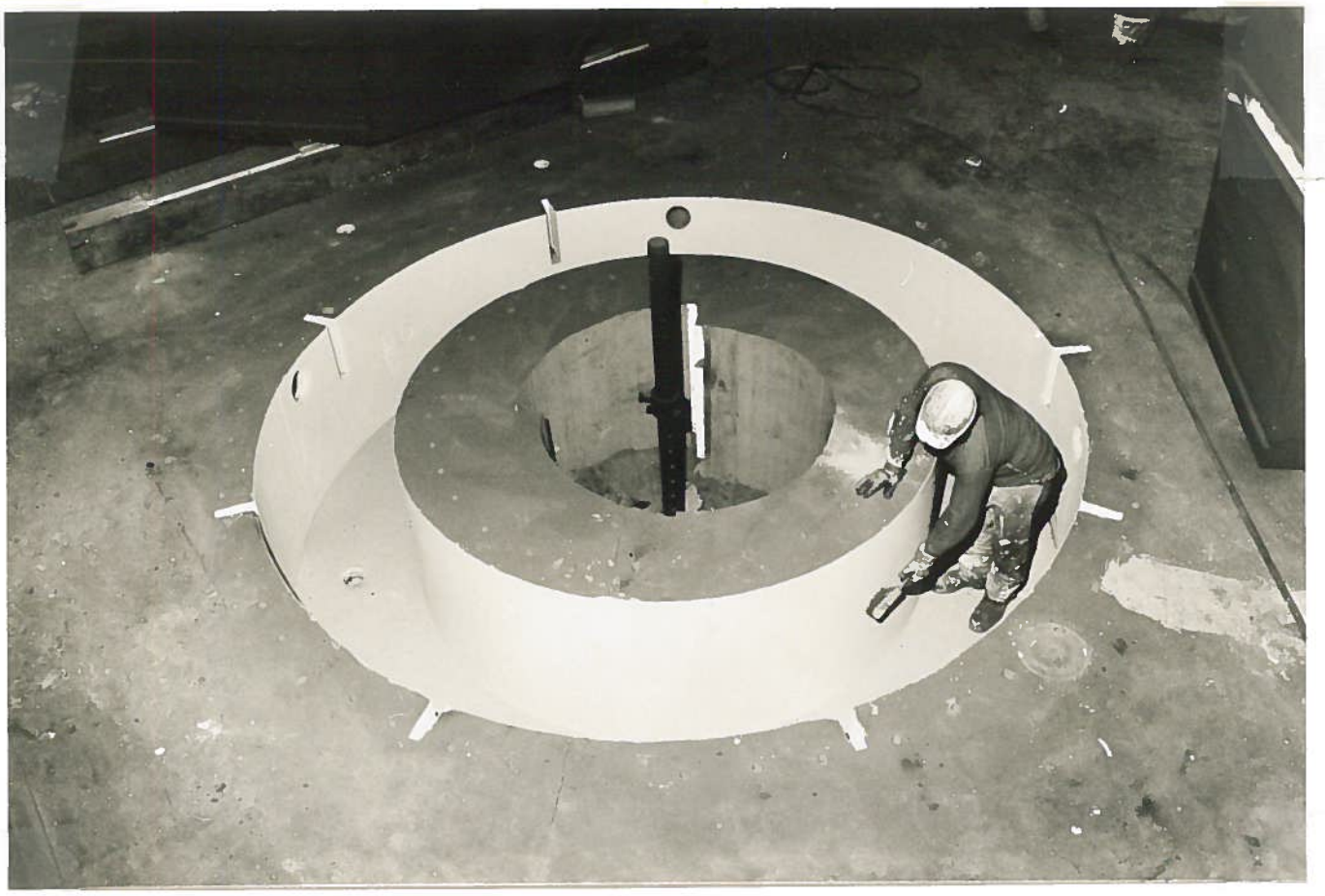

FIG. 18 - Pattern for the casting of the rings.

FIG. 19 - Styropore pattern for the casting of the pole caps.

FIG. 20 - View of the rings after casting.

FIG. 21 - View of the lower pole cap and lower ring after casting.

the material. The mechanical properties are nevertheless sufficient to give a good safety factor with respect to the mechanical stresses expected in the magnet.

3.4.1.- Casting characteristics

As just mentioned the yoke elements are cast under vacuum, by means of two styropore pattern (Figs. 18-21). The three holes of 500 mm diameter for the RF dee stems were also included in the casting mold. The extra-material allowed in the casting was of the order of 40-50 mm on all dimensions. In order to provide the maximum mirror image symmetry with respect to the chemical homogeneity and magnetic properties, symmetric elements were cast from the same heat, i.e.:

- heat 1 = upper and lower pole caps;
- heat 2 = upper, lower and central rings;
- heat 3 = upper and lower pole plates.

For each heat number the chemical, mechanical and magnetic properties were checked.

Moreover a core sample was obtained for the whole pole thickness in correspondance of the central hole in the upper and lower pole caps and shall be used for any future check which might be necessary. After casting the yoke elements were annealed following the cycle described in Fig. 22.

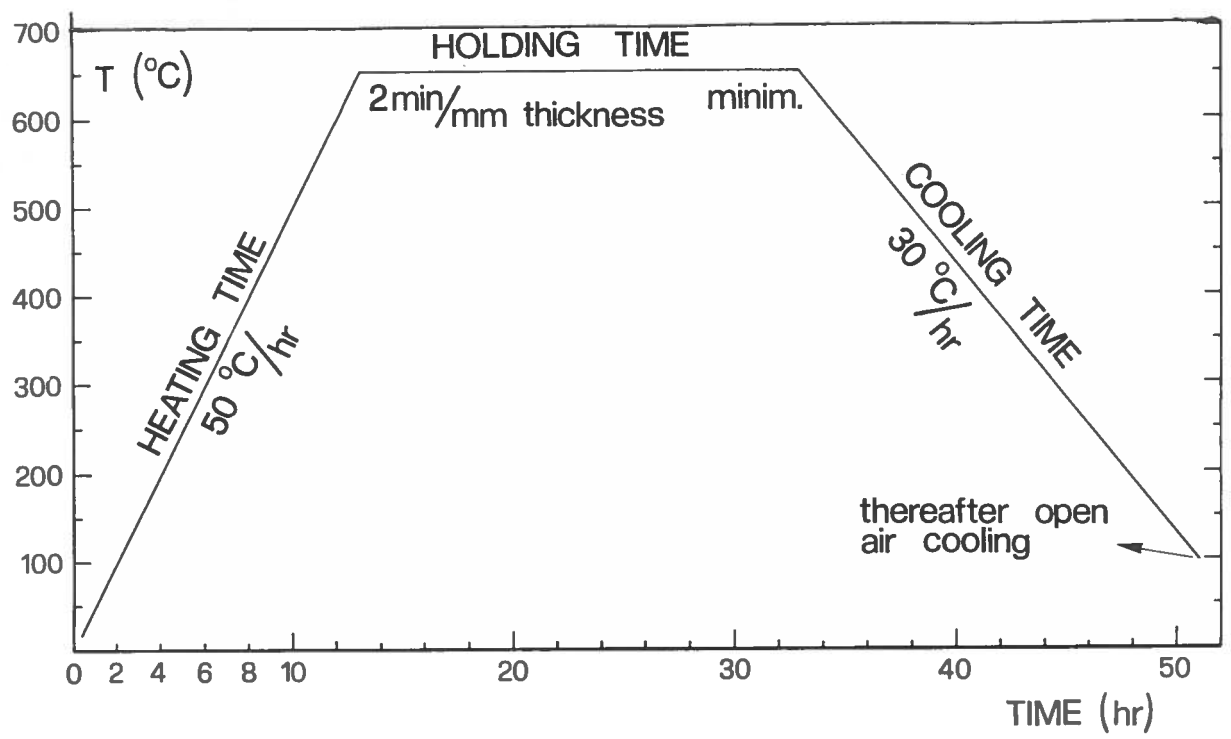

FIG. 22 - Annealing cycle for the casted elements of the yoke.

3.4.2.- Chemical characteristics of the iron

The chemical composition of the iron was certified by HOESCH for each heat. Certified values are reported on Table IX. As a comparison prescription values for the supplier are reported on the same Table as well as a control analysis carried out by us.

TABLE IX Chemical composition of the iron of the magnet yoke

Element	Max. allowed content (%)	HOESCH certified value (%)			Check analysis (%)
		Heat 1	Heat 2	Heat 3	
C	0.08	0.007	0.009	0.004	0.015
Si	0.25	0.03	0.02	0.01	0.03
Mn	0.45	0.21	0.24	0.18	0.24
P	0.015	0.008	0.011	0.015	0.009
S	0.01	0.011	0.017	0.019	0.01
Cr	0.09				0.001
Ni	0.14				0.02
Mo	0.05				0.01
Cu	0.1				0.01
O_2 (dissolved)	0.008				0.0022
N	0.01				0.0096
Al	0.03			0.033	0.048

3.4.3.- Magnetic properties of the iron

Magnetic properties of the iron are certified by HOESCH for values of H up to 30.000 At/m. Typical values of B are of the order of 2.05 T. In Table X we report the magnetization values for the 3 heats of the cyclotron yoke as measured by Hoesch, together with the coercitive field after excitation to 30.000 At/m. Measurements are carried out on a standard torus of the following dimensions:

- Outer diameter D = 114 mm;
- Inner diameter D = 75.85 mm;
- Height h = 15 mm.

TABLE X Magnetic properties of the iron of the magnet yoke.

Field intensity H (At/m)	Magnetic induction B (Tesla)			Magnetization M=B-μ_oH (Tesla)			Coercitive field H_c (A/m)		
	Heat			Heat			Heat		
	1	2	3	1	2	3	1	2	3
1000	1.53	1.53	1.57	1.53	1.53	1.57			
2000	1.63	1.63	1.64	1.63	1.63	1.64			
2500	1.66	1.65	1.67	1.66	1.65	1.67			
5000	1.74	1.74	1.75	1.74	1.74	1.74	100	90	110
10000	1.85	1.85	1.86	1.84	1.84	1.85			
15000	1.94	1.93	1.94	1.92	1.91	1.92			
20000	2.00	1.99	2.00	1.97	1.96	1.97			
25000	2.06	2.05	2.06	2.03	2.02	2.03			
30000	2.10	2.09	2.10	2.06	2.05	2.06			

Accuracy of the measurements: H: ± 10 At/m ; B: ± 0.02 T

An independent check, for one sample, carried out by the Istituto Elettrotecnico Nazionale "G. Ferraris", Turin, has confirmed the certified values. However since the most important parameter is really the saturation value of the iron, measurements of the saturation curve were carried out on a cylindrical sample (Ø 12 mm, length 210 mm) up to saturation. These measurements used the permeameters of the "G. Ferraris", Turin, and "E. Marelli", Milan, with an overall accuracy of ± 0.5%. The same measurements were also carried out on a sample machined from commercial ARMCO iron, with substantially the same results.

The measured values are listed on Table XI. A typical magnetization curve for the iron of the yoke is shown in Fig. 23. From the curve we can deduce that the saturation value of M for the magnet yoke is of 2.135 Tesla at an excitation value H = 130000 At/m, with an accuracy of 0.5%.

TABLE XI Magnetization values of the iron of the magnet yoke

Field intensity H (At/m)	Magnetic induction B (Tesla)	Magnetization $M = B - \mu_o H$ (Tesla)
1800	1.6	1.60
4300	1.7	1.70
8500	1.8	1.79
14000	1.9	1.88
21000	2.00	1.97
34000	2.10	2.06
65000	2.20	2.12
130000	2.30	2.135
210000	2.40	2.136
290000	2.50	2.135
Accuracy of the measurements: ±0.5%		

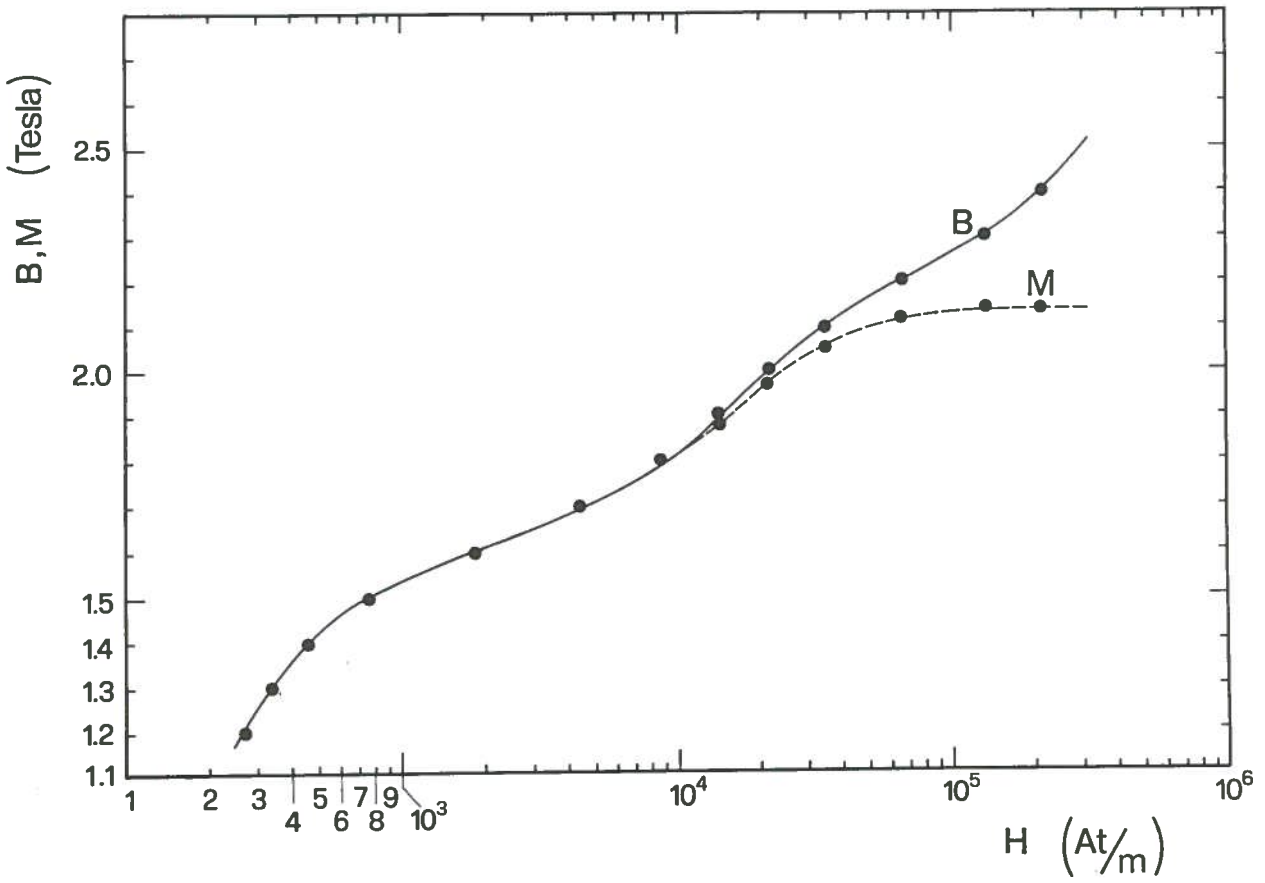

FIG. 23 - Experimental magnetization curve of the iron of the yoke.

3.4.4.- Mechanical properties

Yield point, tensile strength and elongation have been measured and certified by HOESCH for each heat of the yoke.

The results are listed in Table XII.

TABLE XII Mechanical properties of the iron of the magnet yoke

	Heat 1	Heat 2	Heat 3
Yield point (N/mm^2)	122	126	145
Tensile strength (N/mm^2)	270	280	289
Elongation (%)	48	50	50

3.4.5.- Ultrasonic testing

The yoke elements have been ultrasonic tested in order to guarantee the absence of inclusions as for the German Norm DIN 1683. This means that a maximum defect-volume/total volume of 0.1% is guaranted with a maximum single defect of 0.5 cm^3.

3.5.- Cladding of a stainless steel layer on the outer surface of the pole caps

A good rustfree surface is necessary on the upper and lower pole caps, where the vacuum tight feedthroughs for the trim coils will be mounted, center plug, etc. For this reason a 4 mm thick layer of stainless steel has been welded, using the submerged arc technique, on the outer surfaces of the pole caps within a diameter of 1950 mm. After machining the cladding is reduced to 2 mm final thickness.

The chemical composition in % of the layer is the following:

C = 0.02 Cr = 24 Ni = 12 Nb = 0.9.

After welding it modifies in:

C = 0.04 Cr = 19.4 Ni = 10.3 Nb = 0.6.

Tests carried out on one sample have shown a totally vacuum tight and rust resistant surface. A macrophotography of three sections of the sample has shown the absence of cracks, inclusions or other unacceptable defects in the welding process.

3.6.- Machining procedure and assembling

We briefly describe the machining schedule for the magnet. The procedure is designed in order to fulfill the tolerance requirements some of which are indeed difficult to achieve.

1. Pole caps and rings have been rough turned with a 10 mm material allowance. Also the holes with a diameter 100 mm have been rough drilled. Fig. 24 shows rough machined rings.
2. The 4 mm thickness stainless steel layer has been welded by the submerged arc technique on the outer surface of the upper and lower pole caps within a diameter of 1950 mm. Figs. 25 and 26 show the welding phase.
3. Rough machined plates: Fig. 27. Finishing of the mating surfaces of the plates with the pole caps. Drilling of the whole set of holes through the plates by numerically controlled machine: Fig. 28.
4. Cutting of the central ring: Fig. 29. Drilling of the holes for fixing to the lower ring. Finishing of the mating surfaces with the lower ring.
5. Finishing of the mating surfaces of the lower ring, mating surface of the lower pole cap with lower ring.
6. Finishing of the mating surface of the upper ring with the upper pole cap, mating surface of the upper pole cap with the upper ring.
7. The upper pole cap and upper ring are stacked together and dowels holes are machined; the same applies to the lower pole cap, lower ring and central ring.
8. The two free surfaces of the upper pole cap and upper ring are machined with the elements assembled in order to achieve a parallelism of 0.4 mm. The same applies to the lower pole cap, lower ring and central ring stacked together.

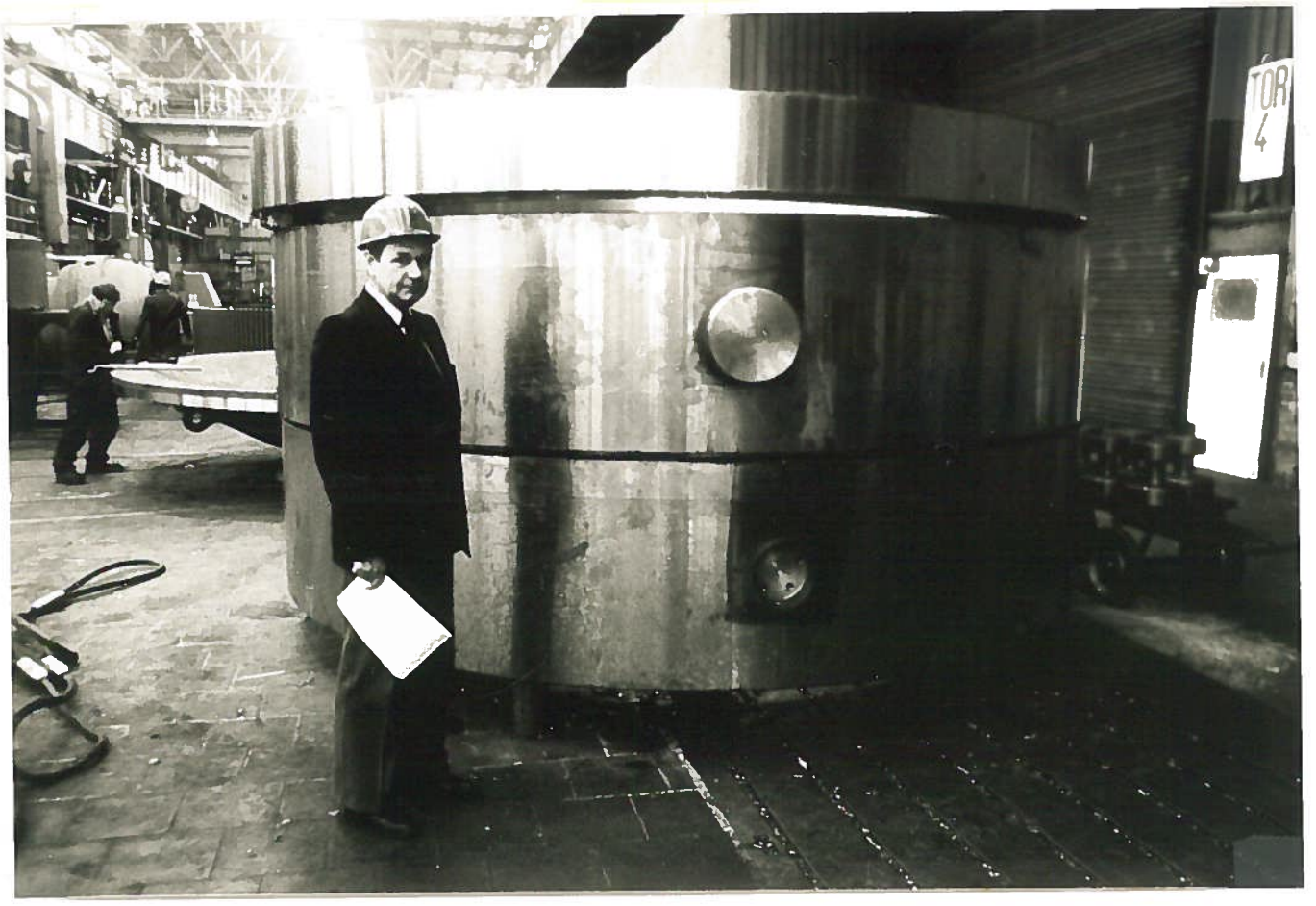

FIG. 24 - View of the rough machined rings.

FIG. 25 - Welding of the stainless steel layer on the pole cap.

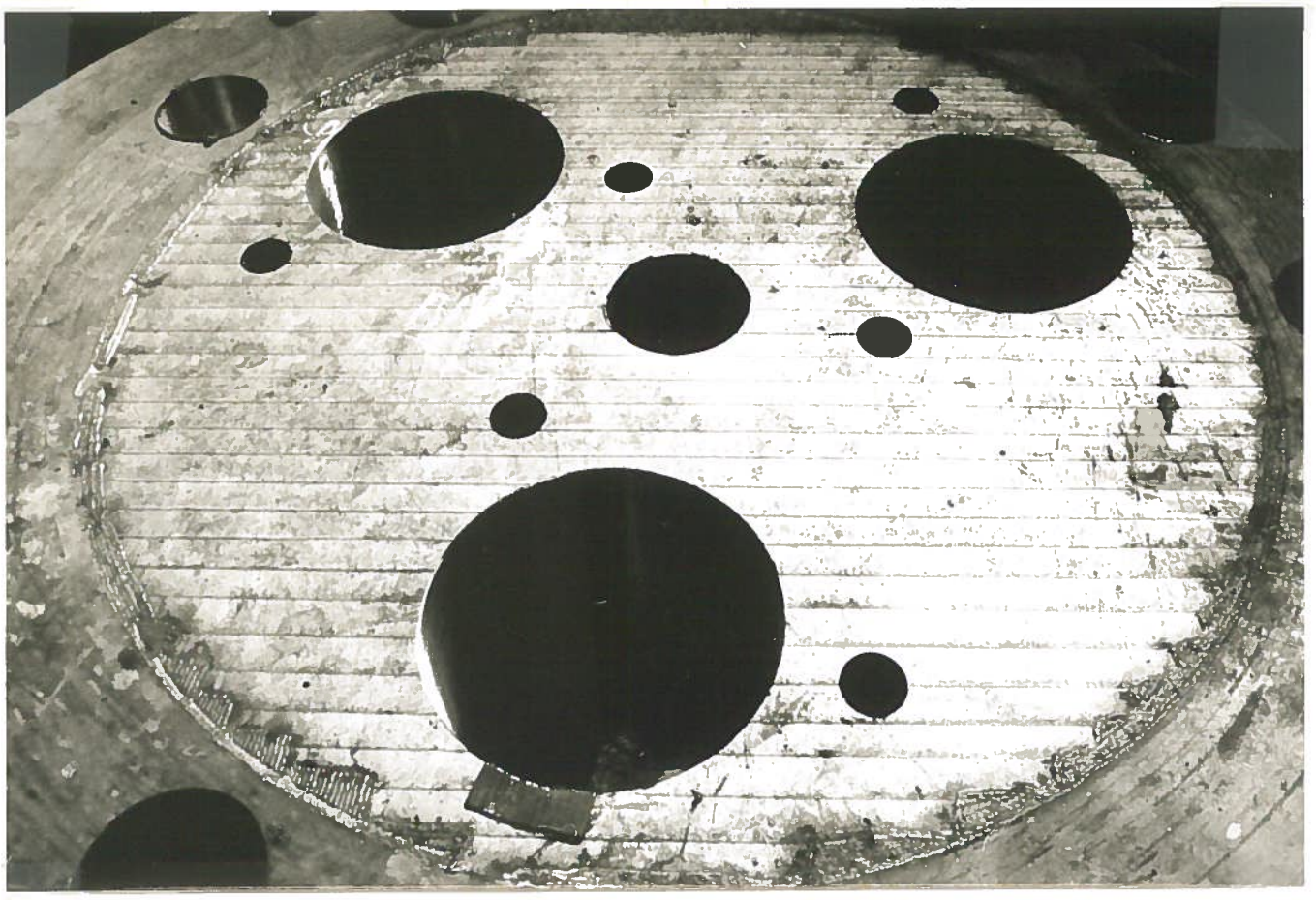

FIG. 26 - Close view of the pole cap after deposition of the stainless steel layer.

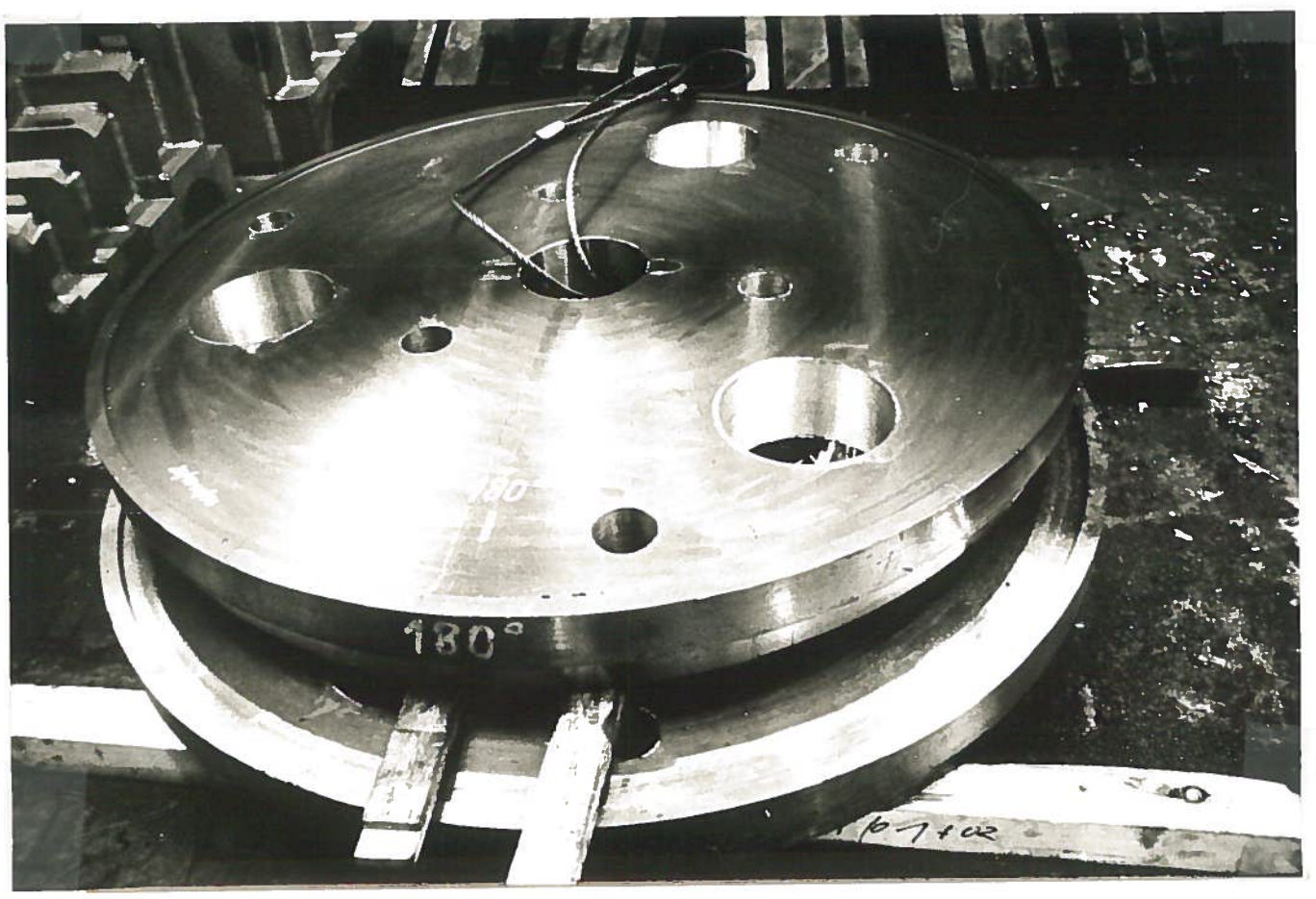

FIG. 27 - View of the rough machined plates.

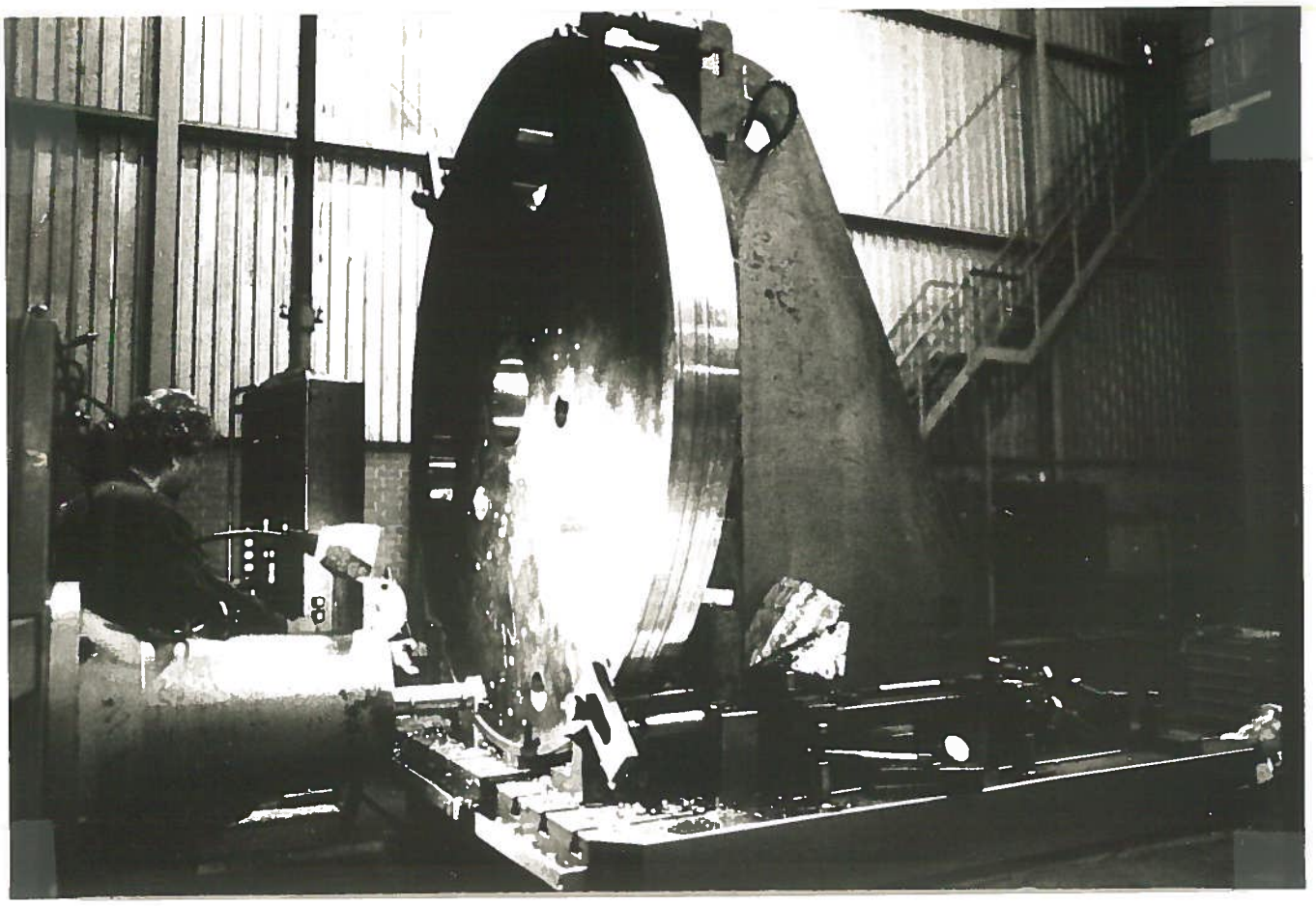

FIG. 28 - Finishing of the holes on the plate by numerical controlled machine.

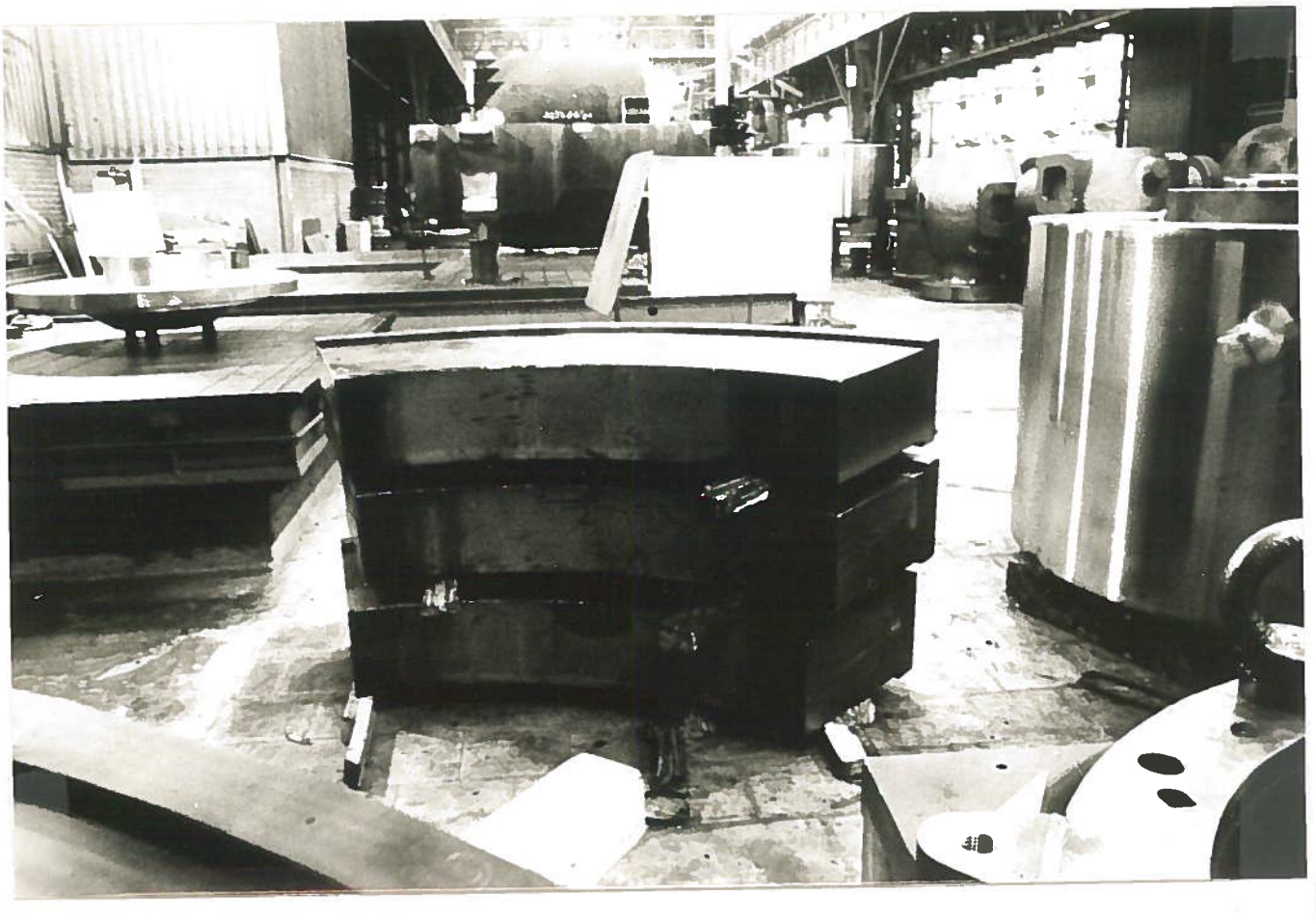

FIG. 29 - View of the central ring after cutting.

9. The plates are mounted and fixed to the relative pole caps without removing the pieces from the machine, and dowels holes are drilled.
10. The external surface of the plate is finished.
11. Pole cap and plate are turned together at the diameter of 1800 mm. This ensures the coaxiality of the two pieces, avoiding positioning errors.
12. Finishing of the inner and outer diameter of the yoke: Fig. 30.

FIG. 30 - View of the lower and central rings after final machining.

13. The whole set of holes in the pole caps is finished. Trimming coils leads holes have been copied from the plate with special tools: Figs. 31-36.
14. All the yoke elements are stacked together: Figs. 37 and 38. After checking the correct coaxiality, dowels holes between the central and upper rings are machined.

3.7.- Azimuthal graduation on the outside of the magnet yoke

In order to provide a suitable frame of reference on the outside of the magnet yoke an azimuthal graduation has been machined on the outer surface

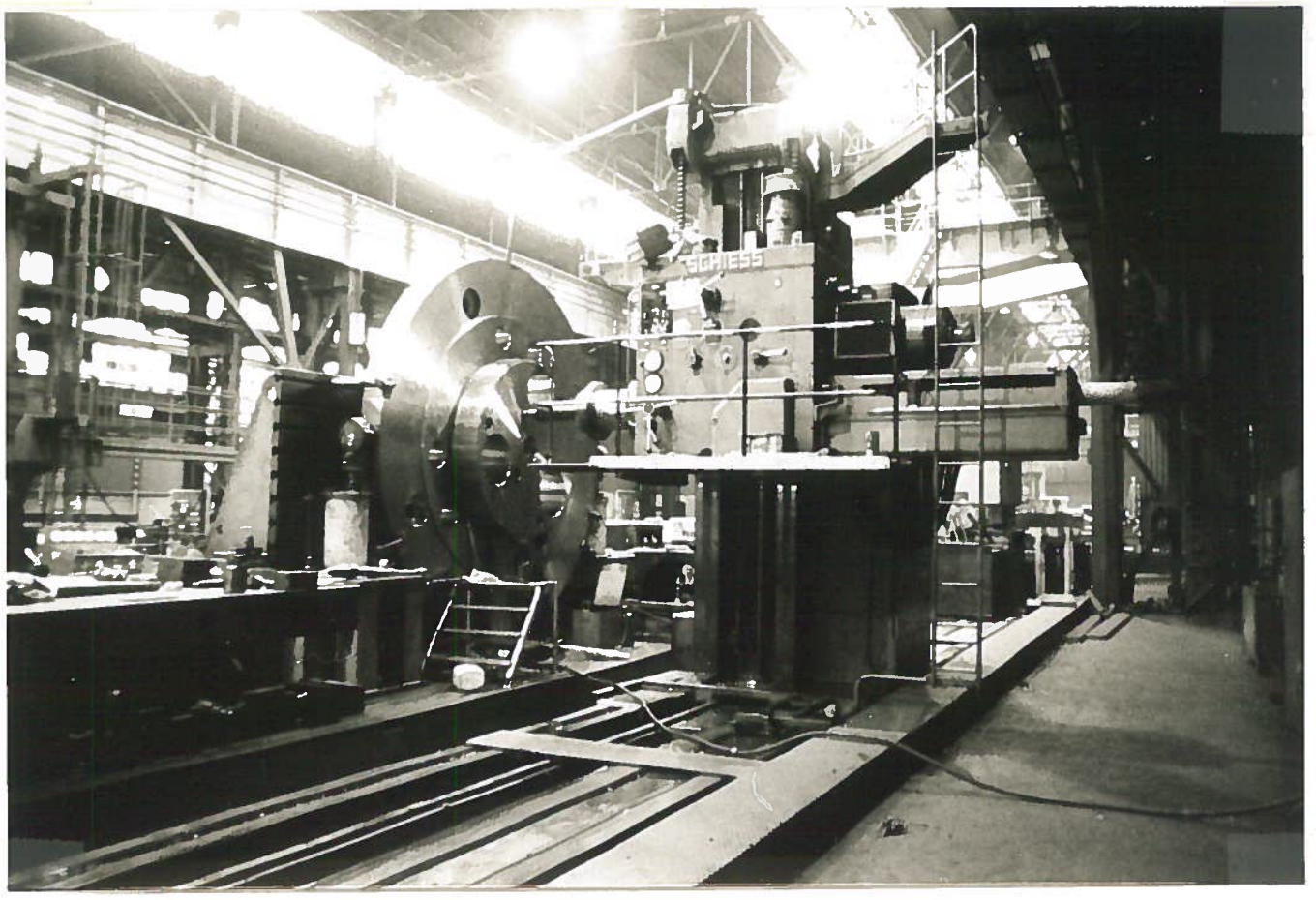

FIG. 31 - Finishing of the holes on the pole cap.

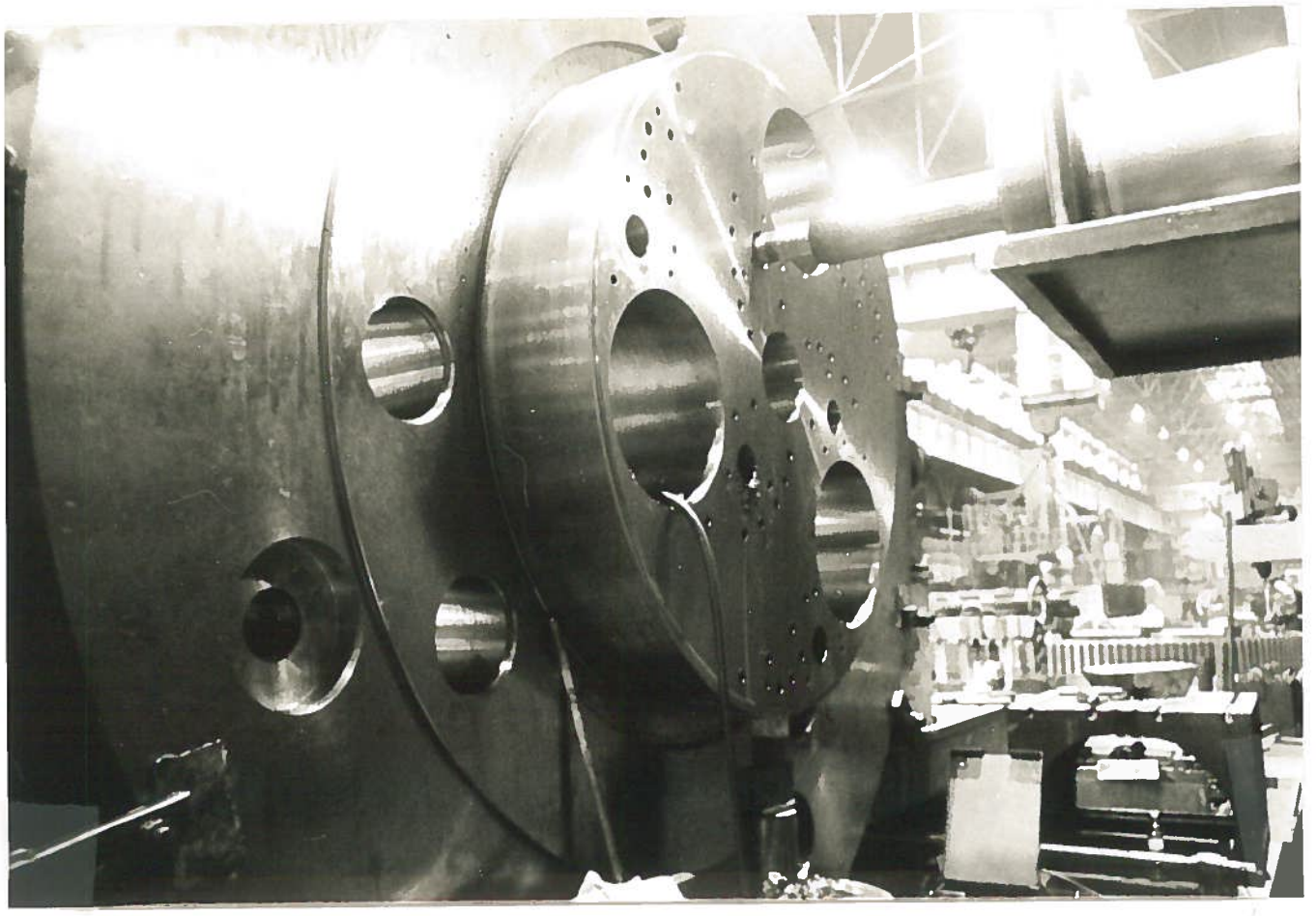

FIG. 32 - Close view of the finishing of the holes on the pole cap.

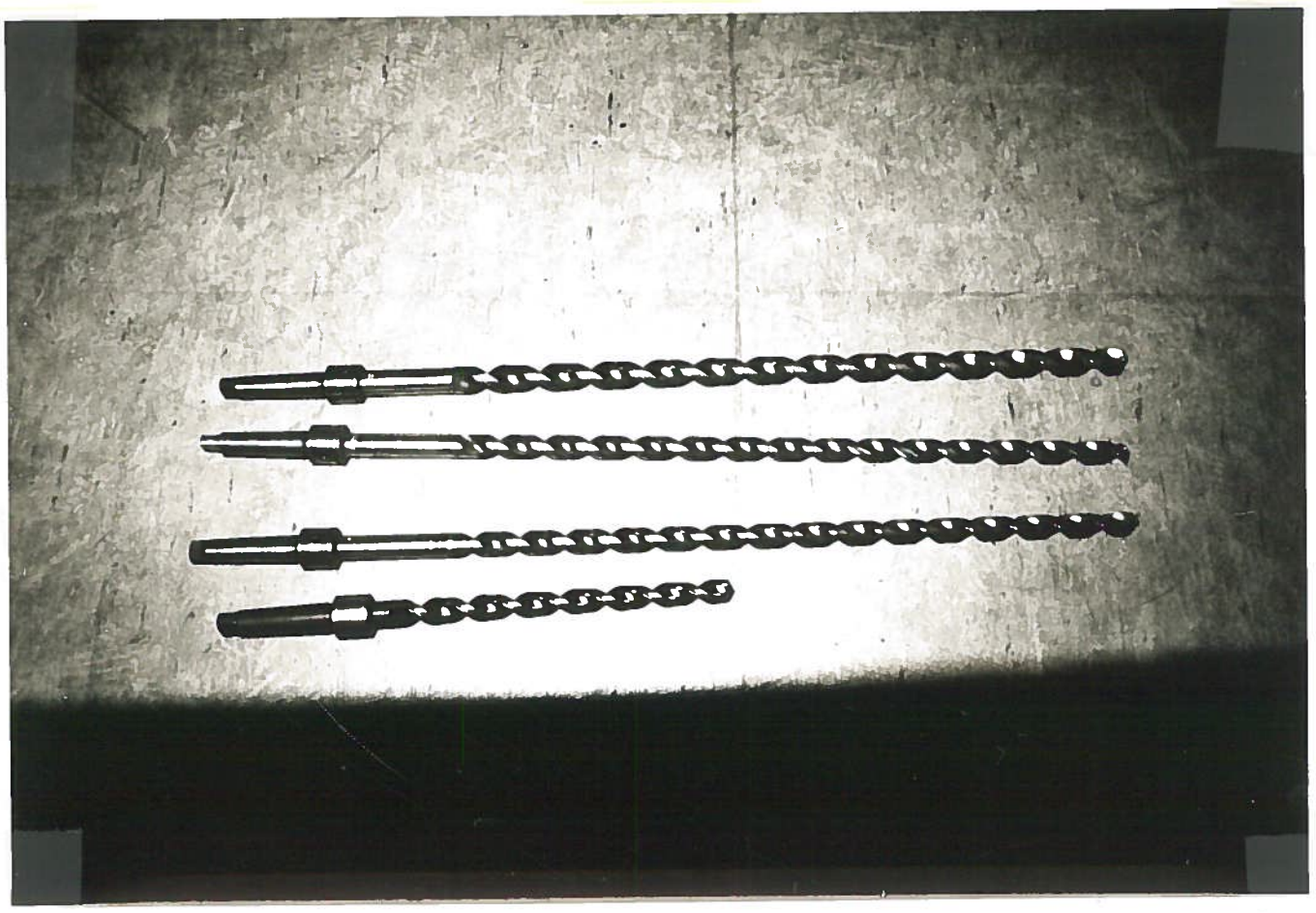

FIG. 34 - Close view of the finishing of trim coils holes on the pole cap.

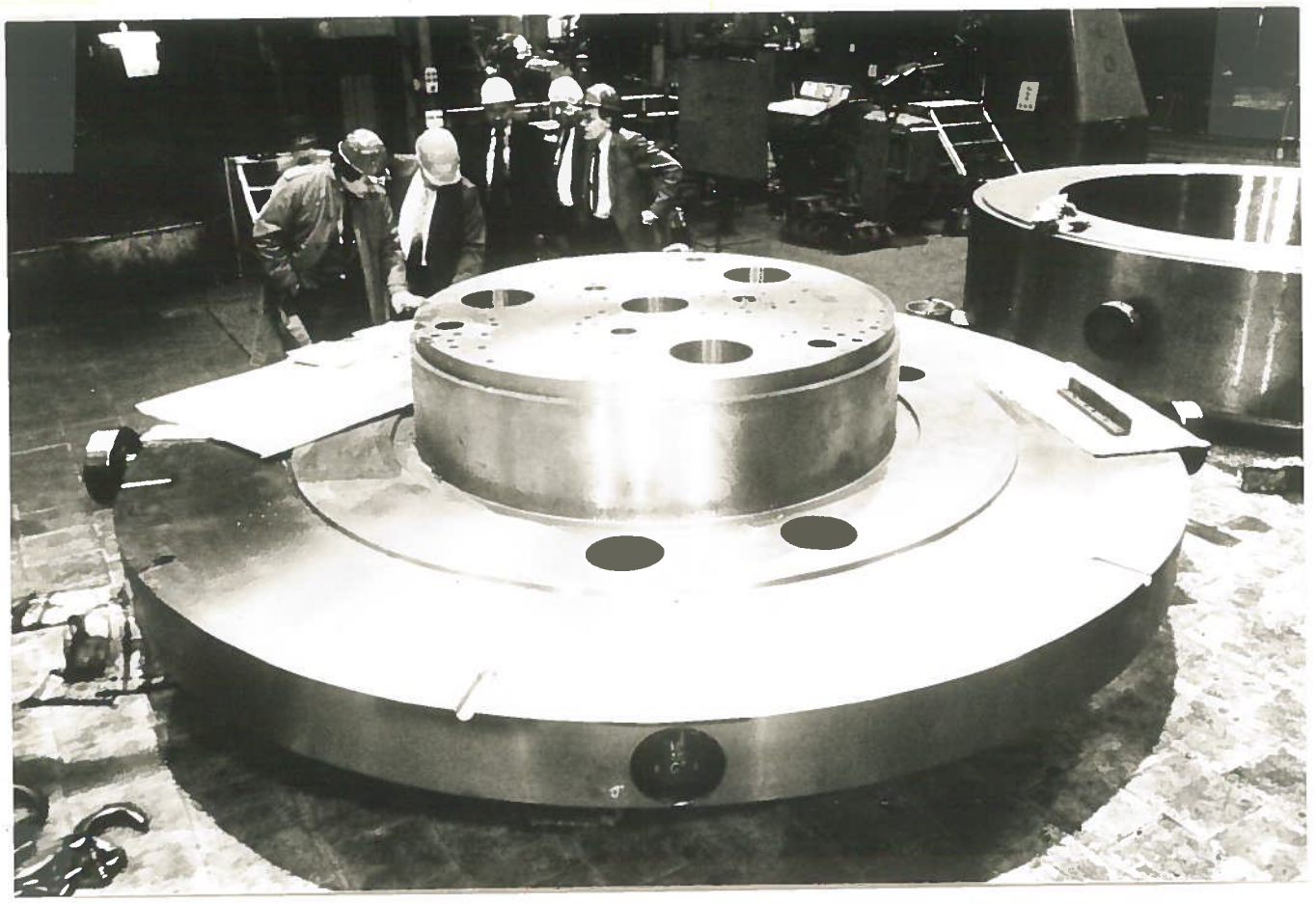

FIG. 35 - View of the finished lower pole cap and plate.

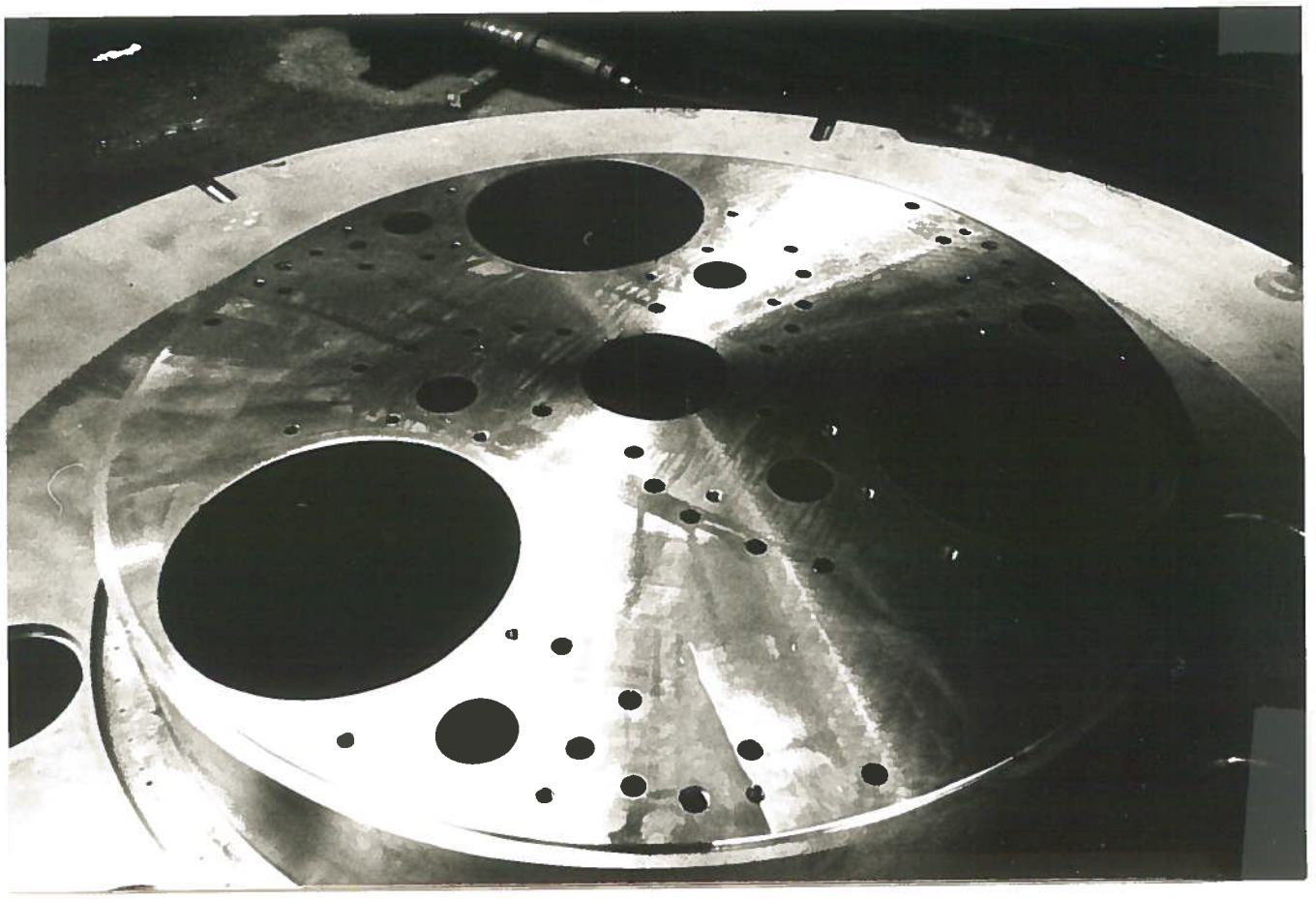

FIG. 36 - Close view of the finished lower pole.

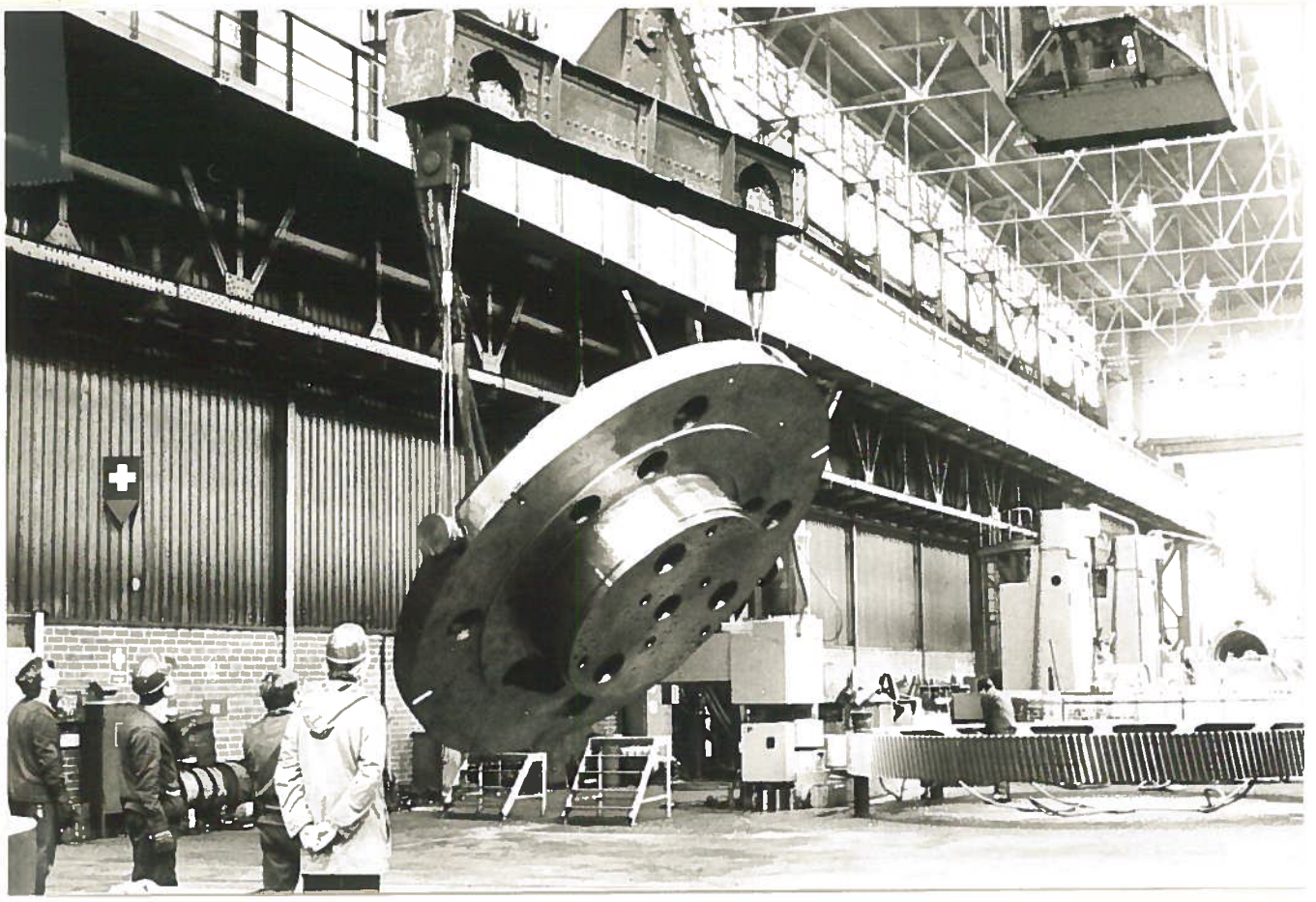

FIG. 37 - Turning of the upper pole cap and plate for the assembling of the magnet.

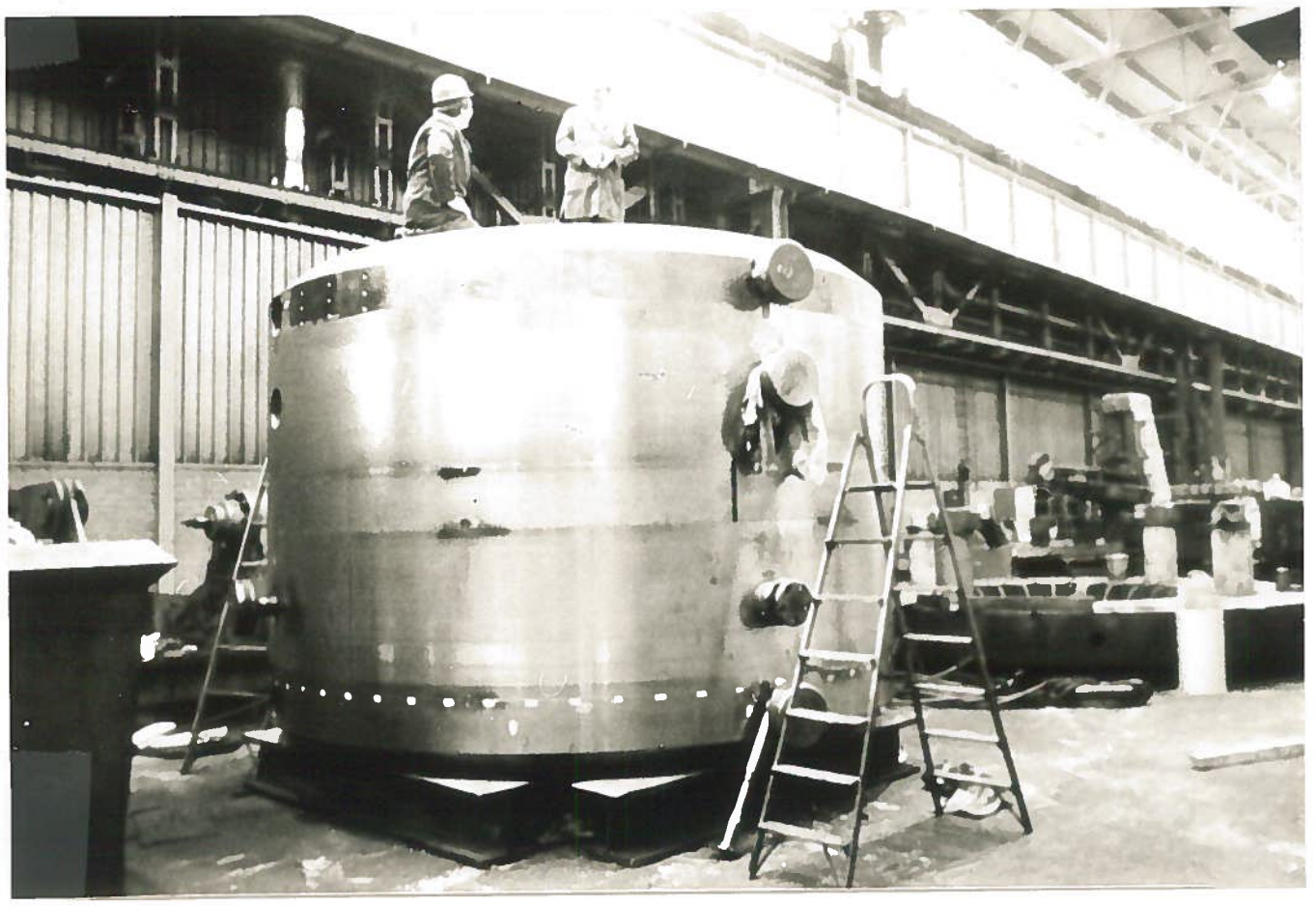

FIG. 38 - View of the magnet yoke fully assembled.

of the lower pole cap at 6° intervals. This has been done in the following way:

The 90° position in the cyclotron frame of reference has been marked on the outside diameter (Ø 1800 mm) of the pole cap and plate with one dot 1 mm diameter, with an accuracy of 0.1 mm. This position has been marked on the outside surface of the lower pole cap with an overall accuracy of 0.15 mm. Thereafter starting from this point the 6° spaced graduation has been machined with a positioning precision of 0.1 mm. Marking is accomplished by lines of 0.25 mm thickness and 20 mm length.

3.8.- Lifting system of the upper pole cap

Since the median plane of the cyclotron is completely blocked by the cryostat, access to the inside of the machine can only be from the top. Consequently we have designed a system for raising and lowering the upper pole cap with high mechanical precision and reliability. The lifting system is manufactured by the firm PFAFF, Augsburg and consists of 4 worm gear screw jacks connected with transmission shafts actuated by an electric motor. The screws, of the self-locking type, are 90° spaced and fixed to the upper ring at the diameter 3020 mm, while the worm gear jacks are fixed to the upper pole cap. A detailed view of the system is shown on Fig. 39. In the following we list the main technical data of the lifting system:

Total load to be lifted	:	Statistical 600 kN Dinamical 600 kN
Load for 1 screw jack	:	Statistical 150 kN Dinamical 150 kN
Nature of load	:	Compression
Nature of buckling	:	Euler I (end of the screw not guided)
Working stroke	:	1810 mm
Screw type	:	Tr120x16
Speed of displacement	:	0.05 m/min
Power of the motor	:	9.2 kW.

The time needed to fully raise by 1810 mm the upper pole cap is 35 minutes and in this configuration the actual clearance between the pole cap (with polar expansions assembled) and the cryostat is 920 mm. The correct

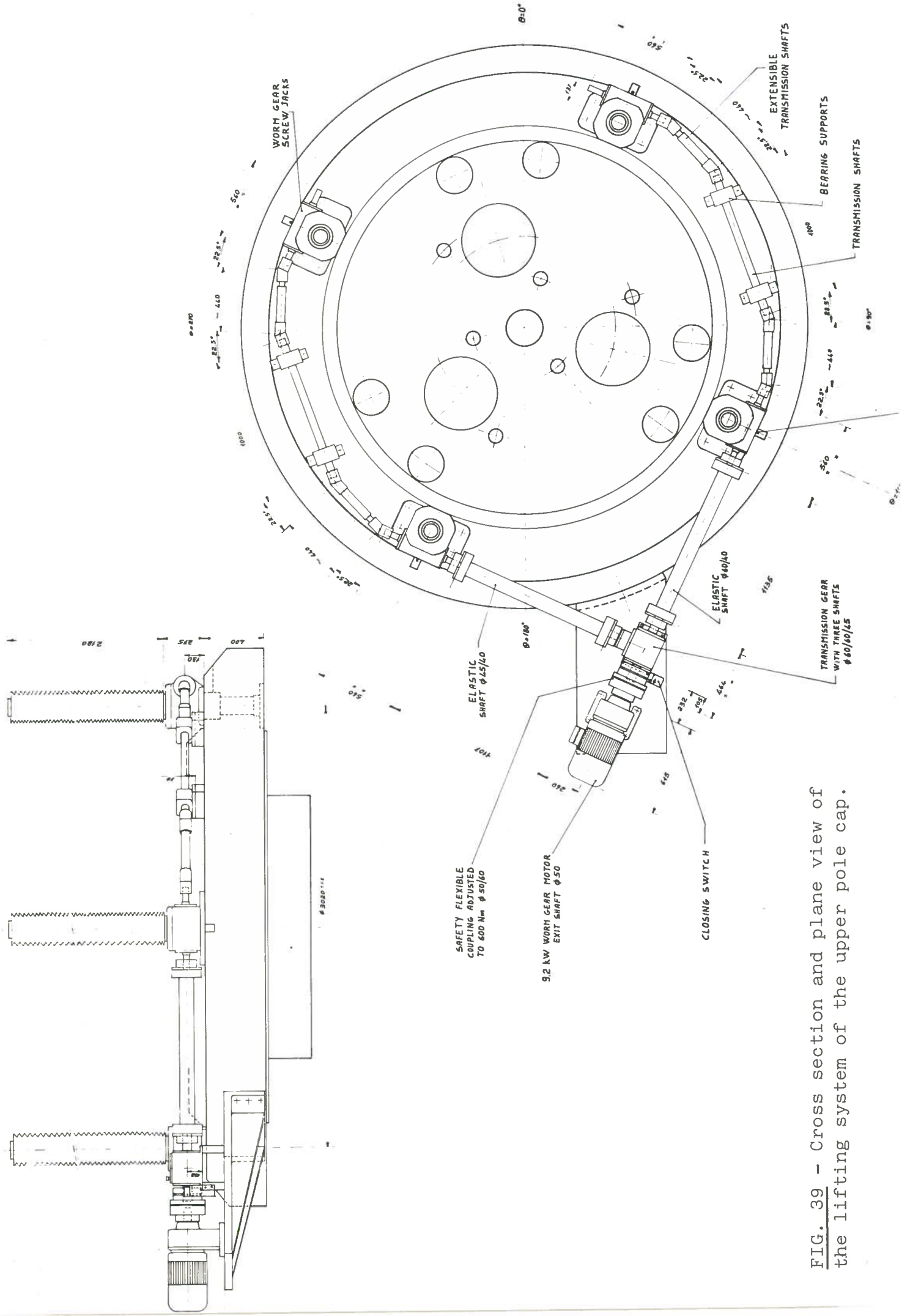

FIG. 39 - Cross section and plane view of the lifting system of the upper pole cap.

functioning of the system during lifting is controlled by measuring the N of turns/min of the worm gear jacks. Moreover the temperature increase of the screws, and the current absorption of the motor are also monitored.

Normal operating conditions values as determined by project choices are the following: the maximum admisible temperature increase for the screws is 100°C, and for the jacks 80°C, while the current absorption must not exceed 20 A.

One critical point of the system is the correct closing of the pole cap. Being the lifting screws of the self locking type a perfect manual closing of the magnet would be tedious and time consuming. Moreover if one attempts to use the power of the motor for a correct closure there is the risk to apply a dangerous traction on the fixing screws of the system to the upper ring. In order to prevent this effect the correct closing is controlled by means of a flexible coupling positioned between the exit shaft of the motor and the transmission gear as shown in Fig. 35. This coupling interrupts the motor supply when the torque on the exit shaft exceeds 600 Nm which is well below the maximum stress admissible on the fixing screws.

A view of the lifting system in operating conditions is shown on Figg. 40 and 41.

4.- POLAR EXPANSIONS

A detailed study of the polar geometry as needed to produce the proper axial focusing together with an isochronous magnetic field, is reported elsewhere[7].

In this paper we shall therefore describe the physical and chemical properties of the iron, the engineering and manufacturing aspects and the way the polar expansions are mounted on the pole caps.

The pole tips have of course a complete mirror image symmetry with respect to the median plane and a 120° azimuthal symmetry.

Each set of polar expansions is constituted by:

- 3 upper hills (the nearest to the median plane);
- 3 lower hills;
- 3 valley shims;
- 1 central plug.

FIG. 40 - View of the lifting system during operation.

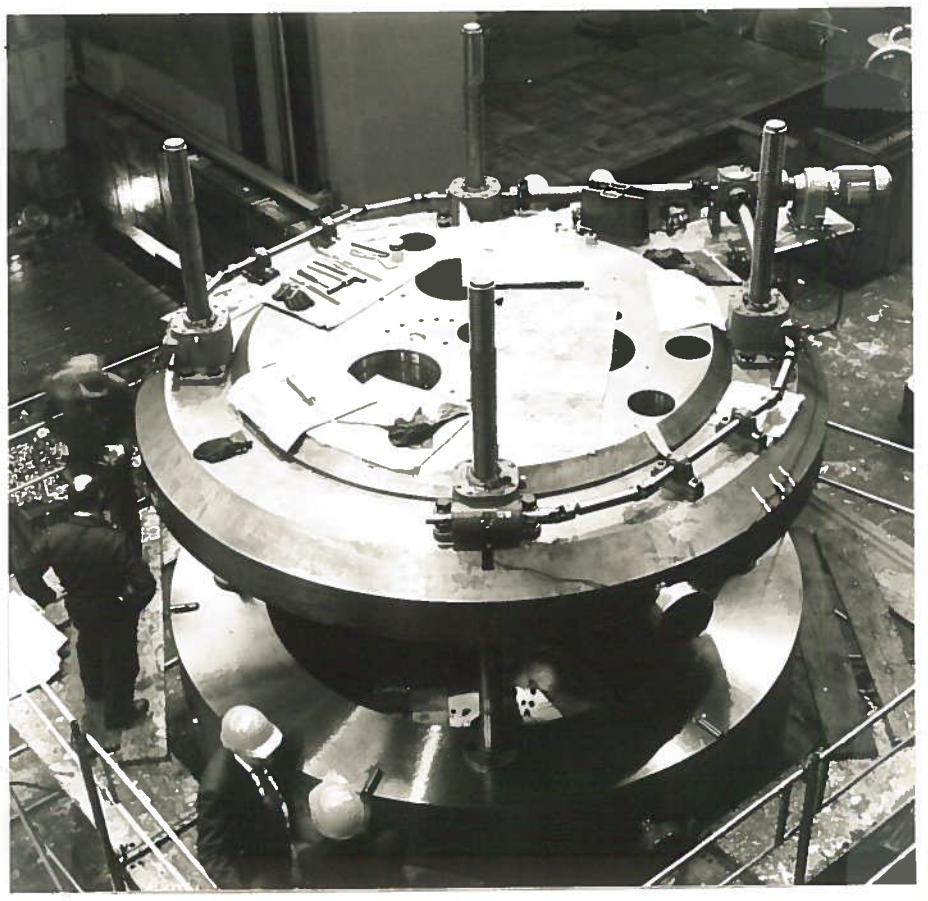

FIG. 41 - Close view of the lifting system.

4.1.- Pole tips design criteria

The hills are split into two parts in order to wind the twenty trim coils around the upper part. Hill and valley radial profiles are shown in Fig. 42.

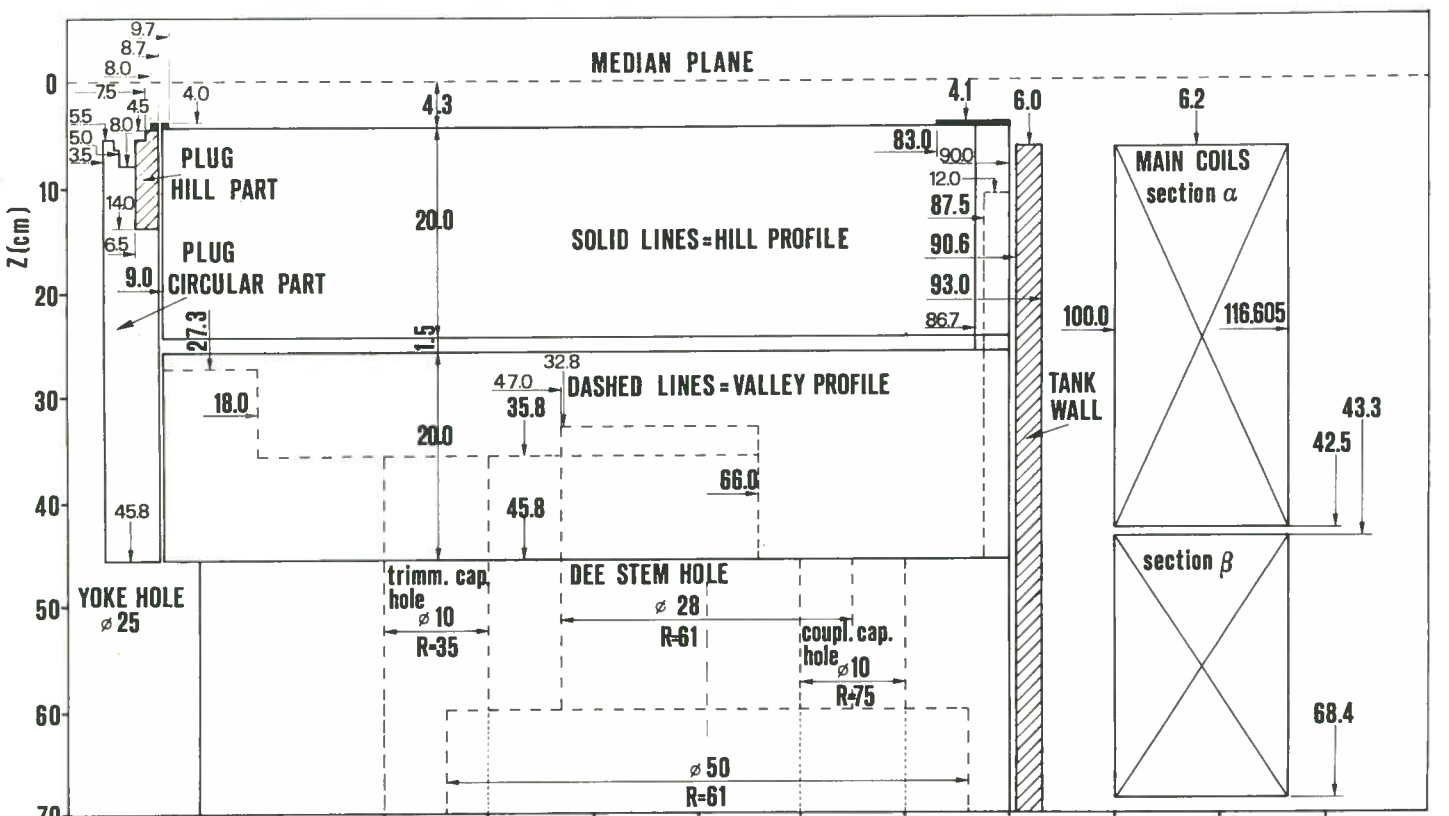

FIG. 42 - Hill and valley radial profiles.

The sectors, of 200 mm height, are 33° wide at the radius of 90 mm where they begin and increase linearly in width up to 46° at R = 400 mm. This width stays constant thereafter up to R = 720 mm, the average spiral constant being 1/45.7 rad/cm. From then on the sectors width increases reaching 52° at R = 867 mm. This is done in order to match the average field produced by the iron to the requirements for minimum trim coil power. The spiral constant also increases in this region, reaching 1/31.4 rad/cm at R = 867 mm, in order to improve the axial focusing. From R = 867 mm to R = 900 mm the sectors are radial, to decrease the axial focusing frequency ν_z, in the region where the $\nu_R+2\nu_z = 3$ resonance limits the machine performances.

Shims of proper height are placed in the valleys, to produce the desired average field shape, as shown in Fig. 42. The first one, which extends from R = 90 mm to R = 660 mm, is 185 mm high from R = 90 mm to R = 180 mm

and 100 mm high from R = 180 mm to R = 660 mm. The second shim is positioned between R = 875 mm and R = 900 mm, has a constant width of 68° and extends up to 120 mm from the median plane.

All the spiral profiles of the hills and valleys are approximated by appropriate arcs of circles. In Tables XIII and XIV we have listed the radius of these circles and the position of their centres in the cyclotron frame of reference for one hill and one valley respectively.

4.2.- Engineering design and assembling of the pole tips

The engineering design of the pole tips had to fulfill these goals:

- Have a minimum number of holes on the upper hills on the side near to the median plane in order to avoid any magnetic perturbation.
- Provide a reasonable mechanical subdivision of the polar expansions in order to maintain some flexibility for any future correction which might be necessary after the magnetic field measurements.
- Easy mounting of the polar expansions on the magnetic yoke.

An overall view of the design of the polar expansions is shown in Fig. 43. Referring to this figure we analyze in some detail the solutions adopted:

4.2.1.- Fixing of the polar expansions to the yoke

The upper hill is bolted to the lower one by means of 24 M8 screws and three dowels 8 mm in diameter. Screws and dowels are on the side away from the median plane in order to avoid the presence of big holes in this region. Holes for the screws are machined through the whole height of the lower sector. The dimension M8 of the screws is dictated by the space allowed on the upper sector around which the trim coils are wound. This space exists only through the spacers positioned between the two parts in which the hill is split. The lower sector together with the upper one is bolted to the pole plate by means of 8 M20 screws and 3 dowels on the side far away of the median plane.

The valley shims which are less critical as far as the magnetic perturbations in the median plane are concerned, are directly fixed to the pole

TABLE XIII Hill profiles in polar coordinates in the CS frame of reference

Concave profiles		Convex profiles	
Center position	Radius of curvature	Center position	Radius of curvature
From R=90 to R=400 mm.			
ρ=290 mm. θ=124 15'	R= 313.134 mm.	ρ=287.86 mm. θ= 72 06'	R= 282.077 mm.
From R=400 to R=720 mm.			
ρ=374.65 mm. θ=157 02'	R= 517.594 mm.	ρ=374.66 mm. θ=111 02'	R= 517.594 mm.
From R=720 to R=867 mm.			
ρ=368.50 mm. θ=160 40'	R= 541.891 mm.	ρ=388.78 mm. θ=150 01'	R= 772.64 mm.

TABLE XIV Valley shim profiles in polar coordinates in the CS frame of reference

Concave profiles		Convex profiles	
Center position	Radius of curvature	Center position	Radius of curvature
From R=90 to R=400 mm.			
ρ=287.87 mm. θ=-192 06'	R= 282.377 mm.	ρ=290 mm. θ=-124 15'	R= 312.834 mm.
From R=400 to R=660 mm.			
ρ=374.660 mm. θ=-231 03'	R= 517.894 mm.	ρ=374.660 mm. θ=-157 03'	R= 517.294 mm.

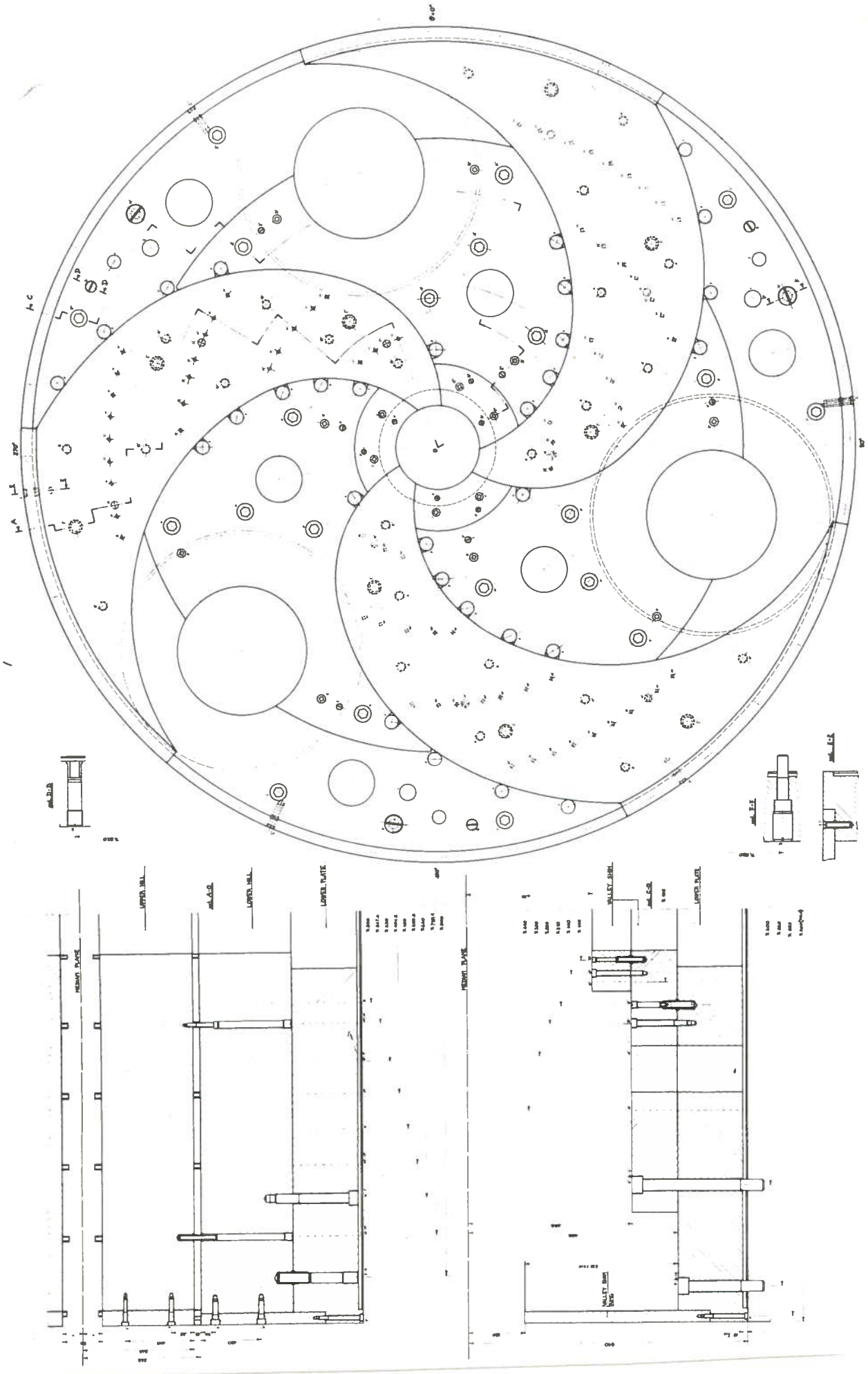

FIG. 43 - Overall view of the lower polar expansions.

plate by means of 3 M12 screws and 2 dowels. The whole set of polar expansions and pole plate is bolted to the pole cap by means of 24 M24 screws. They are all through the valleys (8 for each) and in fact 15 (5 for each valley) go through the valley shims.

Such a solution makes the polar expansions and the relative plate mechanically independent from the yoke.

4.2.2.- Subdivision of the polar expansions

- Upper hill: as mentioned above the hills are split into two parts in order to make possible the winding of the trim coils around the upper one. The upper sector is actually machined into two parts: the first from R = = 90 to R = 867 mm; the second with constant width from R = 867 to R = 900 mm. This subdivision allows to further modify the outer part without having to handle the whole hill. The two parts of the upper sector are fixed together by 12 M12 screws and 2 dowels radially placed. The spiral profile of the upper sector shows an edge chamfering with a curvature radius of 20 mm to allow the winding of the trim coils. A detailed view of an upper hill is shown in Fig. 44.
- Lower hill: also the lower hill is divided into two parts: the first starting from R = 90 to R = 875 mm, and the second from R = 875 to R = 900 mm. This choice has been dictated from the necessity to machine the vertical valley shims as a single ring for better mechanical stability. So we included in this structure also that part of the lower sector between R = 875 and R = 900 mm. Also the lower hill presents an edge chamfering of 8 mm radius of curvature on the side facing the upper hill. A detailed view of a lower hill is shown in Fig. 45.
- Valley shims: the valley shim with a spiral profile has also been divided into two parts of constant height. The first one, from R = 90 to R = = 660 mm, is 100 mm high; the second one from R = 90 to R = 180 mm is 85 mm high. The latter is fixed to the first one by means of 2 M10 screws and 2 dowels 8 mm in diameter. Moreover, in order to give a reasonable clearance, the valley shims are 0.3 mm narrower, on each side of the spiral profile, with respect to the mathematical design. Holes are provided on each side of the shims in correspondance of the trim coils leads holes on the plate, as shown in Fig. 46.

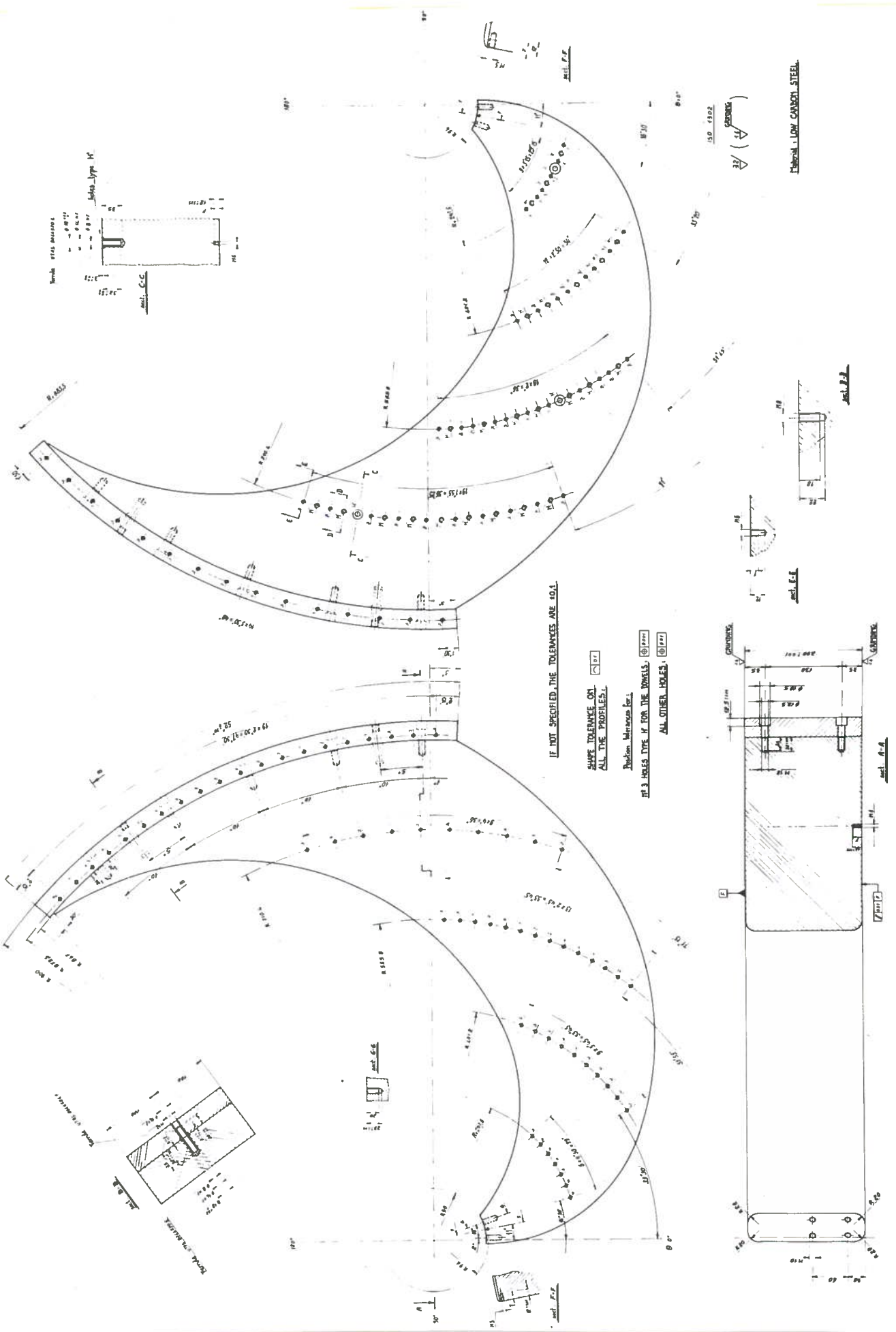

FIG. 44 - Cross section and plane view of an upper hill.

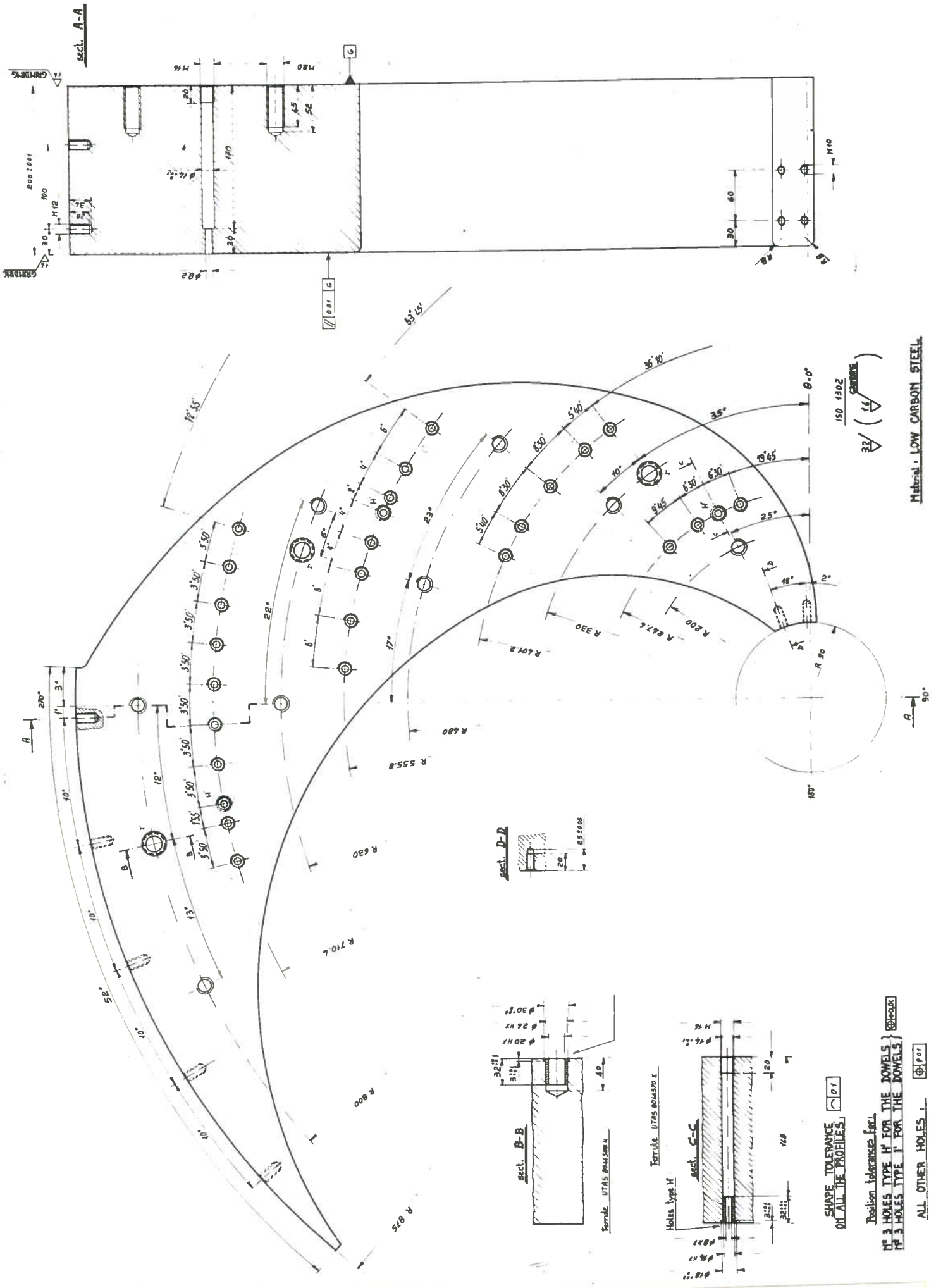

FIG. 45 - Cross section and plane view of a lower hill.

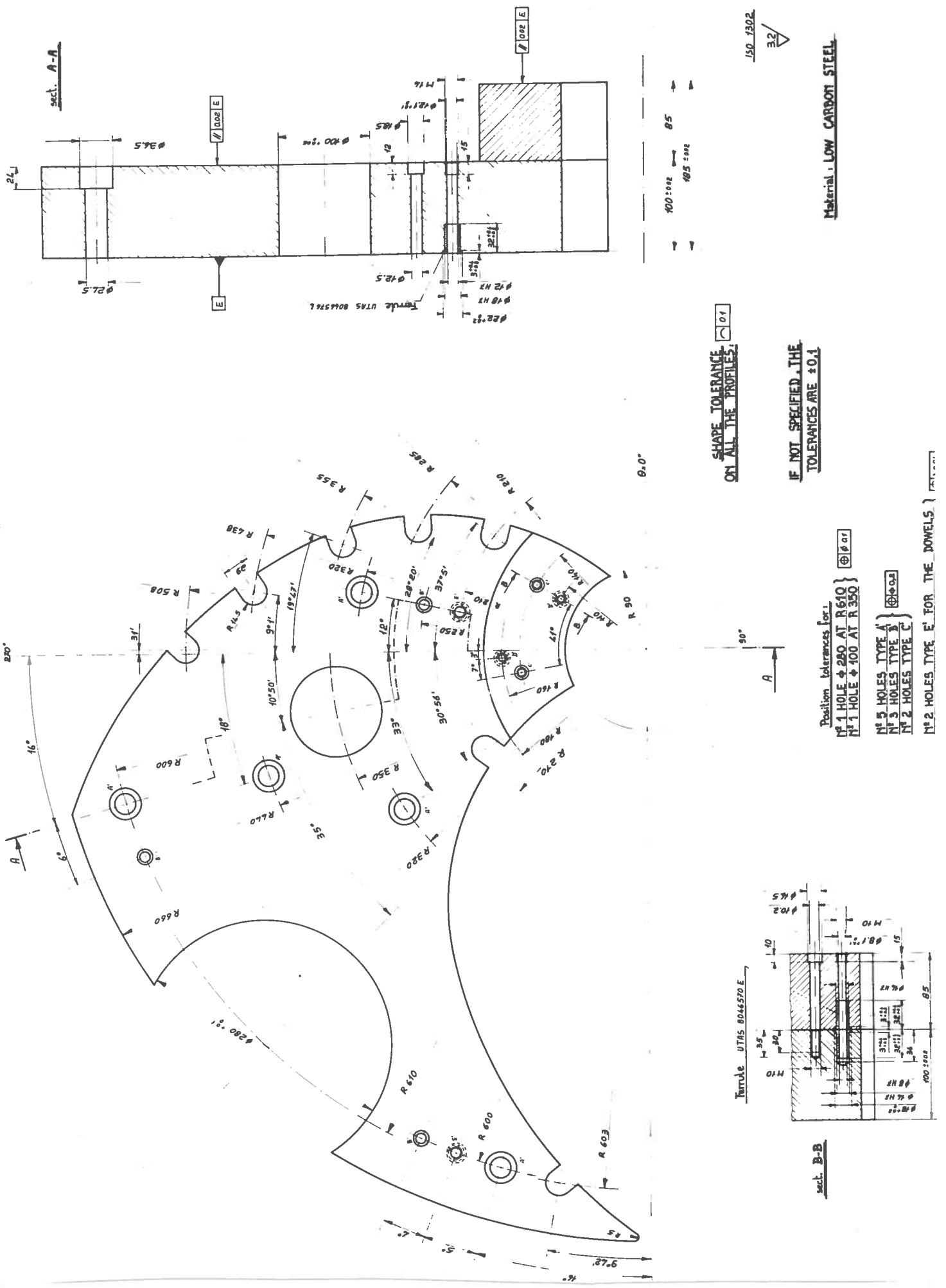

FIG. 46 - Cross section and plane view of a valley shim.

As mentioned previously the vertical valley shim which is 25 mm thick, is a single ring in order to give sufficient rigidity to the structure. Windows 52° wide are provided in correspondance of the upper sectors. The ring is fixed by means of 36 M8 screws to the plate and by 10 M12 screws to the lower sector. Positioning of the ring is accomplished by means of 6 radial dowels, 8 mm in diameter. A view of the ring is shown in Fig.47. The weights of the polar expansions elements are given in Table XV, while Table XVI lists the positions of all the holes in the pole tips, specifying their function.

TABLE XV Weights of polar expansions

Number	Element	Material	Weight
6	Upper hill	Low carbon steel, rolled	466 kg.
6	Radial part of the upper hill	Low carbon steel, rolled and calendered	42 kg.
6	Lower hill	Low carbon steel, rolled	479 kg.
6	Valley shim	Low carbon steel, rolled	192 kg.
2	Ring	Low carbon steel, rolled and calendered	377 kg.
2	Plate	Low carbon steel, casted	2533 kg.
Total weight of one set of the polar expansion when assembled on the relative plate			6447 kg.

- Trimming coils spacers: there are 6 spacers, 15 mm height, on each side of the upper hill. An exception is the outer one, nearer to the median plane, which is 6 mm in height. This provides more axial space for the electrostatic deflector, which for low magnetic fields, must slide sensibly inward. The function of the spacers is to maintain in the correct position the set of trim coils which are epoxy impregnated together with the relative spacers. Those between the upper and the lower hills also ensure the

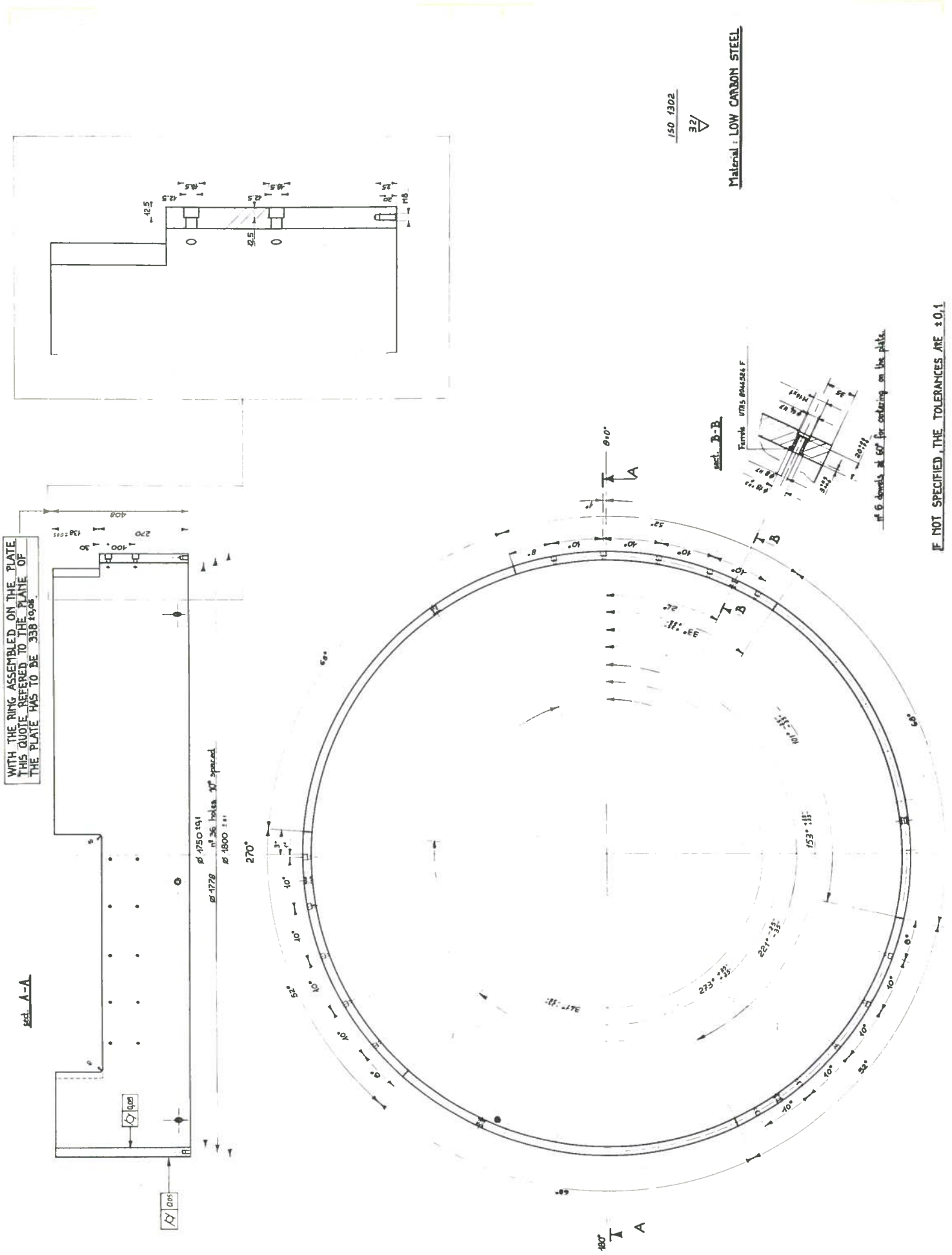

FIG. 47 - Cross section and plane view of a ring.

TABLE XVI Description of the holes in the pole tips

N. of holes / Type	Function	Position in the cyclotron frame of reference	Position tolerance (mm)
24 ;for M 20 screws	Fixing of the lower sector to the relative plate	R=200 θ = 95° =215° =335°	0.1
		R=330 θ = 75° =195° =315°	
		R=480 θ = 70° =190° =310°	
		R=480 θ = 47° =167° =287°	
		R=630 θ = 52° =172° =292°	
		R=630 θ = 30° =150° =270°	
		R=800 θ =30° =150° =270°	
		R=800 θ = 5° =125° =245°	
9 ;for ⌀ 20 dowels	Positioning of the lower sector on the relative plate	R=330 θ = 85° =205° =325°	0.01
		R=630 θ = 47° =167° =287°	
		R=800 θ = 8° =128° =248°	
72 ;for M 8 screws	Fixing of the upper sector to the lower one	R=247.6 θ =100°15' =220°15' =340°15'	0.1
		R=247.6 θ = 87°15' =207°15' =327°15'	

N. of holes / Type	Function	Position in the cyclotron frame of reference	Position tolerance
		R=247.6 θ { = 77°30' =197°30' =317°30'	
		R=401.2 θ { = 86°50' =206°50' =326°50'	
		R=401.2 θ { = 78°10' =198°10' =318°10'	
		R=401.2 θ { = 71°40' =191°40' =311°40'	
		R=401.2 θ { = 61°10' =181°10' =301°10'	
		R=401.2 θ { = 55°30' =175°30' =295°30'	
		R=555.8 θ { = 66°15' =186°15' =306°15'	
		R=555.8 θ { = 60°15' =180°15' =300°15'	
		R=555.8 θ { = 56°15' =176°15' =296°15'	
		R=555.8 θ { = 50°15' =170°15' =290°15'	
		R=555.8 θ { = 46°15' =166°15' =286°15'	
		R=555.8 θ { = 40°15' =160°15' =280°15'	
		R=555.8 θ { = 34°15' =154°15' =274°15'	
		R=710.4 θ { = 47°05' =167°05' =287°05'	
		R=710.4 θ { = 43°15' =163°15' =283°15'	
		R=710.4 θ { = 39°25' =159°25' =279°25'	

N. of holes / Type	Function	Position in the cyclotron frame of reference	Position tolerance (mm)
9 ; for ⌀ 8 dowels	Positioning of the upper sector on the lower one	R=710.4 θ { = 35°35' =155°35' =275°35'	0.01
		R=710.4 θ { = 31°45' =151°45' =271°45'	
		R=710.4 θ { = 27°55' =147°55' =267°55'	
		R=710.4 θ { = 24°05' =144°05' =264°05'	
		R=710.4 θ { = 18°20' =138°20' =258°20'	
		R=710.4 θ { = 14°30' =134°30' =254°30'	
		R=247.6 θ { = 93°45' =213°45' =333°45'	
		R=555.8 θ { = 54°15' =174°15' =294°15'	
		R=710.4 θ { = 21°15' =141°15' =261°15'	
30 ; for M 12 screws	Fixing of the two parts of the upper sector	R=867 θ { = 29° =149° =269°	0.1
		R=867 θ { = 19° =139° =259°	
		R=867 θ { = 9° =129° =249°	
		R=867 θ { =119° =239° =359°	
		R=867 θ { =109° =229° =349°	
6 ; for ⌀ 8 dowels	Positioning of the two parts of the upper sector	R=867 θ { = 24° =144° =264°	0.01

N. of holes / Type	Function	Position in the cyclotron frame of reference	Position tolerance (mm)
9 ; for M 12 screws	Fixing of the valley shim to the relative plate	R=867 θ { =114° =234° =354°	0.1
		R=250 θ { = 42° =162° =282°	
		R=600 θ { = 8° =128° =248°	
		R=600 θ { = 85° =205° =325°	
6 ; for ⌀12 dowels	Positioning of the valley shim on the relative plate	R=210 θ { = 42° =162° =282°	0.01
		R=600 θ { = 71° =191° =311°	
6 ; for M 10 screws	Fixing of the two parts of the valley shim	R=140 θ { = 61° =181° =301°	0.1
		R=140 θ { = 20° =140° =260°	
6 ; for ⌀8 dowels	Positioning of the two parts of the valley shim	R=110 θ { = 61° =181° =301°	0.01
		R=160 θ { = 27° =147° =267°	
36 ; for M 8 screws	Fixing of the ring to the relative plate	R=889 θ_o = 9° 10° spaced	0.1
6 ; for ⌀8 dowels	Positioning of the ring on the relative plate	R=875 θ_o = 24° 60° spaced	0.01
30 ; for M 12 screws	Fixing of the ring to the lower sector	R=875 θ { = 29 =149 =269	0.1
		R=875 θ { = 19 =139 =259	

N. of holes / Type	Function	Position in the cyclotron frame of reference	Position tolerance (mm)
24 ; for M 24 screws	Fixing of the plate to the relative pole through the valley	R=875 θ = 9° =129° =249° R=875 θ =119° =239° =359° R=875 θ =109° =229° =349° R=320 θ = 42° =162° =282° R=320 θ =117° =237° =357° R=440 θ = 12° =132° =252° R=600 θ = 14° =134° =254° R=600 θ = 76° =196° =316° R=820 θ = 50° =170° =290° R=820 θ = 67° =197° =317° R=820 θ = 85° =205° =325°	0.1
3 ; for ϕ 20 dowels	Positioning of the plate on the relative pole	R=820 θ = 55° =175° =295°	0.01

right positioning of the sectors.

Spacers are bolted to the relevant hill by a lot of screws whose number was dictated by the strength of the radial magnetic forces acting on the trim coils when energized.

Table XVII lists the mean radius of curvature of the spacers together with the number of screws.

We briefly mention that all these solutions have been checked on a full scale prototype of two sectors, the valley in between and the relevant plate. The prototype, shown in Fig. 48 was cast in aluminum, in order to reduce its weight. It has proved extremely useful for verifying the machining procedure and for assembling a full set of trim coils. Machining was carried out with a numerically controlled milling machine and measuring tests have shown that a precision of 0.05 mm can be achieved. This is deemed sufficient for the cyclotron.

FIG. 48 - View of the aluminum full scale prototype of two sectors, the valley in between and the relevant plate.

TABLE XVII Mechanical configuration of the spacers on the lower side of the sector.

Number of the spacer	Material	Mean radius (mm)	Number of fixing screws	Angular amplitude	Heigth (mm)	Width (mm)
1	AISI 304	94	3	9	15	8
2	AISI 304	247.6	6	35 35'	15	13
3	AISI 304	401.2	8	39 50'	15	13
4	AISI 304	555.8	11	41 14'	15	13
5	AISI 304	710.4	10	41 27'	15	13
6	Low carbon steel	883.5	15	52	15	34

TABLE XVIIa Mechanical configuration of the spacers on the upper side of the sector.

Number of the spacer	Material	Mean radius (mm)	Number of fixing screws	Angular amplitude	Heigth (mm)	Width (mm)
1	AISI 304	94	3	9	15	8
2	AISI 316	247.6	7	35 35'	15	13
3	AISI 316	401.2	10	39 50'	15	13
4	AISI 316	555.8	14	41 14'	15	13
5	AISI 316	710.4	10	41 27'	15	13
6	AISI 316	872.5	20	52	6	13

4.3.- Mechanical tolerances

As the polar expansions are of noticeable importance from the point of view of the magnetic field, the prescribed tolerances are rather tight. To this end a special mechining procedure, mostly numerically controlled, has been followed, in order to obtain a mirror immage symmetry and a 120° symmetry within 0.1 mm at worst.

This value of the final tolerance, referred to the completely assembled magnet, does not seem so tight, but we must take into account the interaction of all the pieces fixed together, namely yoke and pole tips.

The main tolerance prescribed on the machining of the polar expansions are listed in Table XVIII.

TABLE XVIII Main tolerances required on the machining of the polar expansions

Shape of sectors and valleys	0.10 mm.
Sectors parallelism	0.01 mm.
Valley parallelism	0.02 mm.
Rings concentricity	0.05 mm.
Lower spacers parallelism	0.01 mm.
Holes for the dowels	0.01 mm.

High stress steel ferrules are inserted in all the holes for the dowels in order to avoid any damages during assembling and disassembling. The coupling between dowels and the relative holes is of the type m6, H7.

4.4.- Physical and chemical properties of the iron

The pole tips are manufactured from low carbon iron, of quality as good as the yoke, and supplied by the same firm.

The iron was supplied as rolled plates of suitable thickness. Successivelly they were flame cut according to roughly the sectors and valleys profile, with the exception of the rings and radial parts of the hills which were rolled. Annealing was carried out after flame cutting. All similar

elements are obtained from the same heat, namely:

- HEAT 1 : upper and lower sectors,
- HEAT 2 : radial elements of the upper sectors,
- HEAT 3 : valley shims,
- HEAT 4 : rings.

Chemical characteristics

The chemical composition is certified by HOESCH for each heat number and typical results are reported in Table XIX together with the prescribed values.

TABLE XIX Chemical composition of the iron of the pole tips

Element	Max. allowed content (%)	HOESCH certified value (%)			
		Heat 1	Heat 2	Heat 3	Heat 4
C	0.08	0.01	0.01	0.01	0.01
Si	0.25	0.01	0.01	0.01	0.02
Mn	0.45	0.23	0.18	0.22	0.25
P	0.015	0.008	0.009	0.01	0.009
S	0.01	0.01	0.01	0.009	0.01
Cr	0.09	0.02	0.03	0.02	
Ni	0.14	0.03	0.02	0.03	
Mo	0.05				
Cu	0.1	0.02	0.02	0.02	
O_2 (dissolved)	0.008				
N	0.01		0.0057	0.0067	
Al	0.03	0.04	0.05	0.05	0.04
Sn		0.007	0.003	0.007	

4.4.1.- Magnetic properties

Magnetic properties of the iron for the polar expansions are certified by HOESCH for each heat number for H values up to 30000 At/m. Measured values are identical to those obtained for the yoke. In Table XX we report typical values for the iron of the sectors. Magnetization values up to sa

TABLE XX Magnetic properties of the iron of the polar expansions

Field intensity H (At/m)	Heat 1		
	Magnetic induction B (Tesla)	Magnetization $M=B-\mu_o H$ (Tesla)	Coercitive field H_c (A/m)
1000	1.52	1.52	
2000	1.63	1.63	
2500	1.66	1.66	
5000	1.74	1.74	
10000	1.86	1.85	90
15000	1.94	1.92	
20000	2.01	1.98	
25000	2.06	2.03	
30000	2.10	2.06	

Field intensity H (At/m)	Heat 2		
	Magnetic induction B (Tesla)	Magnetization $M=B-\mu_o H$ (Tesla)	Coercitive field H_c (A/m)
1000	1.54	1.54	
2000	1.64	1.64	
2500	1.66	1.66	
5000	1.75	1.74	
10000	1.86	1.85	90
15000	1.94	1.92	
20000	2.01	1.98	
25000	2.06	2.03	
30000	2.10	2.06	

Accuracy of the measurements: H: $\pm$ 10 At/m
B: $\pm$ 0.02 T

Field intensity H (At/m)	Heat 3		
	Magnetic induction B (Tesla)	Magnetization $M=B-\mu_0 H$ (Tesla)	Coercitive field H_c (A/m)
1000	1.53	1.53	
2000	1.64	1.64	
2500	1.66	1.66	
5000	1.75	1.74	
10000	1.86	1.85	90
15000	1.94	1.92	
20000	2.01	1.98	
25000	2.06	2.03	
30000	2.10	2.06	

Field intensity H (At/m)	Heat 4		
	Magnetic induction B (Tesla)	Magnetization $M=B-\mu_0 H$	Coercitive field H_c (A/m)
1000	1.39	1.39	
2000	1.55	1.55	
2500	1.59	1.59	
5000	1.68	1.68	
10000	1.79	1.78	130
15000	1.87	1.85	
20000	1.94	1.91	
25000	1.99	1.96	
30000	2.03	1.99	

Accuracy of the measurements: H: ± 10 At/m
B: ± 0.02 T

turation were measured with the procedure used for the yoke as described in chapter 3.4.3.

The results are shown in Table XXI and are substantially the same as for the yoke.

4.4.2.- Mechanical properties

Yield point, tensile strength and elongation for each heat are shown in Table XXII. Because of the lamination process they look a little better when compared to those for the yoke.

4.4.3.- Ultrasonic testing

All the iron for the polar expansions has been tested by HOESCH according to the German Norm Stahl-Eisen 072-class 2. In Table XXIII we report the surface and the maximum number of acceptable defects. Moreover a control check carried out by us has confirmed the prescribed values. One set of sectors has shown small defects, within the prescribed norm, approximately at a radius of 400 mm, and they have been picked up as lower sectors (those further away from the median plane).

4.4.4.- Trim coils spacers

Spacers are made of stainless steel with the exception of the lower N. 6 which is in low carbon iron of the same quality as the sectors. The initial choice was to use AISI 304 steel, but tests carried out after the machining process have shown an unacceptable magnetization. Typical magnetization values for H values up to 175000 At/m are listed in Table XXIV. For these reason we have kept the AISI 304 spacers only for the lower ones, i.e., those farther away from the median plane. We have then used AISI 316 steel for the spacers closer to the median plane. Their typical magnetization values are a factor 10 lower as listed in Table XXV.

4.4.5.- Screws for the assembly of the sectors

All the screws for the assembly of the polar expansions were selected in accordance to their magnetic properties. With the exception of the stainless steel spacers, whose fixing screws are in AISI 304, all the screws are of the class 8.8. Mechanical and chemical characteristics of

TABLE XXI Magnetization values of the iron of the pole tips

Field intensity H (At/m)	Magnetic induction B (Tesla)	Magnetization $M = B - \mu_0 H$ (Tesla)
Heat 1:hills		
29115	2.079	2.042
59583	2.191	2.117
89678	2.238	2.125
119775	2.278	2.128
145706	2.312	2.129
177330	2.346	2.130
184740	2.362	2.130
Heat 2: radial parts of the upper hills		
410	1.255	1.255
990	1.506	1.505
4060	1.700	1.695
12230	1.880	1.865
24480	2.030	2.000
39590	2.135	2.085
59280	2.184	2.110
89330	2.232	2.120
119250	2.270	2.120
145300	2.307	2.125
175900	2.346	2.125
Heat 4: rings		
29080	2.075	2.039
59479	2.188	2.113
89592	2.234	2.121
119513	2.274	2.124
143971	2.306	2.125
172852	2.343	2.126
183867	2.357	2.126
Accuracy of the measurements: ± 0.5 %		

TABLE XXII Mechanical properties of the iron of the pole tips

	Heat 1	Heat 2	Heat 3	Heat 4
Yield point (N/mm^2)	175	174	193	194
Tensile strength (N/mm^2)	283	297	289	306
Elongation (%)	40	40	40	40

TABLE XXIII Accettable defects on the iron for the polar expansions according to the German norm Stahl-Eisen 072-class 2

Minimum area of the defects taken into account (cm^2)	Maximum admissible area of the defects (cm^2)	Maximum number of allowed defects for m^2	Mean number of defects for m^2
0.5	1	30	15

TABLE XXIV Magnetization values of the stainless steel AISI 304 used for the lower spacers

Field intensity H (At/m)	Magnetic induction B (Tesla)	Magnetization $M=B-\mu_o H$ (Tesla)
8794	0.017	0.00660
14293	0.027	0.00950
44188	0.074	0.01905
74067	0.116	0.02317
103642	0.155	0.02525
133304	0.193	0.02637
157415	0.224	0.02718
182133	0.256	0.02779
Accuracy of the measurements: ± 0.5 %		

TABLE XXV Magnetization values of the stainless steel AISI 316 used for the upper spacers

Field intensity H (At/m)	Magnetic induction B (Tesla)	Magnetization $M= B-\mu_o H$ (Tesla)
4335	0.0055	0.000152
10250	0.01321	0.000330
21680	0.02785	0.000610
36555	0.04680	0.000864
51475	0.06572	0.00104
66260	0.08445	0.00119
81180	0.10333	0.00132
98870	0.12571	0.00147
115180	0.14631	0.00158
132960	0.16876	0.00168
148050	0.18782	0.00178
164790	0.20896	0.00188
Accuracy of the measurements: ± 0.5 %		

TABLE XXVI Mechanical and chemical characteristics of the screws used in the pole tips

Class	8.8
Tensile strength R (N/mm^2) min.	800
max.	1000
Yield strength $R_p(0.2)$ (N/mm^2) min.	640
Elongation A (%) min.	12
Chemical analysis (%)	$0.32 \leq C \leq 0.5$
	$P \leq 0.04$
	$S \leq 0.05$

TABLE XXVII Magnetization values of the iron of the screws used in the pole tips

Field intensity H (At/m)	Magnetic induction B (Tesla)	Magnetization $M = B - \mu_o H$ (Tesla)
2315	1.3159	1.313
8220	1.7613	1.751
22920	1.9538	1.925
39575	2.0257	1.976
54570	2.0605	1.992
69575	2.0864	1.999
84560	2.1102	2.004
99300	2.1317	2.007
114310	2.1526	2.009
129230	2.1733	2.011
144400	2.1934	2.012
156550	2.2097	2.013
177360	2.2368	2.014

Accuracy of the measurements: ± 0.5 %

these screws are listed in Table XXVI while the magnetization values are presented in Table XXVII.

4.5.- Machining procedure of the pole tips

The machining of the pole tips was carried out by the firm Frigostamp in Turin, with the exception of the rolling, and welding of the rings and radial parts of the hills, which were done by ATB, Brescia.

A stainless steel grinded plate has been the basis for the machining of the sectors and valleys. Holes for suitable dowels were drilled on the plate and hills and valleys were machined using these dowels as a reference. In this way we have avoided any positioning errors between similar elements and furthermore any repositioning for successive machining using the plate will be done with the greatest accuracy. In the following we describe the machining procedure for each element of the polar expansions.

4.5.1.- Lower and upper sectors

The planes are rough machined with 2 mm allowance. Rough machining of the profiles with a copying milling machine with 2 mm allowance: Fig.49. Two dowels holes which will be the reference for any further machining are drilled. Grinding of the planes with 0.5 mm allowance. Drilling of the whole set of holes with numerical controlled machine and screw treads machining: Fig. 50. Milling of the profiles with 0.2 mm allowance and mechanical check. Finishing of all the profiles: Fig. 51. Chamfering machining: Fig. 52. The finished radial parts are mounted on the relative upper sectors and thereafter the planes are grinded to the required tolerance.

4.5.2.- Radial parts of the upper sectors

Flame cutting of the radial parts of the sectors, rolling and annealing: Figs. 53 and 54. Rough machining and annealing: Fig. 55.

Final machining and assembly on the upper sectors.

4.5.3.- Valley shims

Rough machining of the profiles with numerical controlled machine with 2 mm allowance. Drilling of the holes for the reference dowels: Fig. 56.

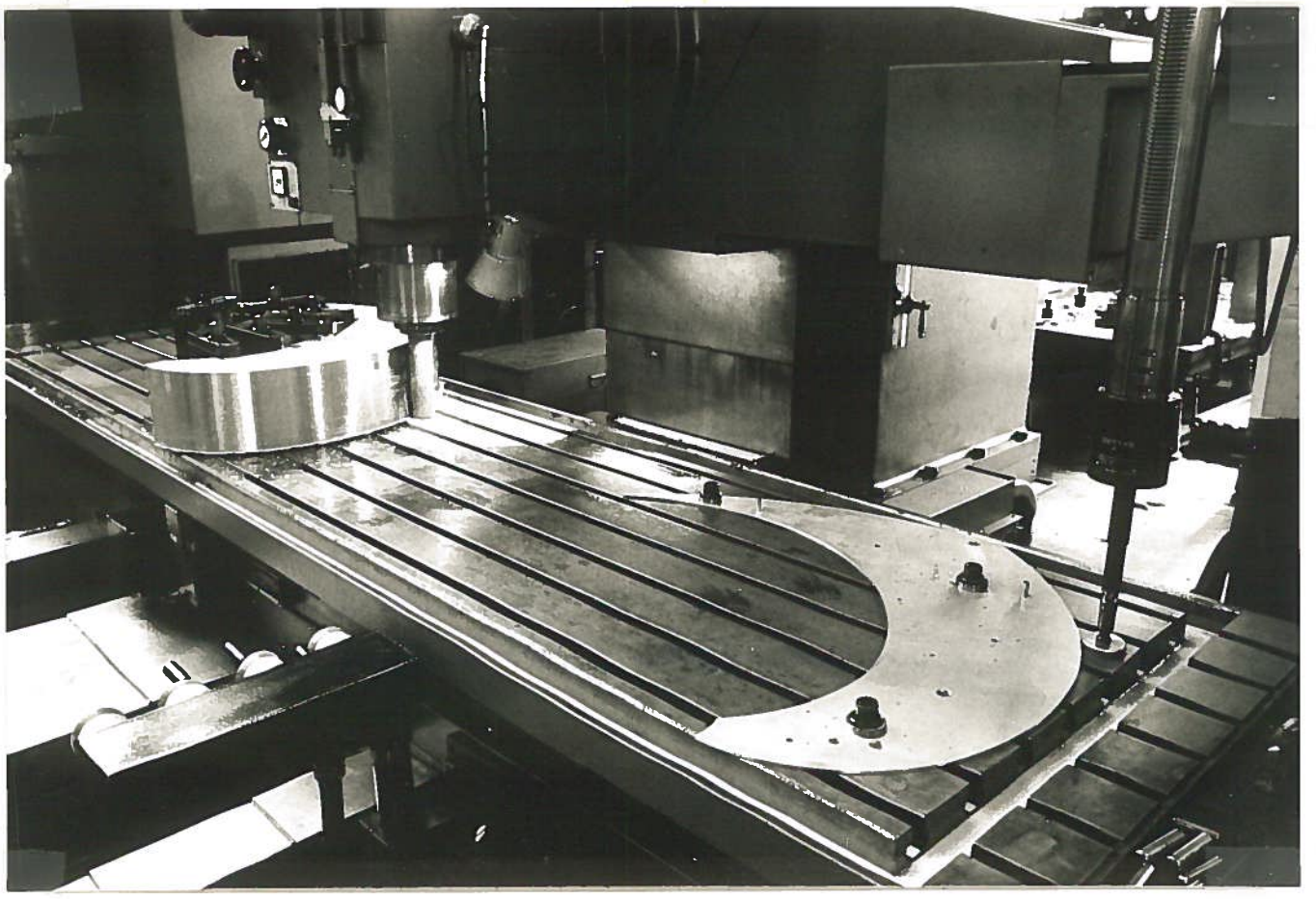

FIG. 49 - View of a sector during rough machining of the profiles with a copying milling machine.

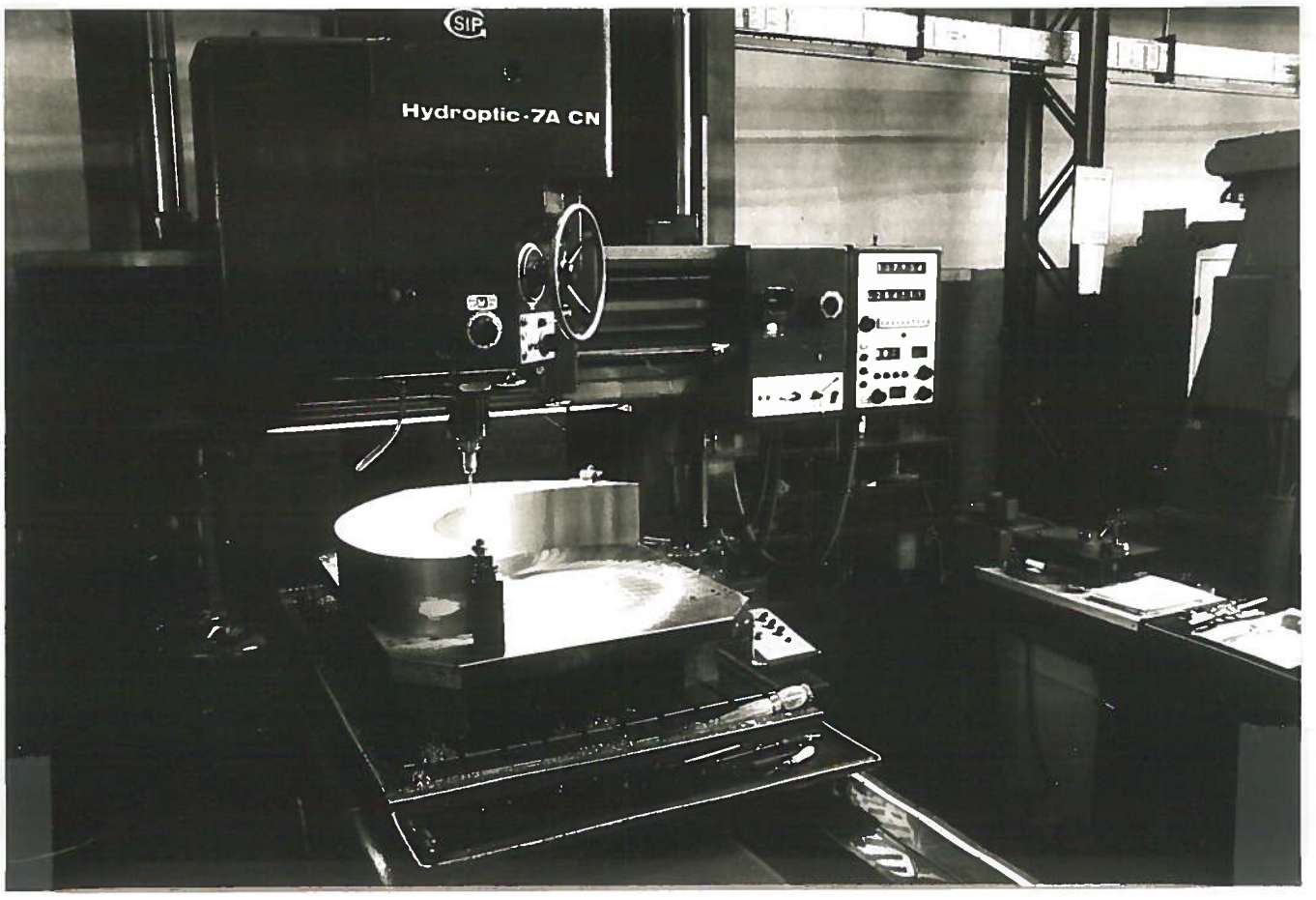

FIG. 50 - View of an upper sector during drilling of holes and screw threads machining with numerical controlled machine.

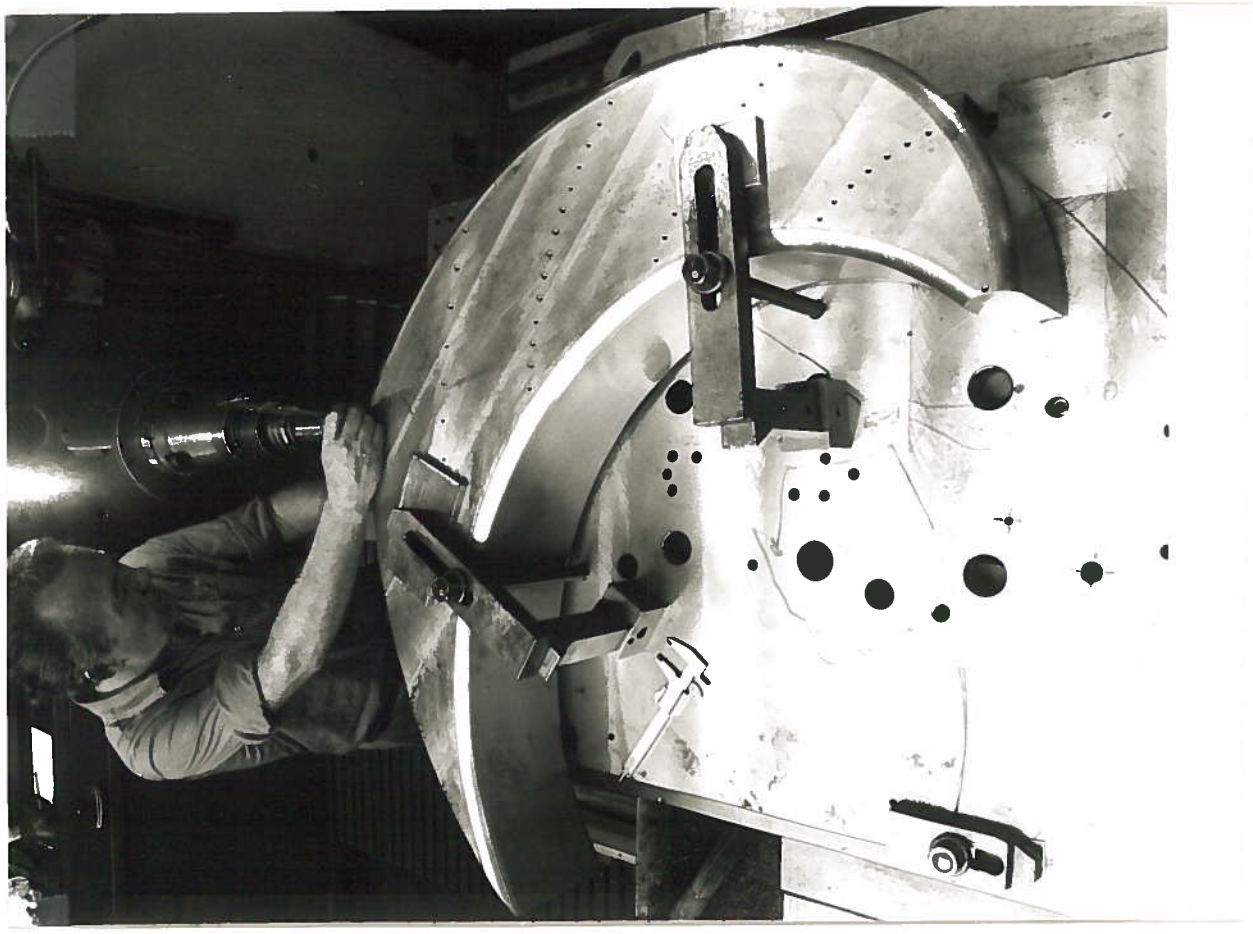

FIG. 52 - View of an upper sector after the chamfering machining.

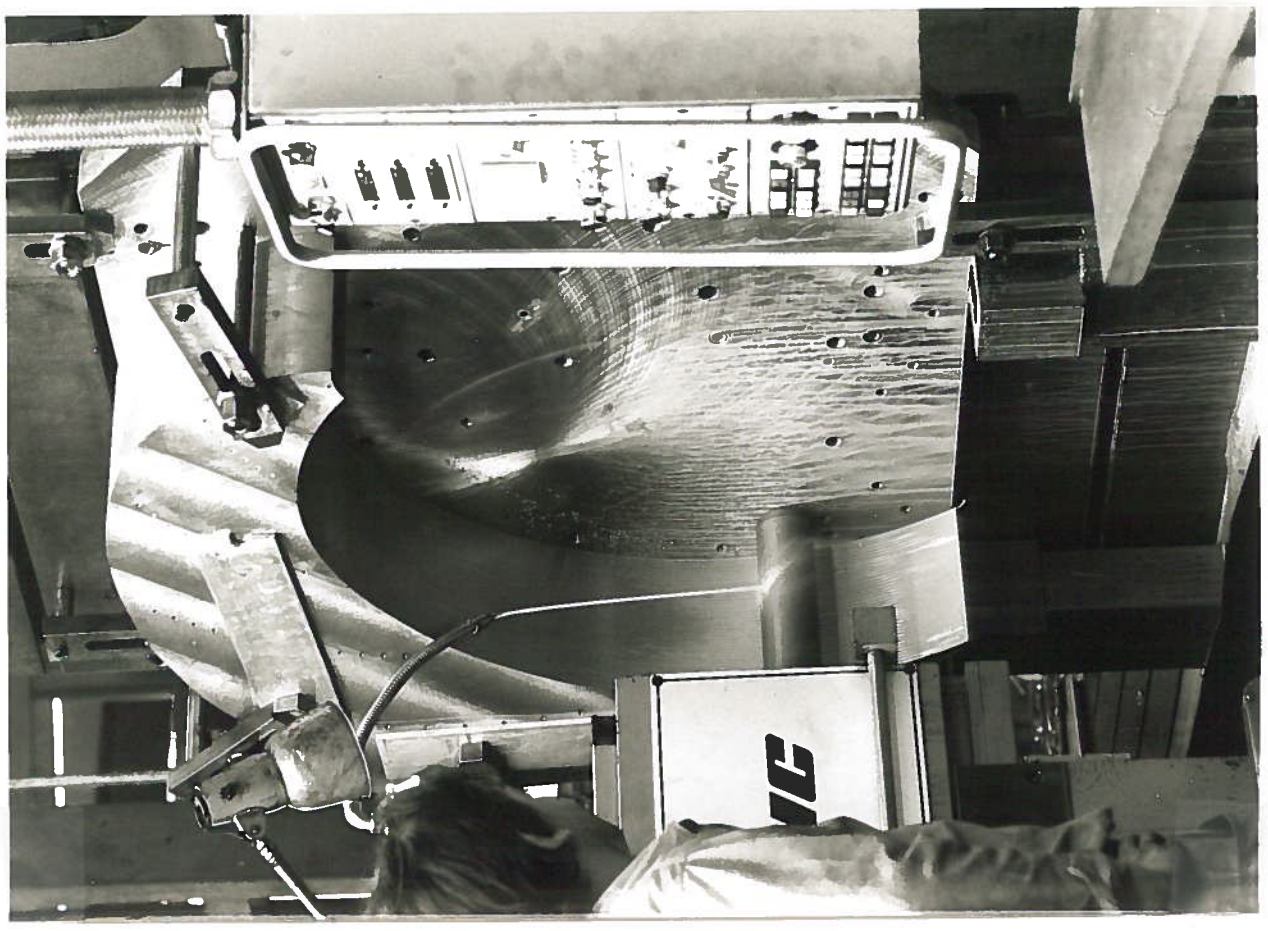

FIG. 51 - Finishing of the profiles of an upper sector.

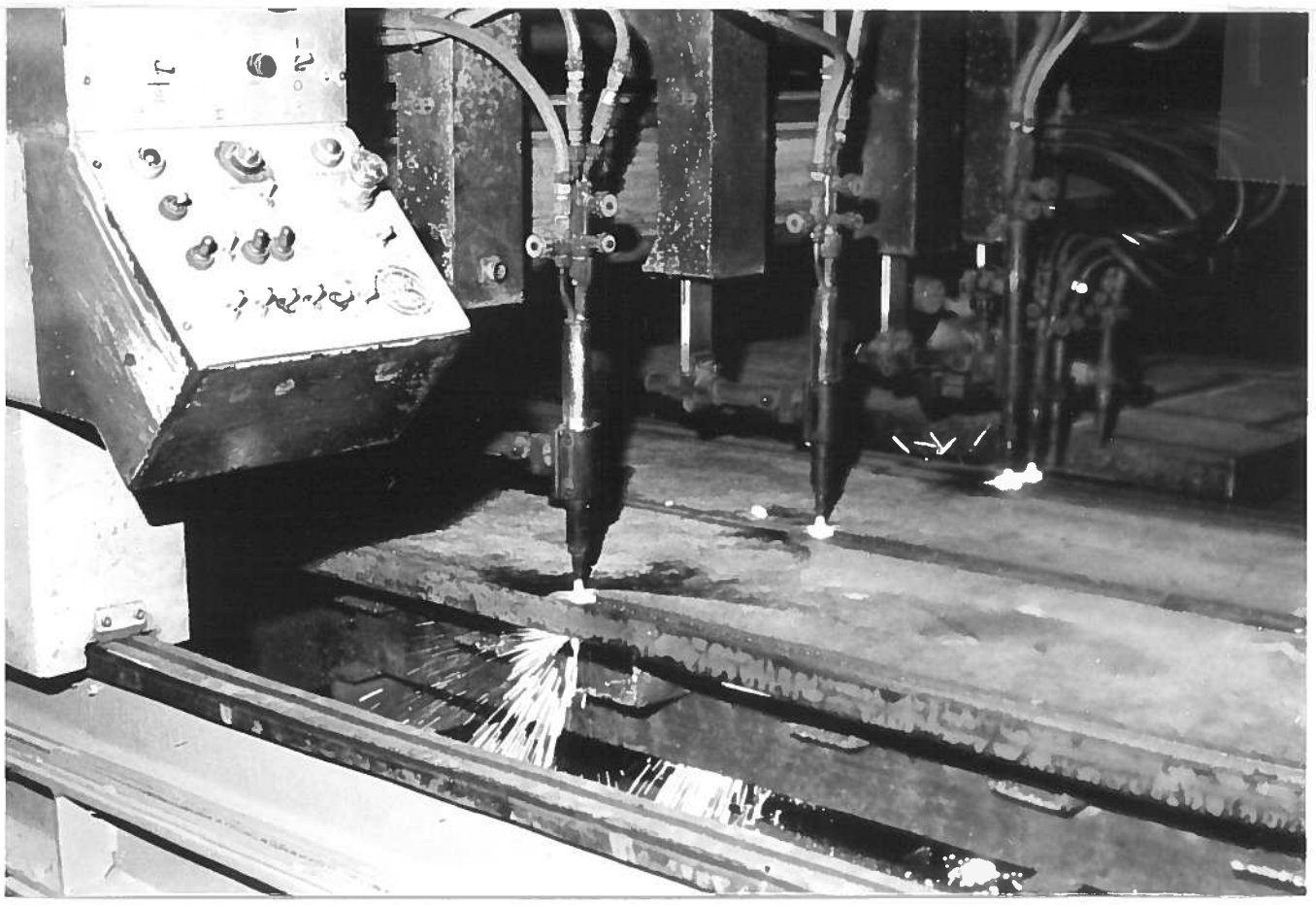

FIG. 53 - Flame cutting of the radial parts of the sectors.

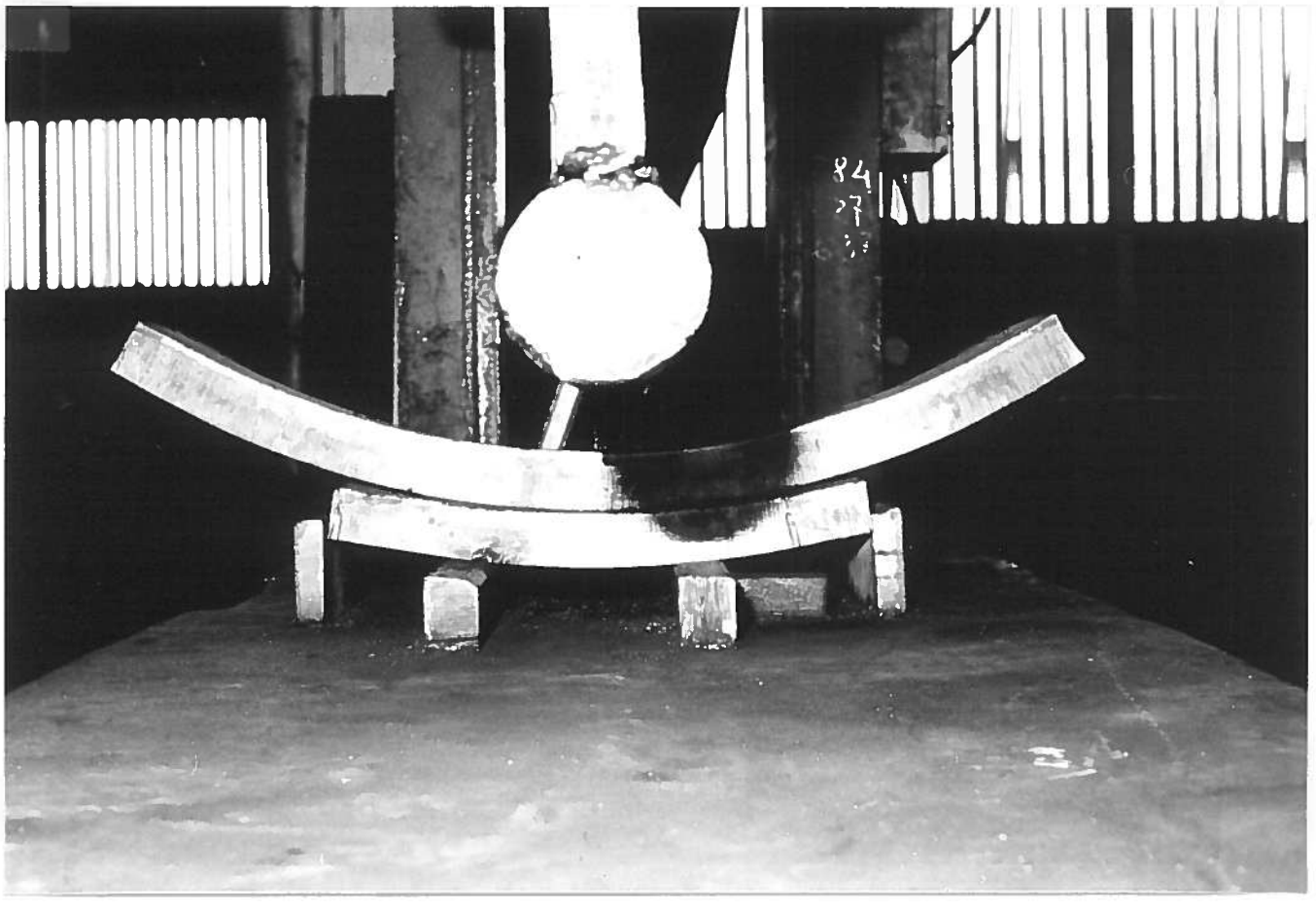

FIG. 54 - Rolling of the radial parts of the sectors.

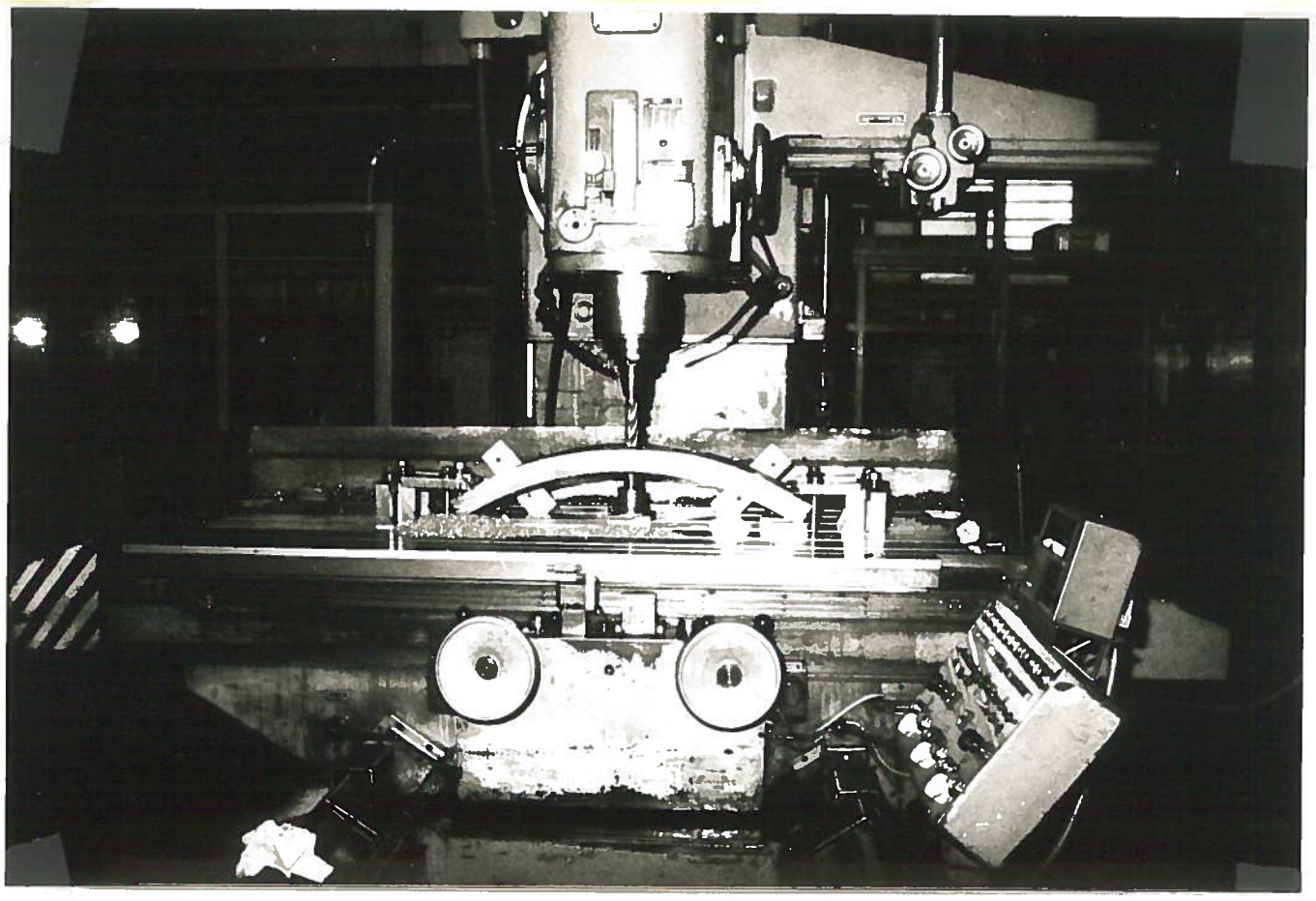

FIG. 55 - Rough machining of the radial parts of the sectors.

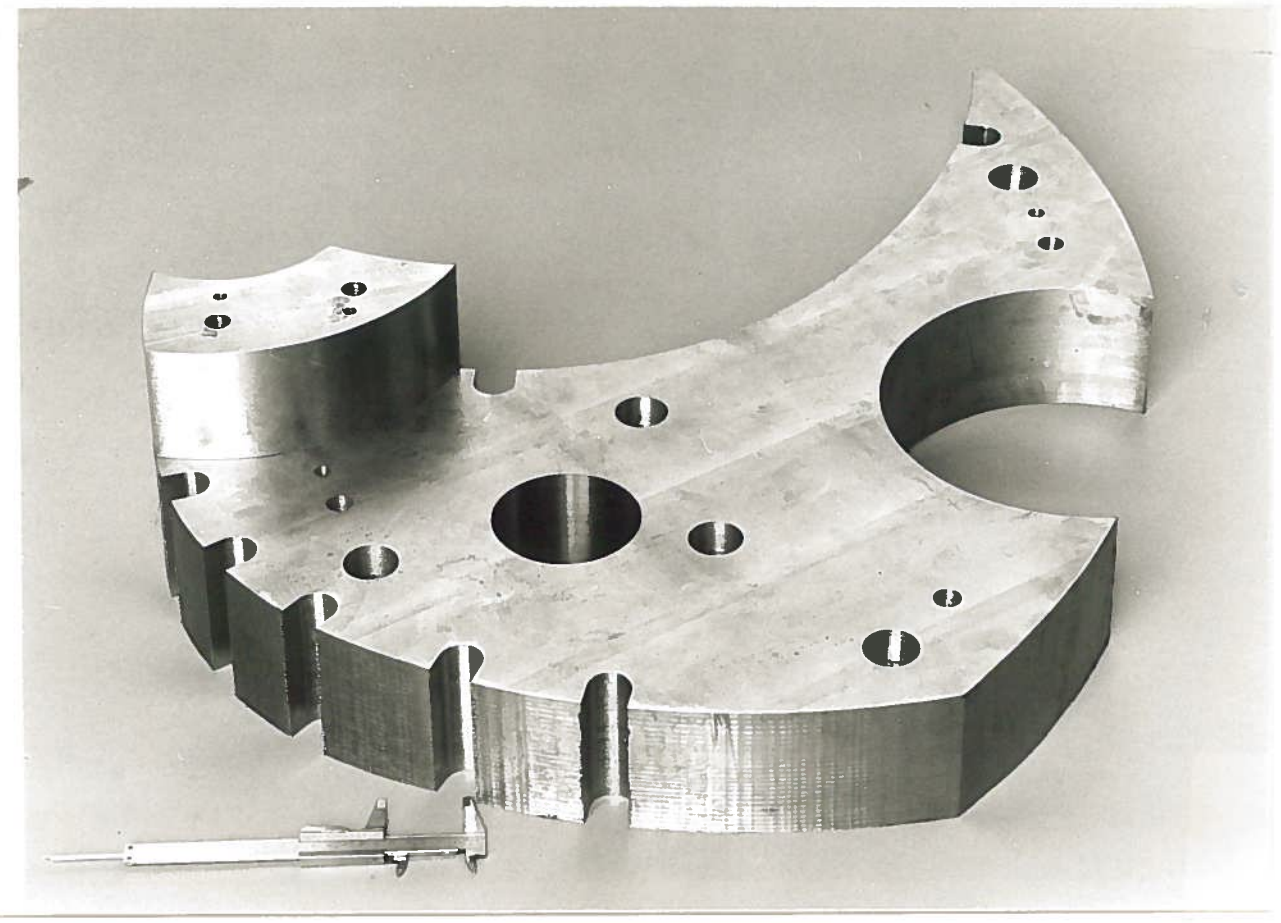

FIG. 56 - View of the rough machined valley shim.

Grinding of the planes with 0.5 mm allowance. Drilling of the entire set of holes including those for the trim coils leads and RF: Fig. 57. Assembling of the two parts of the valley shims. Finishing of all the profiles: Fig. 58. Grinding of the planes: Fig. 59.

4.5.4.- Rings

Rings are calandered from the plates and welded with electrodes of the same quality of iron. Thereafter they are annealed: Figs. 60 and 61. Rough turning of the rings and rough machining of the 52° windows with 2 mm allowance. Rings are once more annealed. Finishing of the mating surface of the ring with the pole plates. Drilling of the fixing holes of the rings and plates. Mounting of the ring on the plate. Rings fixed on the relative plate are turned to the final dimensions. 52° windows and dowels holes are numerically controlled machined.

4.5.5.- Spacers

The stainless steel spacers are obtained from straight plates. First the plain surfaces are machined and holes are drilled by numerical controlled machine and thereafter the circular profiles are spark machined: Figs. 62-64. The 6 low carbon iron spacers are directly numerically controlled machined from rolled bars: Fig. 65. Finally all the spacers between the upper and lower sectors are grinded to final dimensions and mounted on the relative sector.

4.5.6.- Assembly

Dowels holes and fixing holes for the assembly of the lower sectors are carefully machined on the plates using as positioning reference the central hole and the coupling capacitor hole at R = 350, θ = 19°10'; Fig. 66. Afterwards all the pole tips are mounted on the relative plates and the shape tolerance and the 120° symmetry are checked using a numerical controlled machine: Fig. 67.

5.- CONCLUDING REMARKS

The magnet yoke has been delivered in March 1983 and assembled in Milan without the pole plates, which were sent to Turin for further machining and mounting of the polar expansions. Also the lifting system has

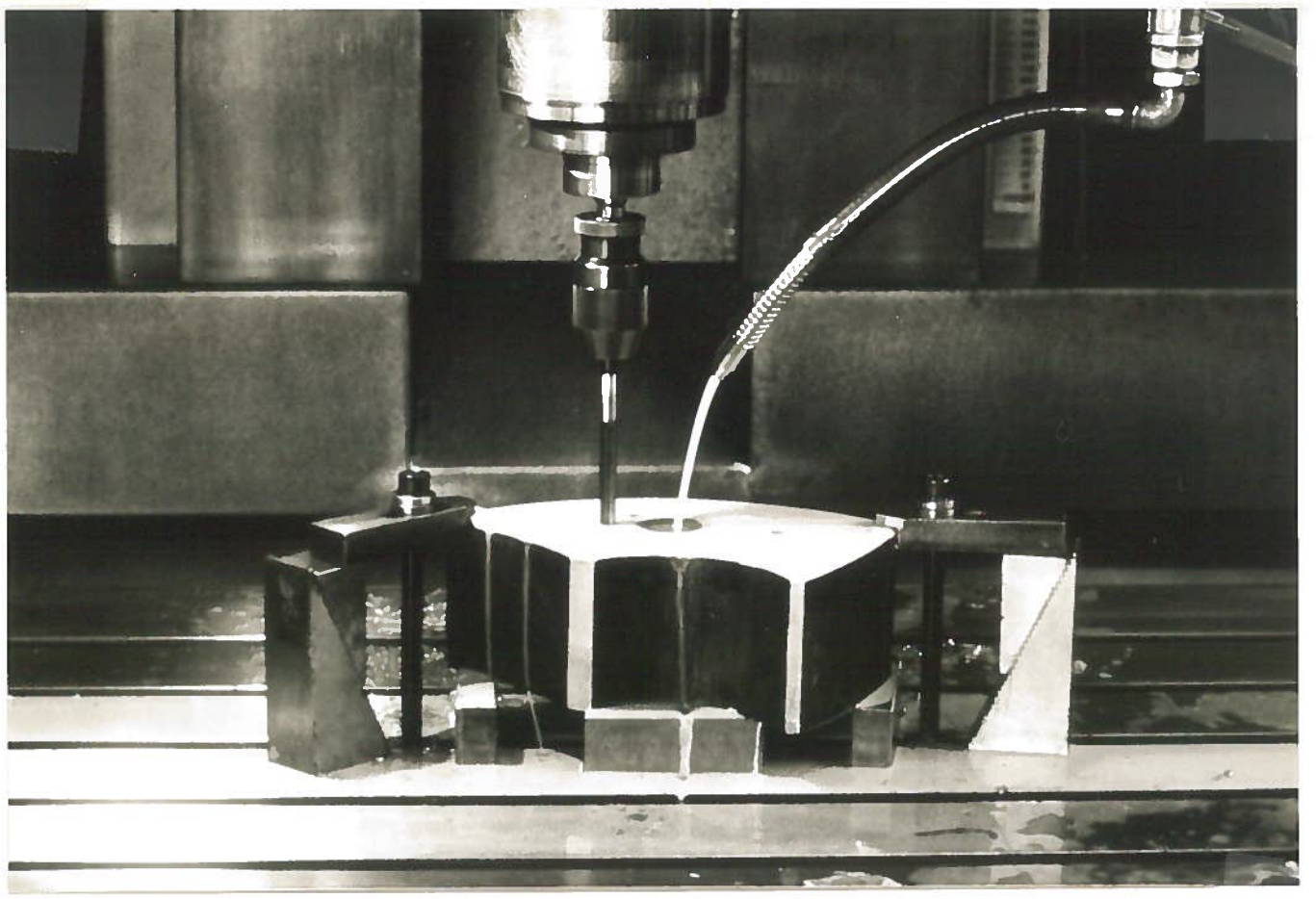

FIG. 57 - View of the valley shim during drilling of the holes.

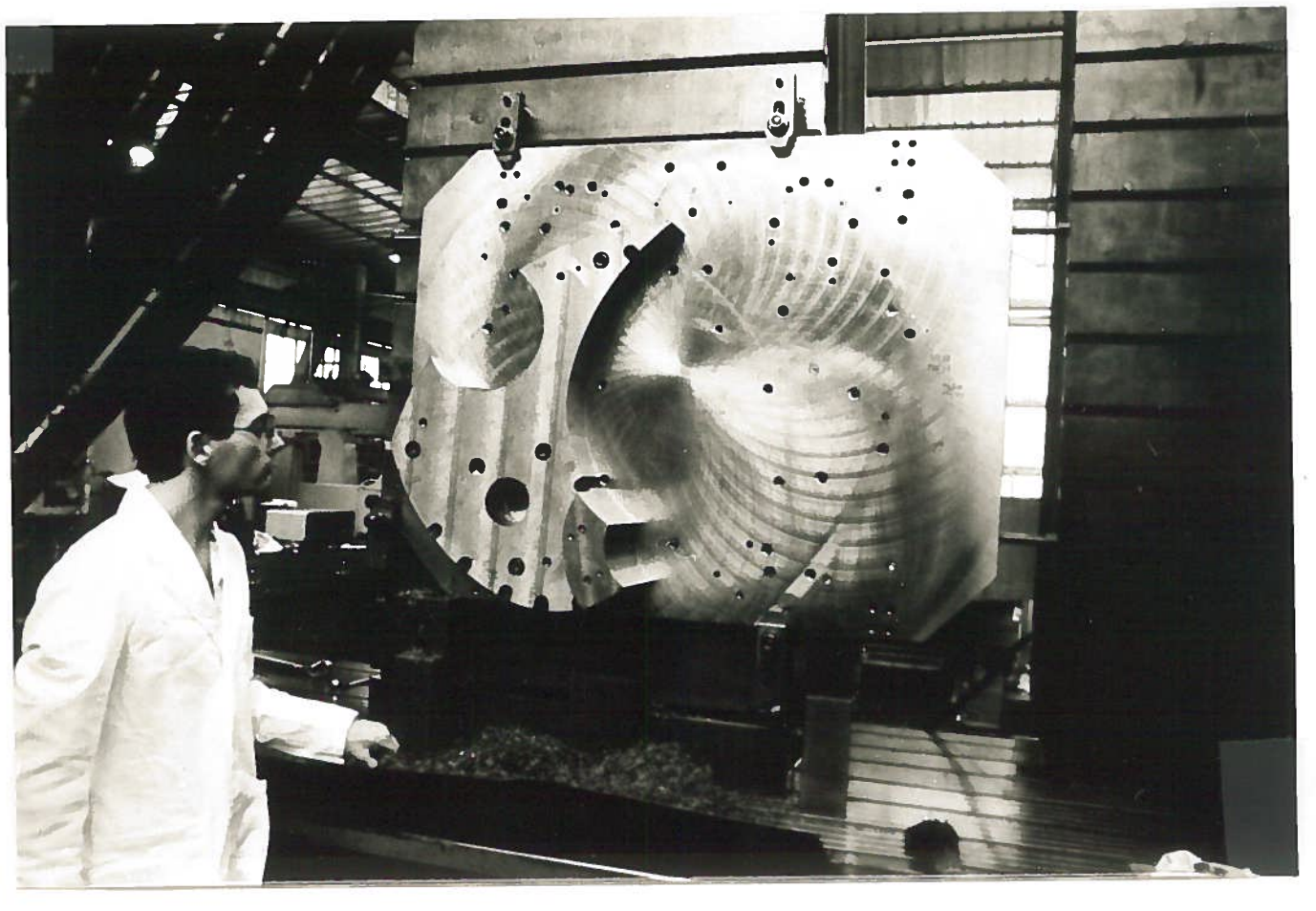

FIG. 58 - Finishing of the profiles of a valley shim.

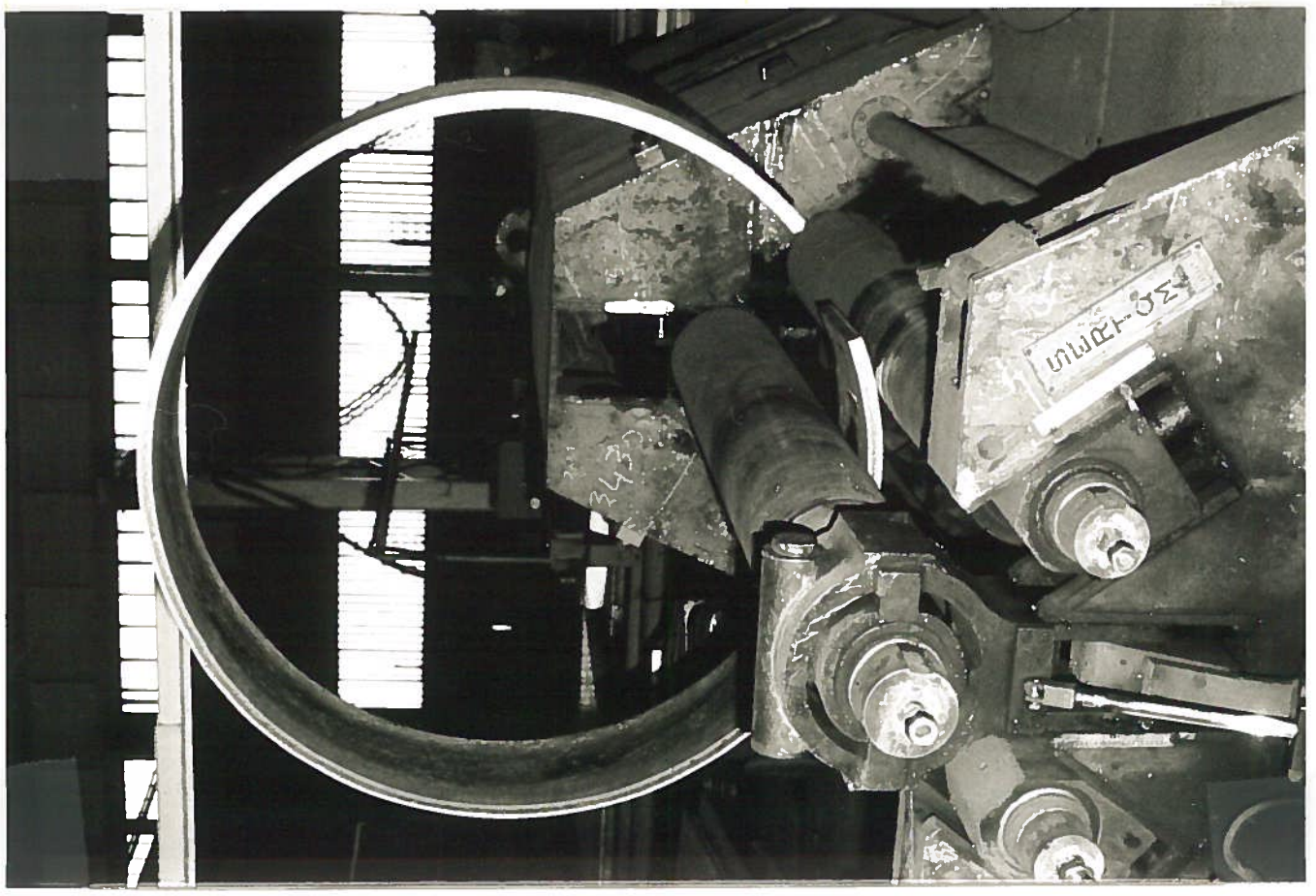

FIG. 60 - View of the ring during calendering.

FIG. 59 - Grinding of the planes of a valley shim.

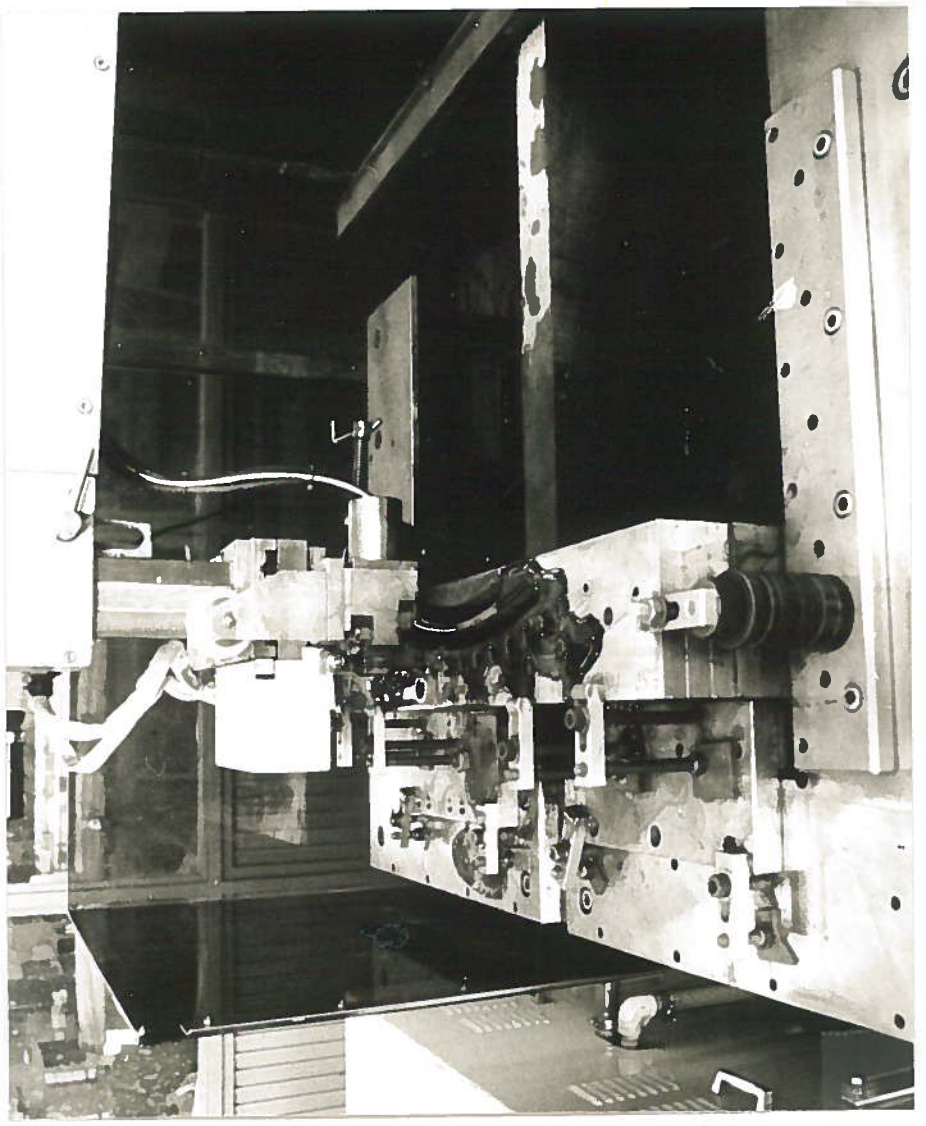

FIG. 62 - View of a spacer during spark machining of the profiles.

FIG. 61 - View of the ring during welding.

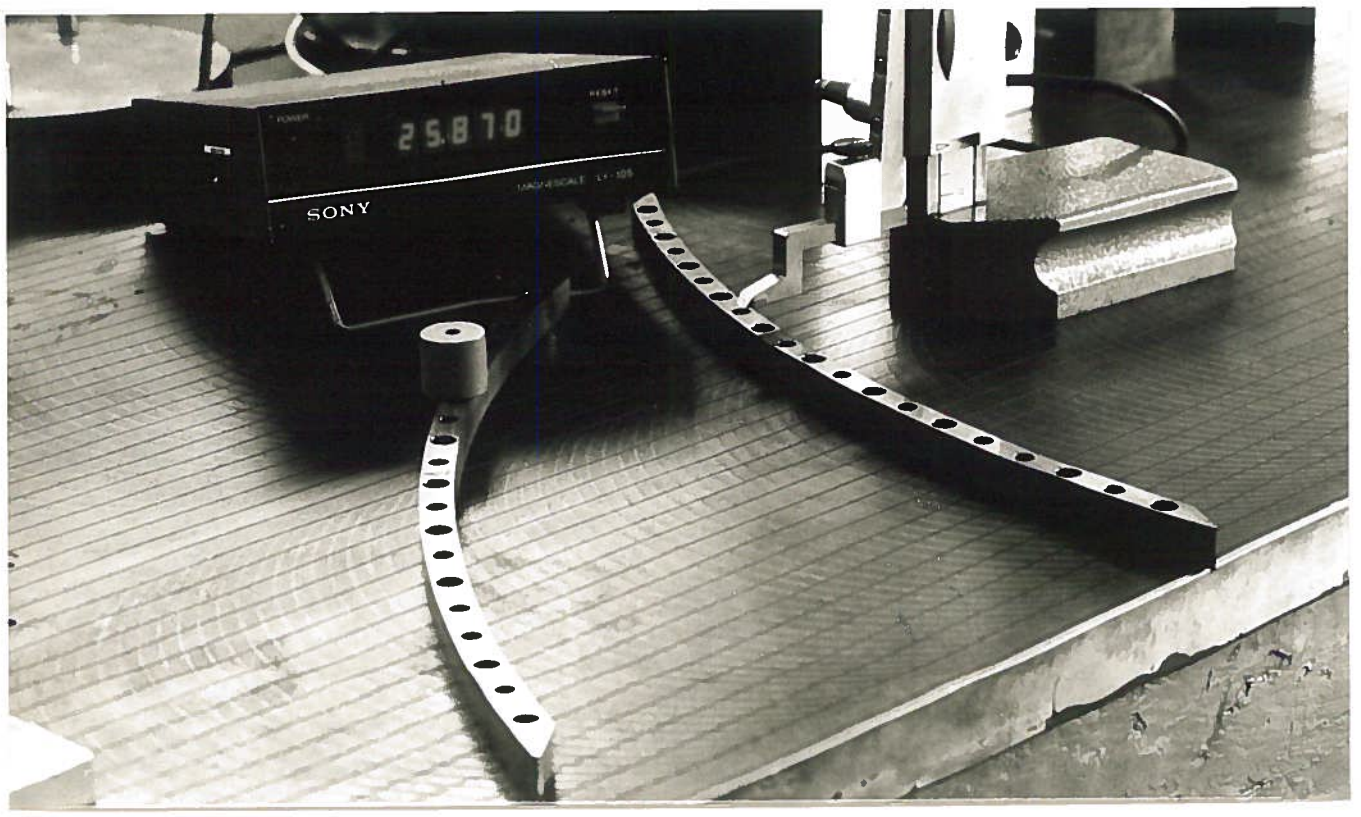

FIG. 63 - View of two spacers after final machining.

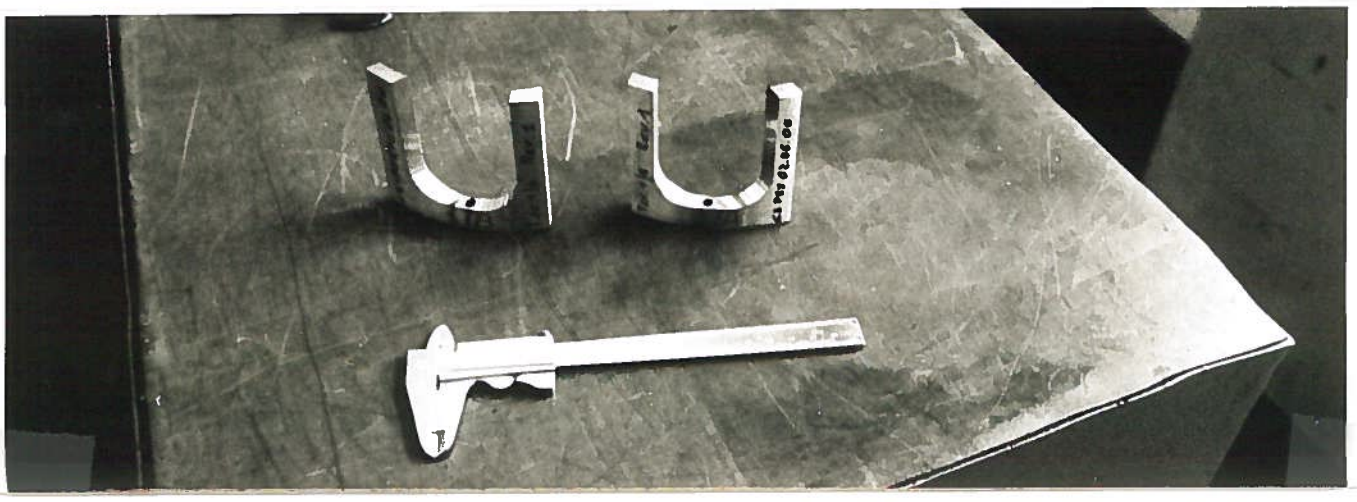

FIG. 64 - View of one set of spacers n.1 after final machining.

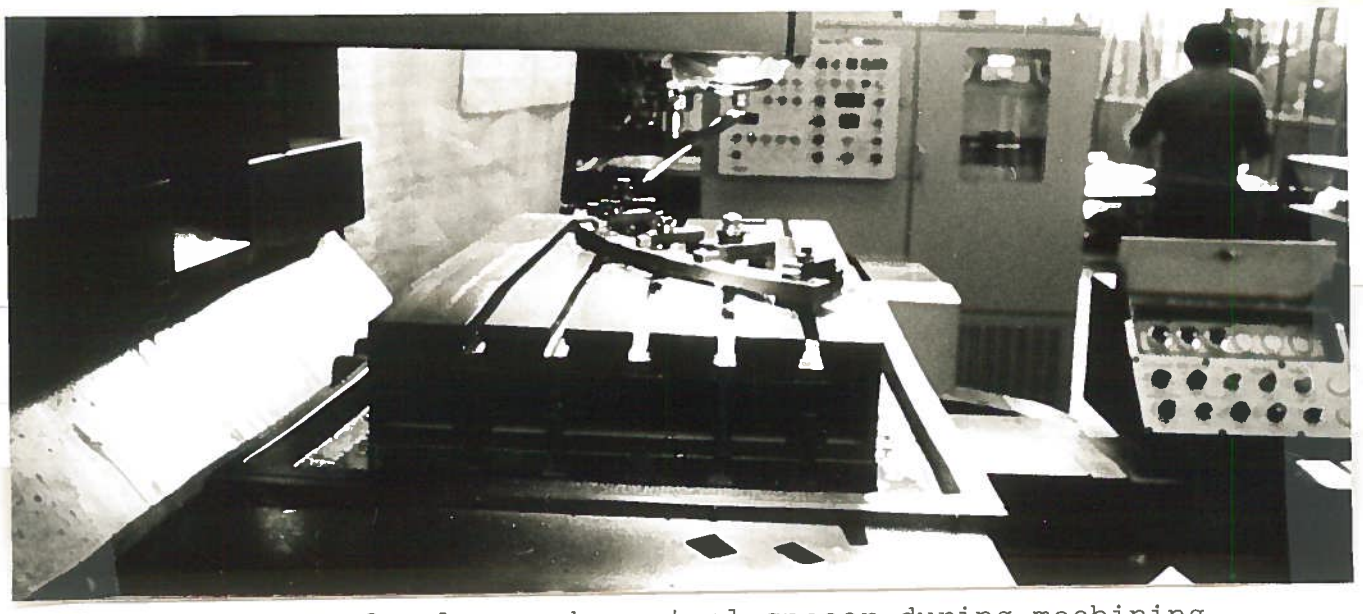

FIG. 65 - View of a low carbon steel spacer during machining.

FIG. 66 - View of one pole plate and ring during machining of the holes for the assembly of the lower sectors.

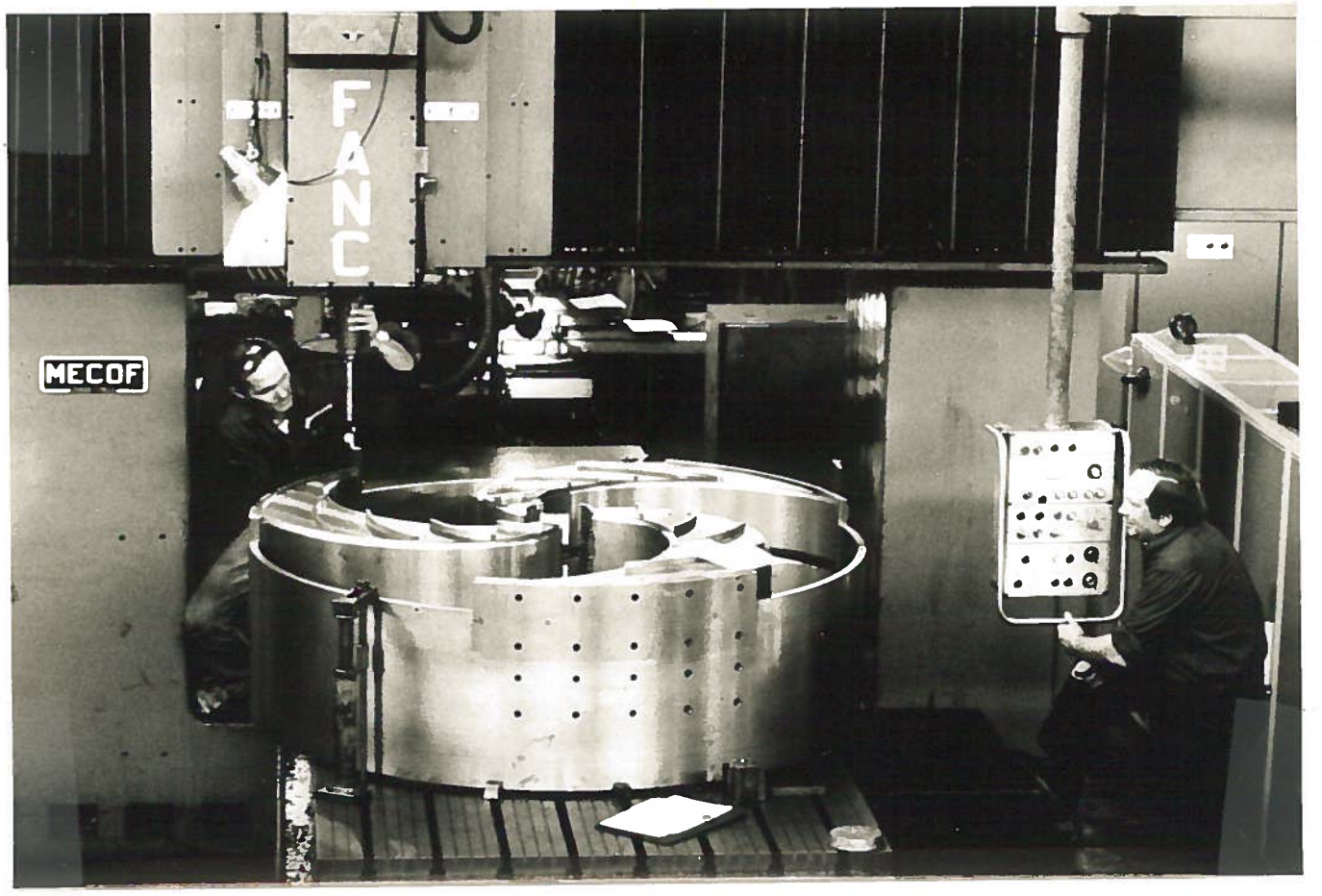

FIG. 67 - View of one set of polar expansions fully assembled on the relevant plate during acceptance tests.

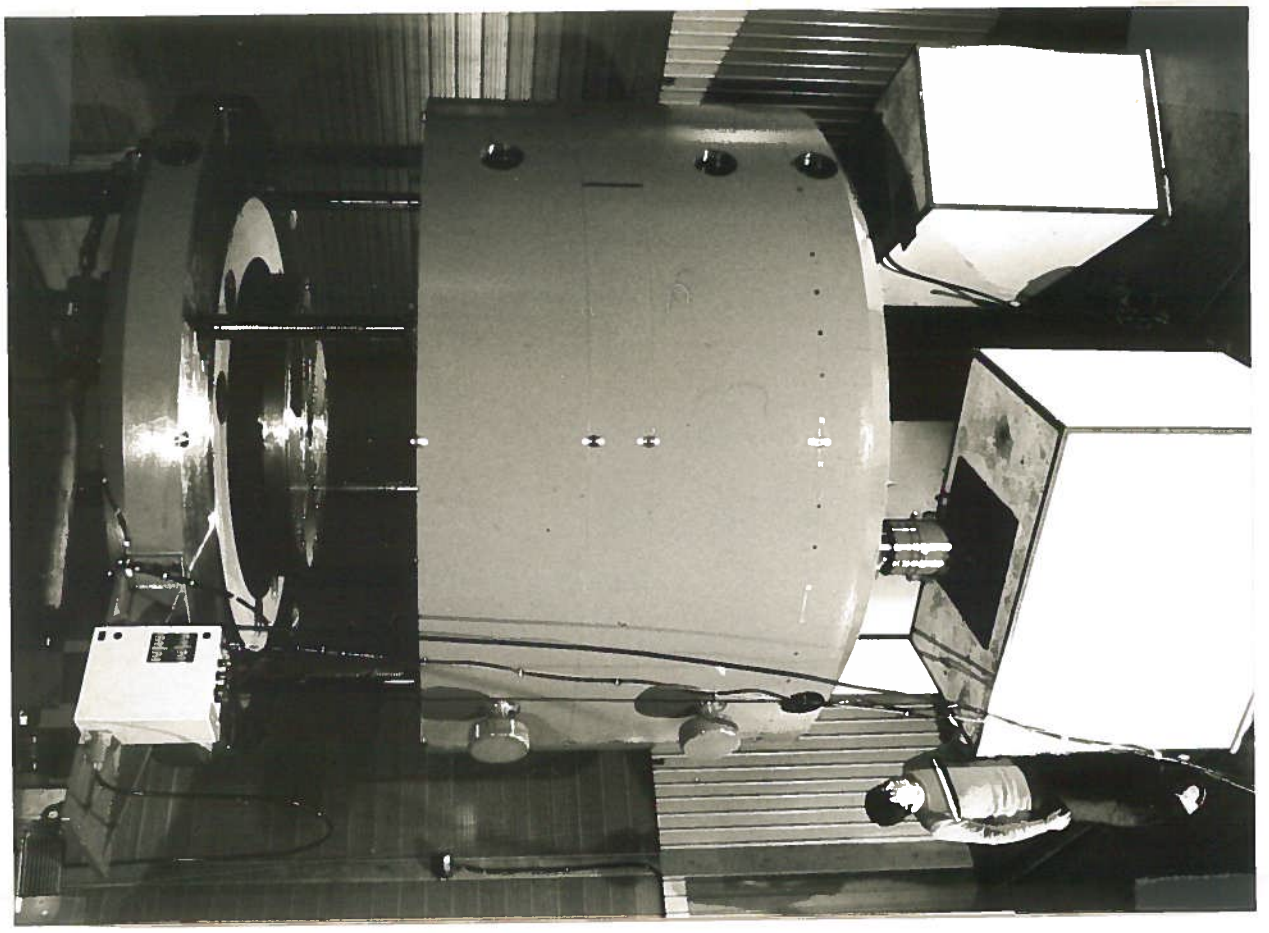

FIG. 69 - View of the magnet yoke assembled in Milan during operation of the lifting system.

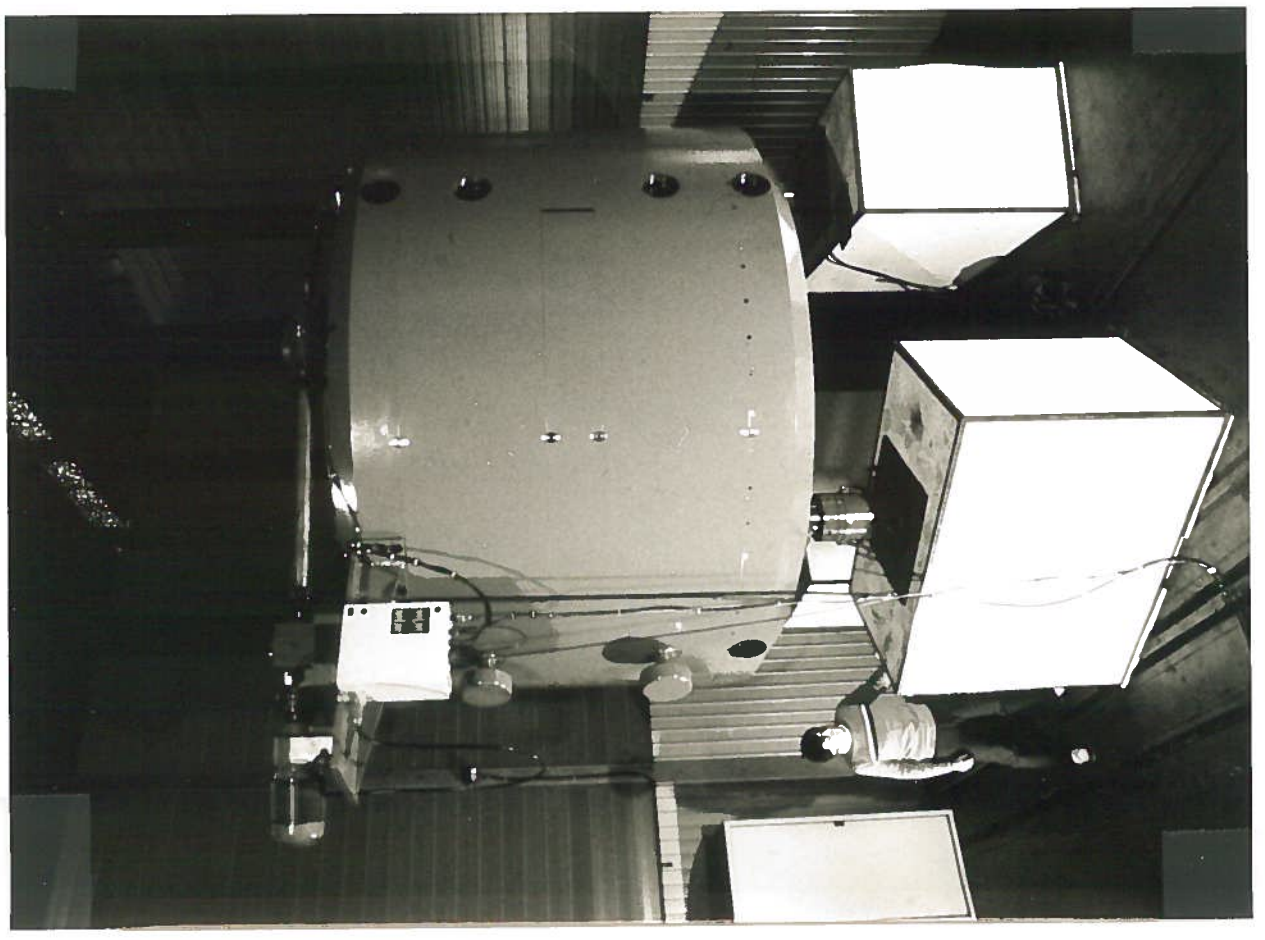

FIG. 68 - View of the magnet yoke assembled in Milan.

been assembled as seen in Figs. 68 and 69. Acceptance tests carried out on the magnet yoke have shown a satisfactory correspondance with required values. Further measurements are now in progress in order to completely map the mechanical characteristics of the yoke.

Machining of the polar expansions has been completed in Turin in October 1983. Afterwards the pole tips have been mounted on the yoke and measurements of the mechanical tolerances with the fully assembled magnet, which are the really important ones, are now in progress.

ACKNOWLEDGEMENTS

Authors wish to express their thanks to Mr. W.Giussani who carried out all the drawings of the magnet with great skill and to Mr. G.Cortesi and to Mr. S.Parmeggiano for their continuous and essential help during the mounting of the magnet in Milan.

REFERENCES

(1) - E.Acerbi et al., The Milan Superconducting Cyclotron Project, IEEE Trans. Nucl. Sci. NS-28, 2095 (1981).

(2) - E.Acerbi et al., The Milan Superconducting Cyclotron Project, Proceedings IX Intern. Conf. on Cyclotrons and their Applications, Caen 1981 (Les Editions de Physique, 1981), p. 169.

(3) - E.Acerbi et al., Status of the Milan Superconducting Cyclotron, IEEE Trans. Nucl. Sci. NS-30, 2126 (1983).

(4) - J.Ouvry, M.Savat and Mlle Brisset, Forces ponderomotrices s'exercant sur un corps aimante e sur des courants, Note CEA N.95 (1954).

(5) - E.Fabrici, Magnetic Forces on the Coils of the Superconducting Cyclotron at the University of Milan, Report INFN/TC-82/10 (1982).

(6) - S.P.Timoshenko and S.Woinowsky-Krieger, Theory of Plates and Shells (McGraw-Hill), p. 66.

(7) - G.Bellomo, C.De Martinis and L.Serafini, Design of the Magnetic Field for the Milan Superconducting Cyclotron, Proceedings IX Intern. Conf. on Cyclotrons and their Applications, Caen 1981 (Les Editions de Physique, 1981), p. 395.